

THE DESIGN AND CONSTRUCTION OF A LINEAR ELECTRON ACCELERATOR

by

John E. Crawford

A thesis submitted to the Faculty of Graduate Studies and Research in partial fulfilment of the requirements for the degree of Doctor of Philosophy.

Radiation Laboratory,
Department of Physics,
McGill University,
Montreal.

April, 1962

Table of Contents

	Page
List of figures	iv
List of tables	v
Abstract	vi
Acknowledgements	vii
Introduction	1
1. Prior knowledge	1
2. Medical accelerators	3
I Design considerations	5
1.1 Power distribution	5
1.2 Basic design aims	8
1.3 Optimum accelerator designs	9
1.4 Machining tolerances	14
II R.F. testing of the constant velocity structure	18
2.1 R.F. tests for v_p , v_g and Q	18
2.2 Determination of shunt resistance r	21
2.3 Impedance measurements	27
III Design and construction of buncher cavities	32
3.1 Choice of α and β	32
3.2 Dimensions of buncher cavities	38
3.3 Phase shift measurements and bandwidth	42

Table of Contents

	Page
IV The electron gun and focusing system	44
4.1 Gun designs	44
4.2 D.C. pulsing system	47
4.3 The present electron gun	49
4.4 Magnetic focusing	51
V Accelerator tests at high power	54
5.1 Experience with magnetrons	54
5.2 Frequency skipping and long-line effect	58
5.3 Measurements of accelerator performance	63
5.4 Improvement of accelerator operation	68
5.5 Present accelerator performance	72
Appendix: The transverse electron motion	75
A.1 Accelerator R.F. fields	75
A.2 Equations of radial motion	78
A.3 Electrons with initial angular velocity	81
Bibliography	85

List of figures

Figure	Subject	Following page
1	Block diagram of accelerator	2
2	Photograph of accelerator	2
3	Optimum loading vs. attenuation	11
4	Energy vs. beam current	12
5	Attenuation vs. a/b	12
6	a and b vs. a/b	12
7	Shunt resistance vs. a/b	12
8	Brillouin diagram	18
9	Bench test apparatus	19
10	Resonances of two-foot section	21
11	Measurement of cavity impedance	23
12	Accelerator cavities	26
13	Apparatus for impedance measurement	27
14	Buncher coupler	30
15	Dummy load coupler	30
16	α and β in the buncher	37
17	Longitudinal orbits - 2800 Mcps	37
18	Longitudinal orbits - 2798 Mcps	37
19	Longitudinal orbits - 2802 Mcps	37
20	Measured phase shift	42

List of figures

Figure	Subject	Following page
21	VSWR near design frequency	43
22	The electron gun	49
23	Axial field in the buncher	53
24 a	Input susceptance vs. phase angle	58
b	Tuning characteristic of a magnetron	
25	Permissible line length	60
26	Beam current pulses	64
27	Energy spectra with early magnetrons	70
28	Output energy spectrum	73
29	Average and peak current vs. filament power	73
30	Photograph - buncher focusing coils	80
31	Transverse buncher orbits with different fields	80
32	Transverse orbits with different angular velocities	83

List of tables

Table		Page
1	Optimum accelerator designs	11
2	Tentative specifications	14
3	Cavity resonances	20
4	Orbit calculations	37
5	Buncher parameters and dimensions	41
6	Accelerator operation	73

Abstract

A linear electron accelerator, intended for radiotherapy and for physics research, has been built for the Royal Victoria Hospital. The electron energy (0.5 Mev) and peak beam current (> 200 ma.) meet the design specifications. The design and construction procedures are described, and the techniques and results of various performance tests are given.

A simplified explanation of magnetron frequency skipping, ascribed to long-line effect, is given. The thesis appendix gives a discussion of transverse accelerator orbits, and describes an approximate method of evaluating the required focusing field.

Acknowledgments

The author gratefully acknowledges the advice and assistance of his supervisor, Dr. W. M. Telford, in every aspect of this work. To Dr. Telford is due much of the accelerator design, and a great deal of its construction.

Many members of the Radiation Laboratory participated in this work, either directly or indirectly. Mr. R. S. Weaver assisted in the programming of the IBM 650 computer, greatly simplifying the calculation of buncher orbits. Of the workshop staff, under Mr. S. Doig, the work of Mr. A. Simard deserves special recognition. Mr. Simard machined all accelerator cavities with great skill and precision, and made many other critical parts.

The project was made possible by grants from the Federal Department of Health and Welfare, which were made available to the Royal Victoria Hospital by the Quebec Provincial Government. Financial assistance was provided for the author in several N.R.C. studentships, and this help is greatly appreciated.

Thanks are due to Dr. L. G. Stephens-Newsham, who offered valuable advice on radiological matters, and provided the facilities of the hospital physics laboratory and workshop.

Introduction

1. Prior Knowledge

The ideas behind linear accelerator technology are by no means recent. Ising¹⁾ in Sweden suggested the use of a spark gap oscillator and transmission lines for the acceleration of particles to high energies, and the first successful linear accelerator was built by Wideröe²⁾ in 1928. With a maximum applied voltage of 25 kv., Wideröe succeeded in accelerating potassium ions to energies of 50 keV. Shortly after, Sloan and Lawrence³⁾ accelerated mercury ions to 1.25 MeV. Beams, Snoddy, and Trotter^{4,5)} obtained energies of several millions of volts with both electrons and protons, using loaded transmission lines.

It is only in the period after the Second World War, however, that electron accelerators similar to the one described in this thesis have become really practical. Radar technology made available magnetrons and klystrons of high efficiency and power and groups in England and the U.S.A. worked independently on the idea of accelerating electrons by means of the travelling wave propagated within a wave guide. An ordinary rectangular or cylindrical guide is useless for this purpose since the phase velocity of the fundamental wave component is greater than the velocity of light. With appropriate loading, this phase velocity can be reduced, and

adjusted to be equal to c , or less. Although various forms of loading have, and are being tried for accelerators, one of the simplest forms available for machining is the disc loaded cylindrical guide.

A typical accelerator system is shown in fig. 1 . A pulsed, high power magnetron provides the R.F. wave, which is changed to a transverse magnetic mode at the input coupler, and propagates with attenuation along the cylindrical disc loaded guide. At the output end a similar coupler guides the wave to the dummy load where the remaining power is dissipated. It is not necessary to throw away this remaining power; an alternative procedure is to provide a feedback loop to the input coupler, permitting recirculation to improve the efficiency, and increase output energy. In any event it is important to suppress the reflected wave by suitable matching procedures. After the accelerator is filled with R.F. power, electrons are injected by a pulsed gun into the input cavities of the guide at a velocity $v_e < c$. If the wave travels at the same velocity the electron can gain energy from the axial electric field, and will be accelerated. In the first cavities of the accelerator it is necessary to vary the phase velocity of the wave to keep step with the electron; after the initial "buncher" section the electron's velocity will be so close to c that for most of the accelerator a uniform repetitive

ACCELERATOR SYSTEM

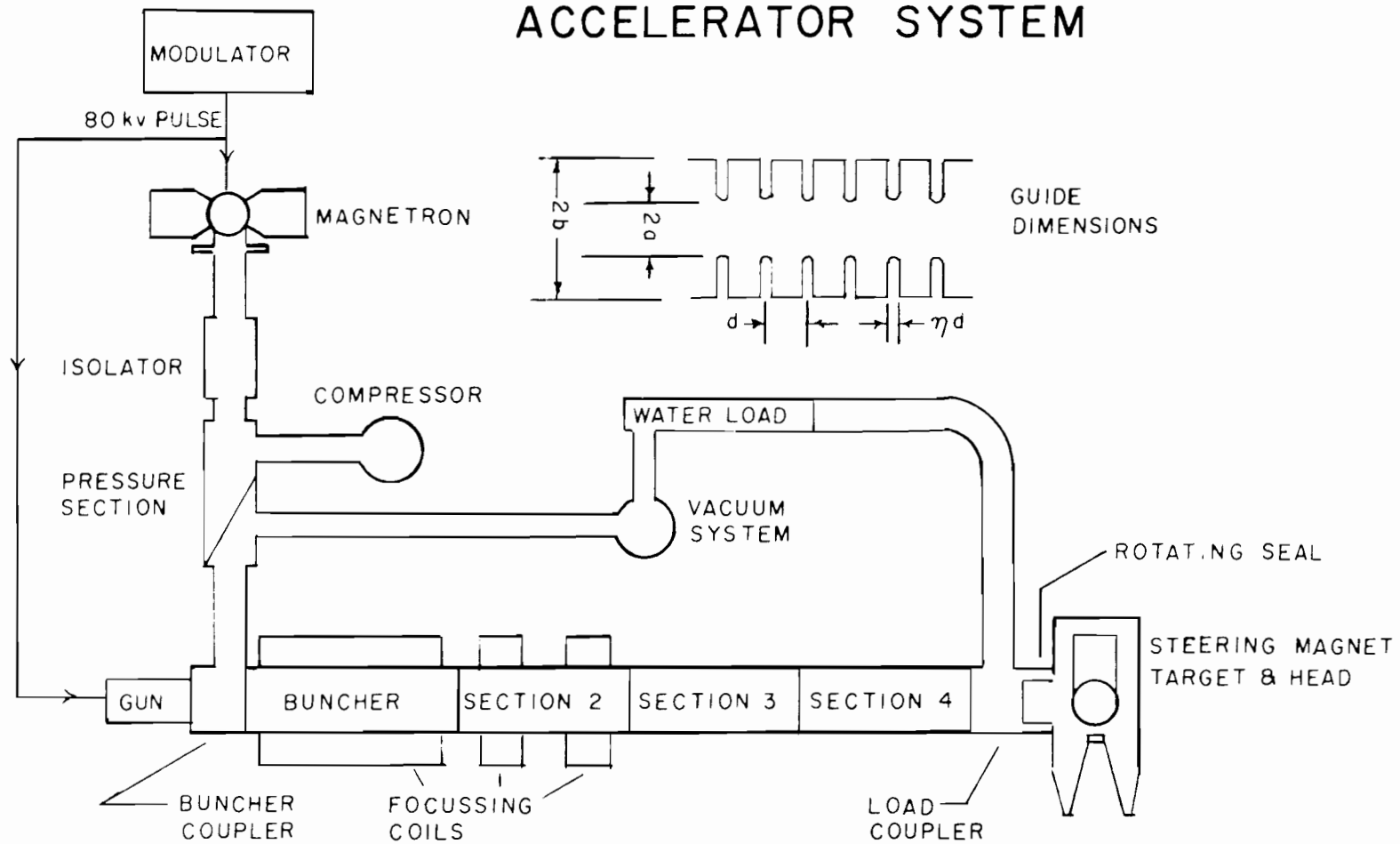


FIGURE 1

structure can be used to increase the energy (mass) of the electron to any desired value. The linear accelerator design, in contrast to the circular, involves insignificant radiative losses, so the only limitation on energy is the power and space available.

2. Medical Accelerators

Although linear accelerators in the billion volt range have been designed at Stanford University, they are becoming more and more popular as sources for medical and radiographical purposes at lower energies. Conventional X-ray tubes are useful for energies below 300 keV, and Van de Graaf accelerators are commercially available up to several MeV. In the therapeutically useful range from about 3 to 30 MeV the linear accelerator provides the most practical source of electrons and X-rays.

The medical advantages of this energy range, compared with the conventional 200 keV machine are:

(a) Ionization equilibrium occurs several centimetres below the surface of the skin; thus, skin burning, a common side effect with lower energy units is greatly reduced. Scanning techniques, which place the tumour site on the axis of rotation, may be used, making the skin dose even smaller.

(b) Depth dose is greatly increased and is relatively independent of the field size chosen. This means that adequate dosage can be delivered to the tumour site, while the damage to nearby healthy tissue is minimized.

(c) With lower energy radiation, selective absorption in different types of tissue (particularly bone) occurs, causing inhomogeneities in the dose delivered to adjacent tissue. With energies above ~ 2 MeV, selective absorption disappears; the delivery of the desired dose is more a matter of prediction than of chance.

The staff of Radiology at Montreal's Royal Victoria Hospital decided to build a linear accelerator for therapy in 1952, and enlisted the aid of the McGill Radiation Laboratory in 1956. It is the purpose of this thesis to describe the design considerations for this device, and to outline the measurements and experiments involved in its construction.

I Design Considerations

1.1 Power distribution in the constant velocity section.

In the "constant velocity" sections of a travelling wave accelerator electrons which have previously reached relativistic voltages (usually >1 MeV) gain energy at the expense of the electromagnetic field. It may be shown that in a disc loaded guide an infinite set of waves, both forward and backward is propagated; the design parameters must be chosen to make the TM_{01} mode travel at the velocity of light to keep step with the electrons. All other components have a negligible effect on output energy; their amplitudes are much smaller, and their different phase velocities are seen by the electrons only as oscillatory disturbances.

A study of power distribution in the guide is basic to the design and permits estimates of output energy to be made. The relations involved are well known, and have been discussed at length in the Stanford report⁶⁾, and by Neal⁷⁾; they are given here briefly by way of introduction, and for later reference.

If w represents energy stored per unit length, and the group velocity of the wave is v_g , then the energy flow equation is simply

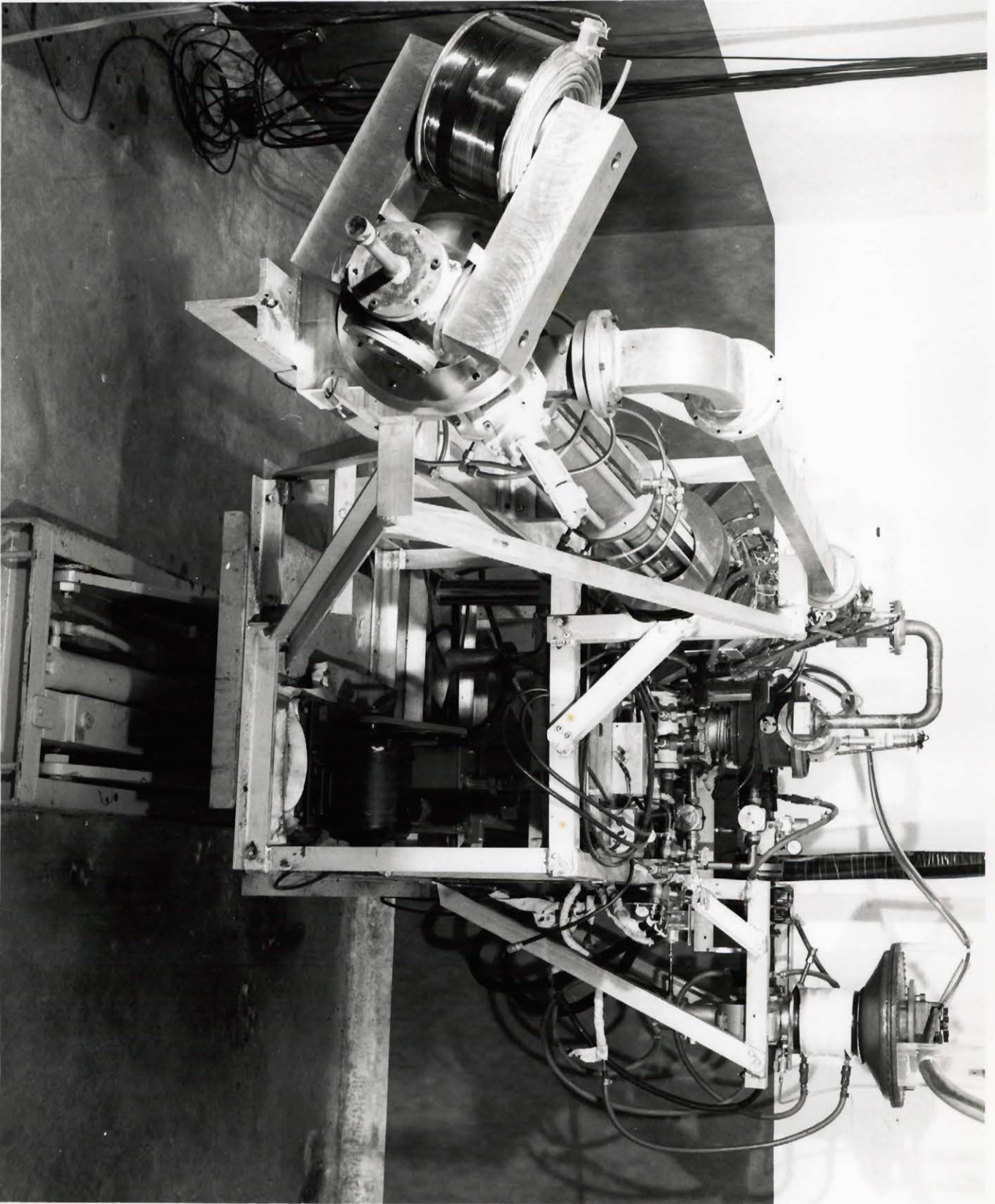
$$P = w v_g \tag{1.1}$$

Figure 2

Photograph of the accelerator

In this picture, taken when the accelerator was under construction, the main components of figure 1 may be seen. The magnetron is at the upper right, and the accelerator tube extends diagonally toward the camera. Power at the output passes through the E bend section and to the dummy load through the long rectangular guide. This upper guide also serves as one branch of the vacuum pump out system.

The beam may be taken out axially, or deflected through 90° by means of the steering magnet (left foreground). The magnet is attached to the dummy load coupler with a rotating vacuum seal; this permits the beam to be swung to the desired treatment angle. It is also possible to raise the whole accelerator 40 inches by the hydraulic lifting table.



Therefore

$$\frac{dP}{dz} = v_g \frac{dw}{dz} \quad (1.2)$$

and since $v_g = \dot{z}$

$$\frac{dP}{dz} = \dot{w} \quad (1.3)$$

Q for the structure is defined in the usual way as

$$Q = \frac{2\pi \times \text{energy stored}}{\text{energy dissipated per cycle}} = \frac{2\pi w}{-\frac{dw}{d\tau}} = \frac{\omega_0 w}{-\frac{dw}{d\tau}} \quad (1.4)$$

Therefore

$$\frac{dP}{dz} = \frac{\omega_0 w}{Q} = -\frac{\omega_0}{v_g Q} P \quad (1.5)$$

The power at a distance z from the input is then

$$P = P_0 e^{-\frac{\omega_0 z}{v_g Q}} \quad (1.6)$$

Since the electric field is proportional to \sqrt{P} ,

$$E = E_0 e^{-\frac{\omega_0 z}{2v_g Q}} = E_0 e^{-Iz} \quad (1.7)$$

where I , the attenuation, is expressed in nepers per metre.

If it is assumed that beam loading is very small (i.e. attenuation due to wall losses \gg attenuation caused by the beam), the output energy of a section of length L will be

$$V = \int_0^L E dz = E_0 L \frac{(1 - e^{-IL})}{IL} \quad (1.8)$$

It is useful to define a shunt impedance r as a figure of merit for an accelerator structure, analogous to the resistance of a parallel LCR resonant circuit. This gives the ratio of the square of axial field to the power lost per unit length:

$$- \frac{dP}{dz} = 2IP = \frac{E^2}{r} \quad (1.9)$$

so that the total energy is

$$V = \sqrt{2IL} \sqrt{P_0 L r} \frac{(1 - e^{-IL})}{IL} \quad (1.10)$$

For purposes of comparing accelerator structures, \bar{r} , a mean shunt resistance may be used. It is defined by

$$\bar{r} = \frac{V^2}{P_0 L} \quad (1.11)$$

$$\text{Therefore } V = \sqrt{P_0 L \bar{r}} = \sqrt{\frac{\bar{r}}{r}} \sqrt{P_0 L r} \quad (1.12)$$

and from 1.10

$$\sqrt{\frac{\bar{r}}{r}} = \sqrt{2IL} \frac{(1 - e^{-IL})}{IL} \quad (1.13)$$

Equation 1.10 gives only an approximation of accelerator energy in the case of low beam current. If loading due to the beam is considered, equation 1.9 must be modified to

$$- \frac{dP}{dz} = 2IP + iE = 2IP + i \sqrt{2IPr}$$

where i is the accelerator current. This may be easily integrated, giving the energy with beam loading:

$$\begin{aligned}
 V &= E_0 L \left[\frac{1 - e^{-IL}}{IL} - \frac{ir}{E_0} \left(1 - \frac{1 - e^{-IL}}{IL} \right) \right] \\
 &= E_0 L \left[\frac{1 - e^{-IL}}{IL} - m \left(1 - \frac{1 - e^{-IL}}{IL} \right) \right] \quad (1.14) \\
 m &= \frac{iE_0}{2IP_0}, \text{ is called the beam loading parameter,}
 \end{aligned}$$

and is simply the ratio of $\frac{\text{energy absorbed by the beam/unit length}}{\text{wall loss/unit length}}$.

With loading

$$\sqrt{\frac{r}{r}} = \sqrt{2IL} \left[\frac{1 - e^{-IL}}{IL} - m \left(1 - \frac{1 - e^{-IL}}{IL} \right) \right] \quad (1.15)$$

1.2 Basic design aims

Considerations of depth-dose curves⁸⁾ show that there is very little medical advantage in increasing electron energy beyond 10 MeV. The design of the X-ray head is further complicated at high energies by the larger steering magnet necessary, and by the increase in shielding material. At 10 MeV, the design energy chosen for the RVH accelerator, the unfiltered X-ray intensity 1 metre away from a gold target on the axis of the beam is about 20 R./minute for every microampere of average beam current; with the filtration required to give suitable dose curves over the treatment area, one may expect perhaps 6 R/minute/microampere. It was therefore decided to design for a current of 20 microamperes in order to have a useful therapeutic dose of 100 R/minute at 1 metre.

The power source chosen for the accelerator was the Raytheon QK 327 magnetron. This tube will provide a 4 megawatt pulse for 2 microseconds at a repetition rate of 330 p.p.s., and is tunable from 2720 to 2880 m.c.p.s. It was not expected that a QK 338 fixed frequency magnetron would be suitably stable in frequency throughout its life, but to provide for this possibility, it was decided to design the accelerator to operate at 2800 m.c.p.s., the nominal frequency of this tube.

The length of the constant velocity accelerator section was chosen to be 2 metres^x. Although the theoretical optimum number of discs per wavelength is $3.5^{(6)}$, the choice of 4 discs per wavelength greatly simplifies the R.F. bench tests with a sacrifice of only 2% in output energy. The resultant disc spacing is therefore $\frac{\lambda_g}{4}$, or 2.677 cm. Disc thickness is relatively unimportant, if it is reasonably small compared with the disc spacing; the value chosen was .579 cm.

1.3 Optimum accelerator designs

The accelerator dimensions which remain to be specified are a and b (see fig. 1). The ratio of $\frac{a}{b}$ determines the attenuation of the

^x see calculation of sec. 1.3

accelerator tube, as well as the value of r for the structure. The problem of choosing the correct attenuation is really that of maximizing $\sqrt{\frac{r}{r}}$ for the expected beam loading parameter m .

By differentiating eq. 1.13, one finds that the value of attenuation required to give maximum output energy at low beam current is $IL = 1.26$, and that for this value $\sqrt{\frac{r}{r}} = .903$. A differentiation of equation 1.15 shows that the condition for maximum $\sqrt{\frac{r}{r}}$ for the loaded accelerator is

$$m = \frac{2 \left(e^{-IL} - \frac{1 - e^{-IL}}{2IL} \right)}{1 - 2 \left(e^{-IL} - \frac{1 - e^{-IL}}{2IL} \right)} \quad (1.16)$$

This condition is plotted in fig. 3. When the value of I has been determined, the shunt resistance r should be found; a calculation of output energy may then be made from equation 1.15. Experimental values of r due to Ginzton, Hansen and Kennedy⁹⁾ have been used for this work. Table 1, computed from these values, lists some optimum accelerator designs (optimum in the sense that $\sqrt{\frac{r}{r}}$ has been maximized.) It is assumed that the accelerator is 2 metres long, has a duty cycle of .00066, and uses a 2800 M.c.p.s. power source with a 4 MW. pulse - the design parameters already chosen for the R.V.H. accelerator.

Table I

Optimum Accelerator Designs								
I_n/m	$m_{opt.}$	i_p (ma)	i_{av} (μ amp)	$\sqrt{P_0 L r}$ (MeV)	$\sqrt{\frac{\bar{r}}{r}}$ Unloaded	$\sqrt{\frac{\bar{r}}{r}}$ Loaded	V (MeV) Unloaded	V MeV at Opt.m.
.05	6.1	622	411	17.5	.43	.28	7.53	4.9
.086	4.0	524	345	17.9	.54	.35	9.67	6.3
.1	2.8	390	258	18.2	.58	.40	10.54	7.3
.2	1.2	224	148	19.1	.74	.58	14.16	11.1
.3	.5	112	74	19.5	.83	.68	16.2	13.3
.4	.3	77	51	19.7	.87	.75	17.1	14.8
.5	.1	29	19	19.9	.89	.85	17.7	16.9
.6	0	(Low)	(Low)	20.1	.90	.90	18.1	18.1
.7	0	(Low)	(Low)	20.2	.90	.90	18.2	18.2

It is apparent from this table that an accelerator using the R.V.H. power source could have an output of some 9 MeV per metre with extremely low beam current. However, an output of 20 μ amp is necessary, and considerable beam loss must be anticipated. It seems desirable, then, to design for fairly high beam loading, and to choose a relatively low value of attenuation. This choice of low attenuation also simplifies the problem of machining tolerances^x, and increases the permissible

^x
See sec.1.4

frequency limits of the source. For this reason the attenuation chosen for the R.V.H. constant velocity section was .086 nepers/metre. It is seen in the table that this gives an output energy of 9.6 MeV under conditions of low loading, and an energy of 6.3 MeV even with the high output beam current of 345 μ amp. If the buncher is designed to increase the velocity of the electron from .5 c to .96 c, 1.5 MeV can be added to the above energies, bringing them to 11.1 MeV unloaded, and 7.8 MeV loaded. A graph of energy vs. average beam current for the attenuation chosen is given in fig. 4.

The problem remaining is to choose values of a and b which will give the desired attenuation. Ginzton, Hansen, and Kennedy⁹⁾ give approximate experimental design curves, but do not guarantee their accuracy to within better than 15%, because of difficulties in the experimental measurements, and theoretical calculations of r and I. The curves, however, give a first approximation to the values of a and b, and the bench tests described in section 2.1 enable one to correct these trial values. The design curves are shown in figures 5, 6, and 7.

It is seen from fig. 5 that a value of $a/b = .365$ will give the desired attenuation. Figure 6 shows that for this ratio the phase velocity will be equal to c if $a = 1.506$ cm and $b = 4.110$ cm.

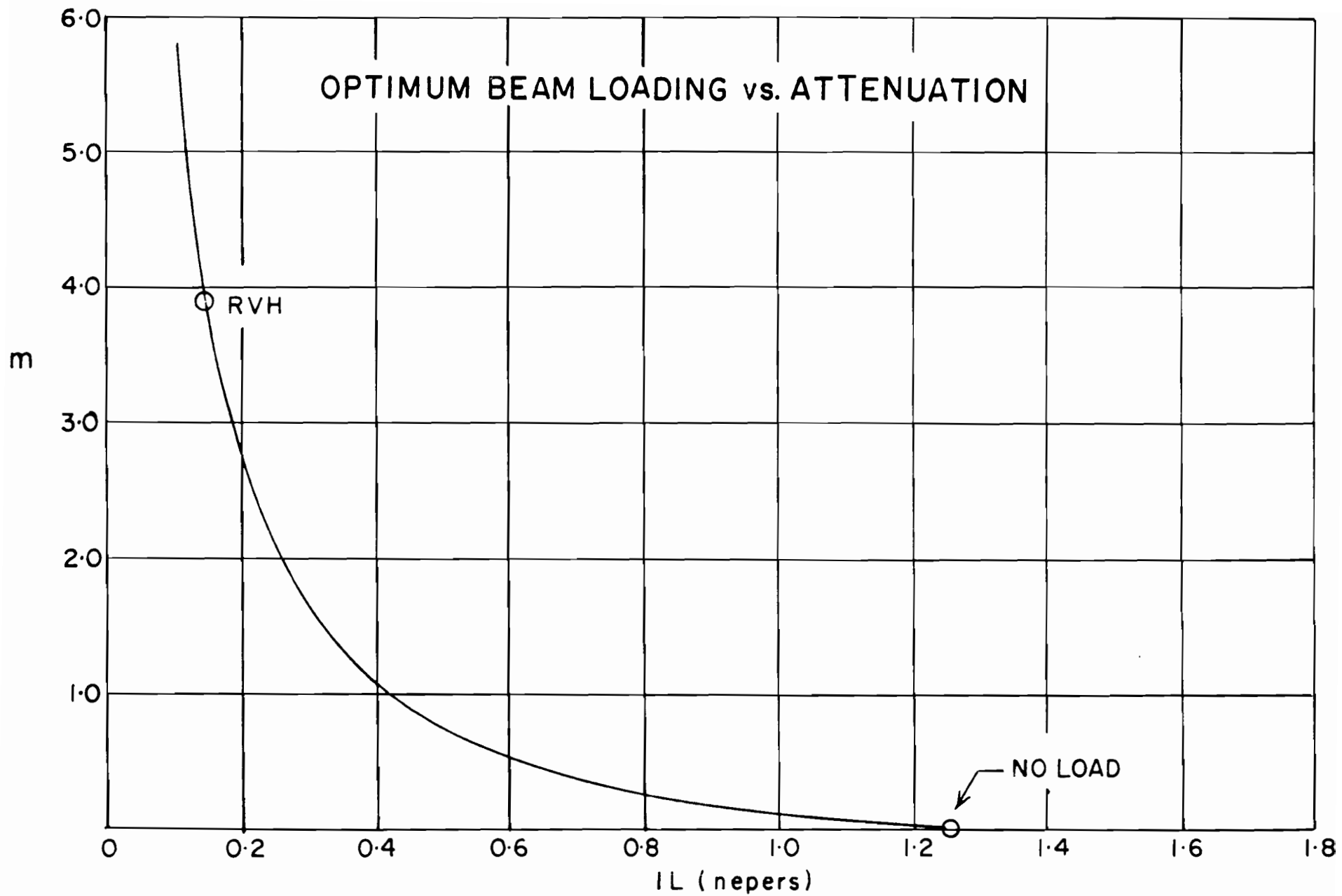


FIGURE 3

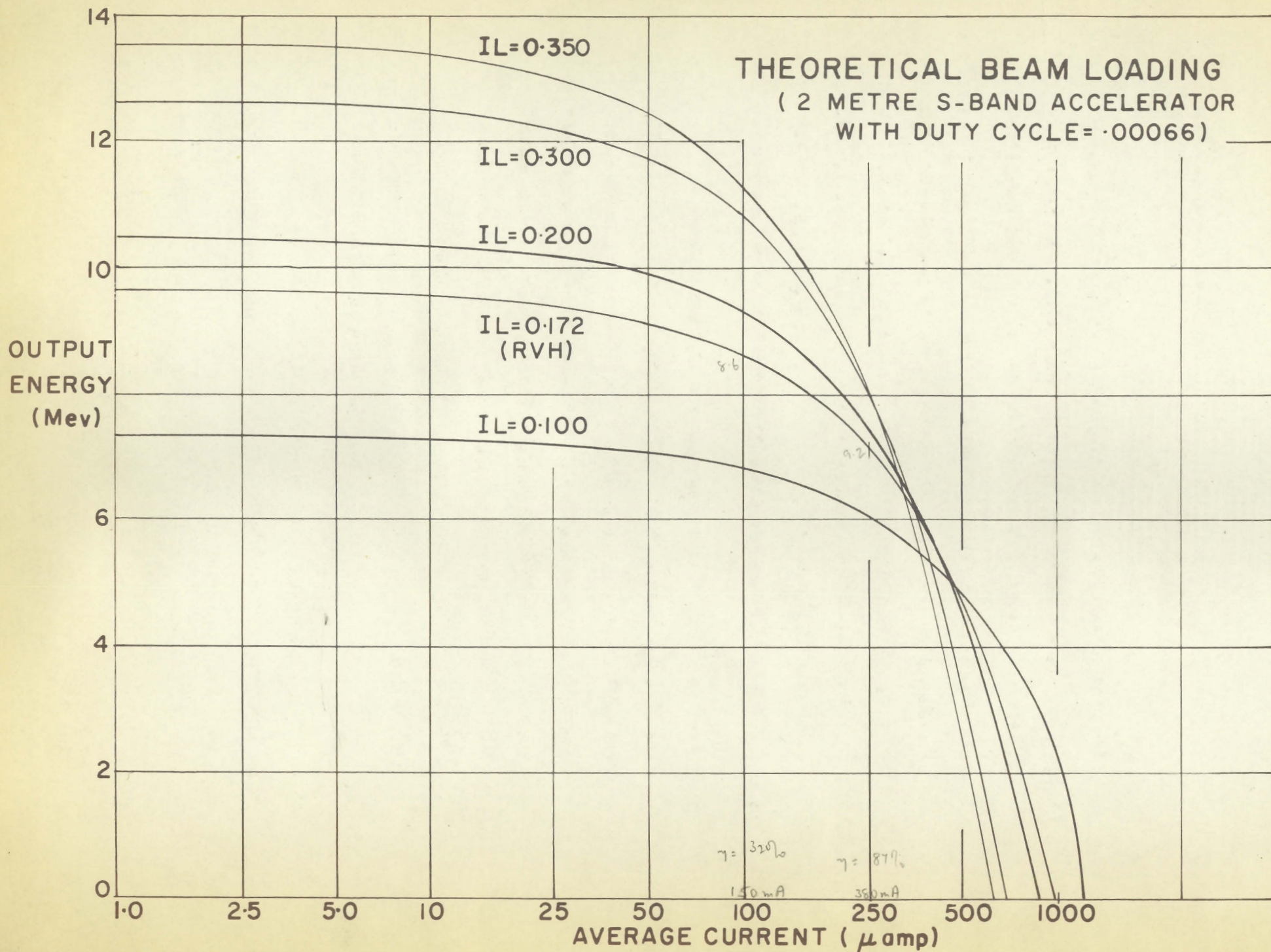


FIGURE 4

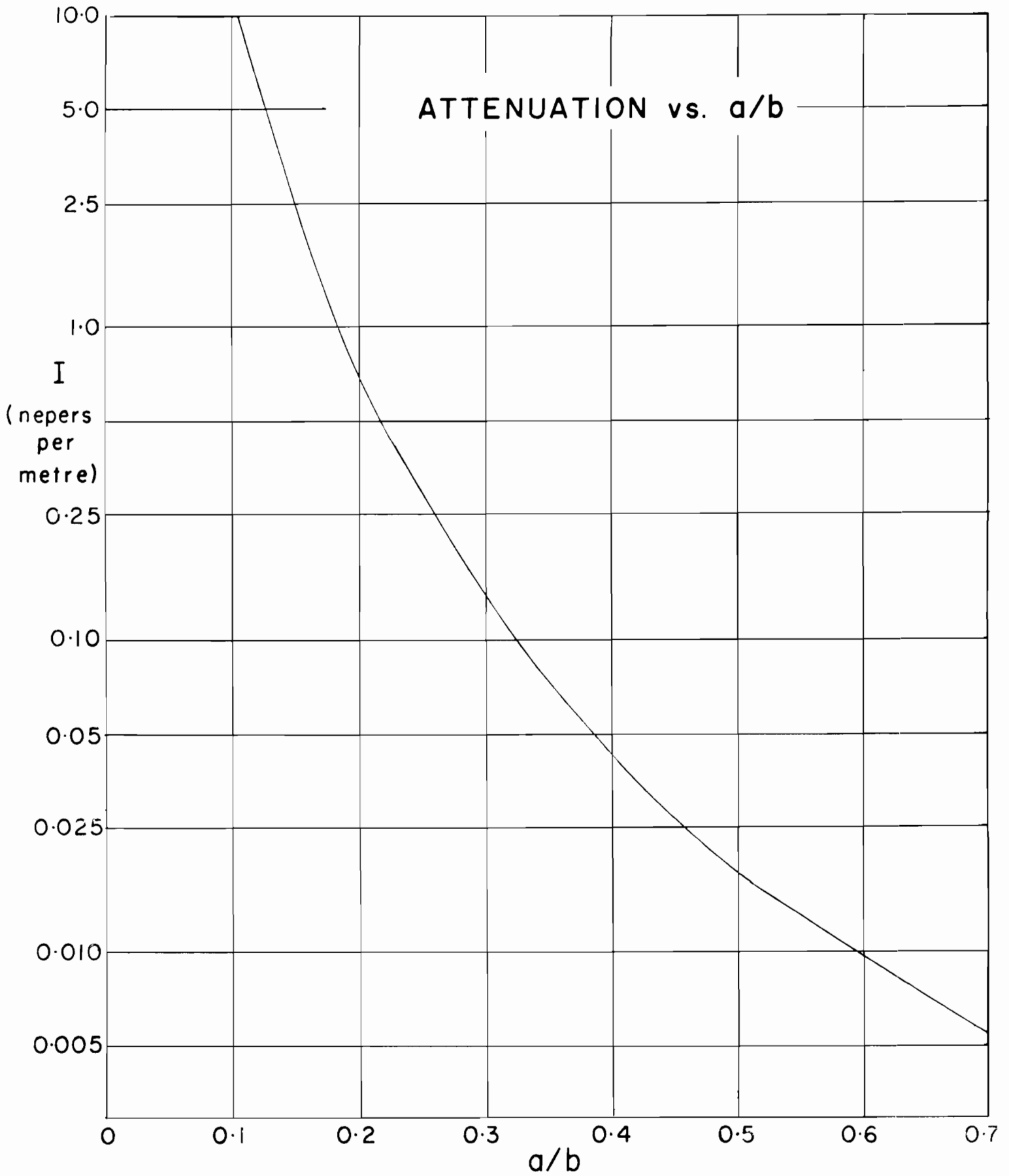


FIGURE 5

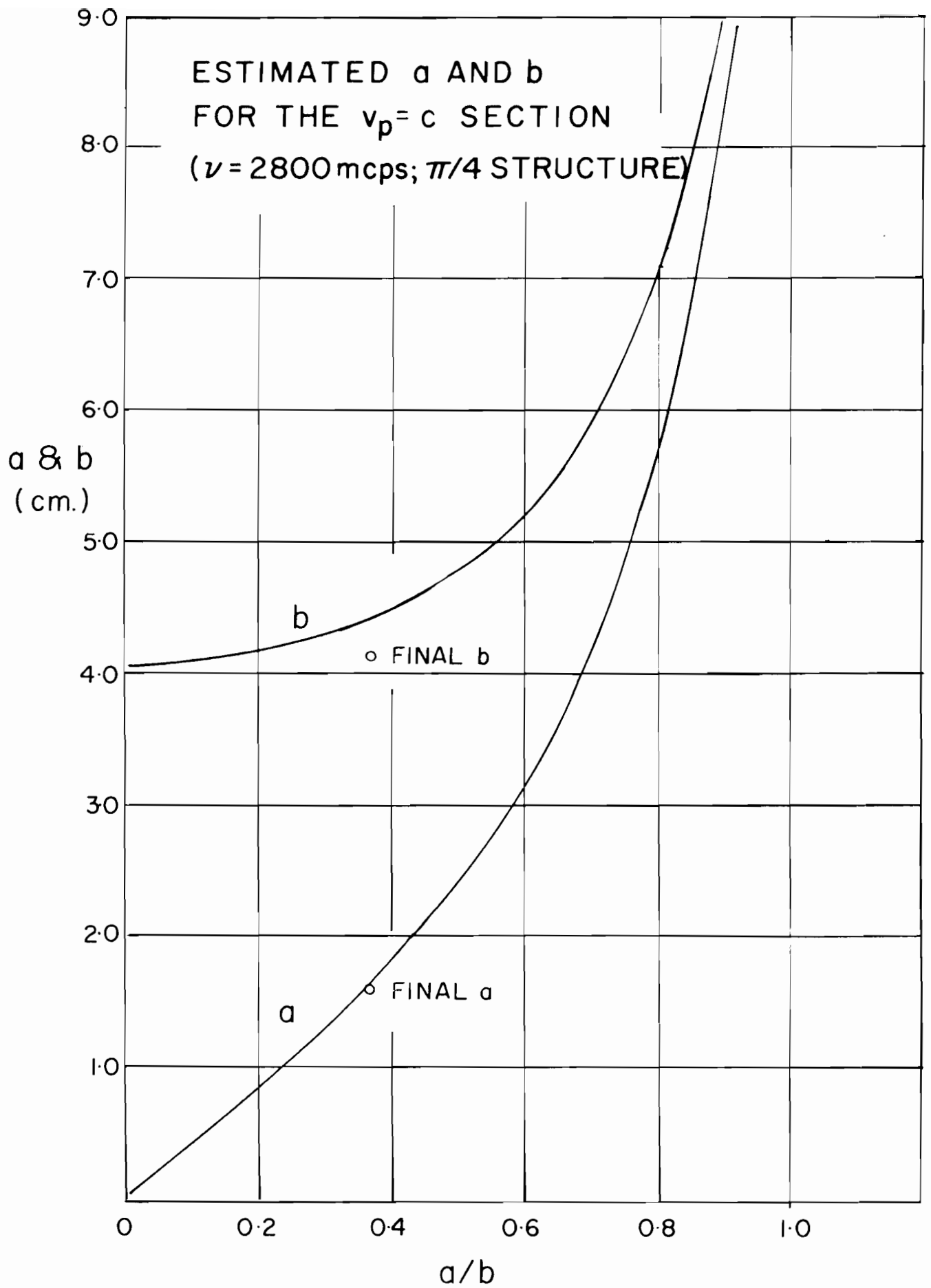


FIGURE 6

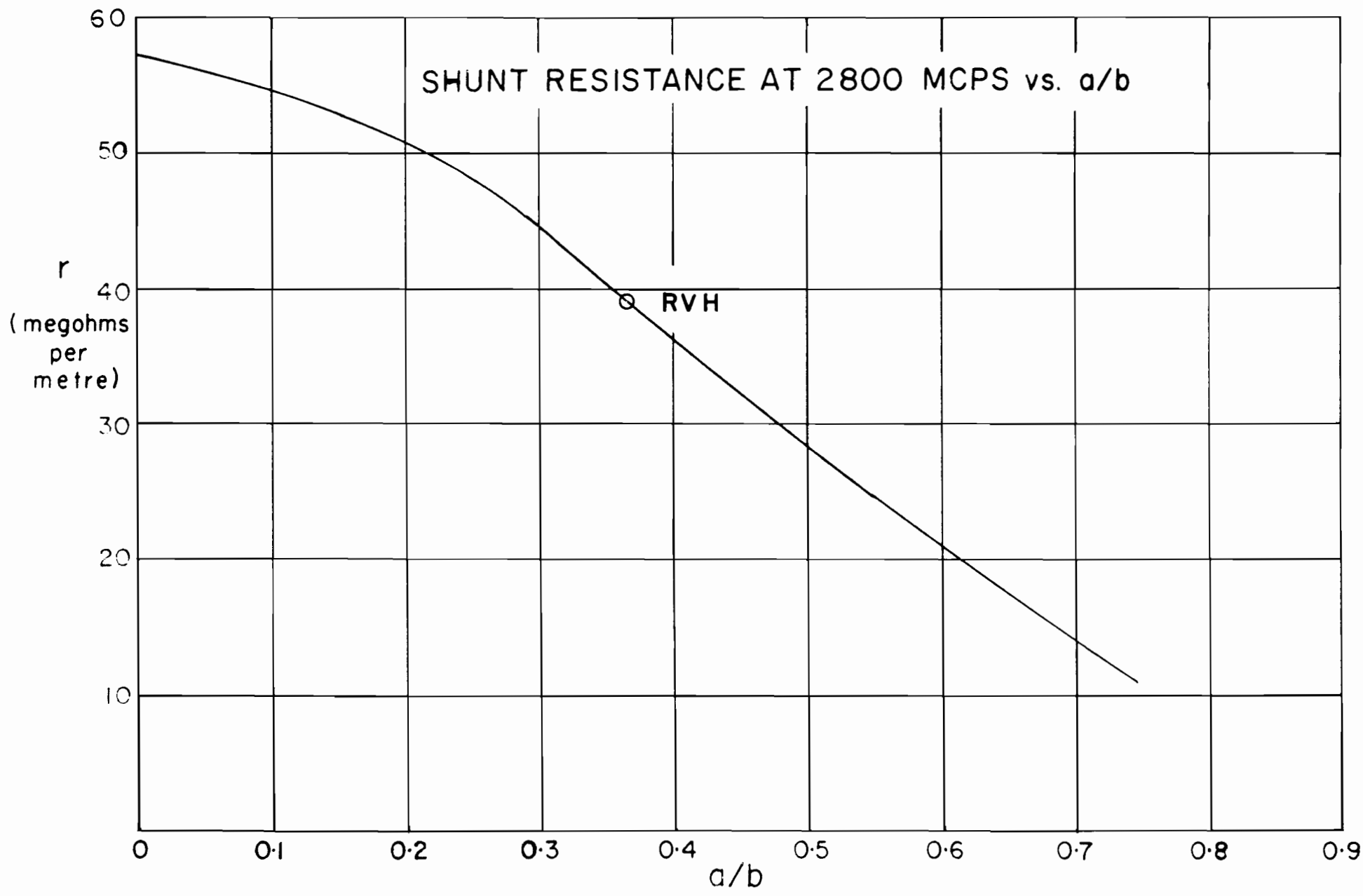


FIGURE 7

For the first cavity, then, it was decided to machine 2a to 1.185", and 2b to 3.233" .

It is of interest to compute v_g/c , a quantity of importance in the discussion of accelerator tolerances. This may be done if Q , in equation 1.7, is known. Q is difficult to measure with high accuracy but theoretical values have been calculated¹⁰⁾ . For the value of 'a' chosen $Q_{\text{Theor.}} \doteq 1.13 \times 10^4$, although imperfect electrical contacts are likely to lower this value. If $Q = 10^4$, the group velocity will be $v_g = .034 c$. The filling time for a two metre accelerator will then be $t_F \doteq 0.2 \mu\text{sec}$.

These tentative design values are listed for reference in Table 2 .

Table 2

Tentative Specifications for R.V.H. Accelerator

L (excluding buncher)	2 metres
I (voltage attenuation)	.086 nepers/metre =.75 db/metre
2a	1.185"
2b	3.233"
ν	2800 m.c.p.s.
λ	10.706 cm.
d	1.055"
$\eta d =$ disc thickness	.233"
r	4×10^7 ohm/metre
P_0	4 megawatts (peak) 2.64 kw. (average)

1.4 Machining Tolerances

If the accelerator is perfectly designed and constructed, a wave of phase velocity $v_p = c$ will propagate through all cavities for the design frequency ν_0 . If the frequency changes, the guide wavelength will change accordingly; a variation in cavity dimensions from the design value will have a similar result.

Some simple calculations indicate the extreme sensitivity of

the accelerator to frequency changes or dimensional errors.

Starting with the definition of v_g :

$$v_g = \frac{d\omega}{d\beta} \quad (\text{where } \beta = \frac{2\pi}{\lambda_g}) \quad (1.17)$$

we have

$$v_g = \frac{d(2\pi \nu_0)}{d\left(\frac{2\pi}{\lambda_g}\right)} = \frac{d\left(\frac{2\pi c}{\lambda_g}\right)}{d\left(\frac{2\pi}{\lambda_g}\right)} \quad (1.18)$$

$$\text{Therefore } \frac{v_g}{c} = \frac{d\left(\frac{1}{\lambda_0}\right)}{d\left(\frac{1}{\lambda_g}\right)} = \left(\frac{\lambda_g}{\lambda_0}\right)^2 \frac{d\lambda_0}{d\lambda_g} = \beta_w^2 \frac{d\lambda_0}{d\lambda_g} \quad (1.19)$$

$$\text{where } \beta_w = \frac{v_p}{c} = \frac{\lambda_g}{\lambda_0} \quad (1.20)$$

From 1.19 and 1.20

$$\frac{\Delta \lambda_g}{\lambda_g} = \frac{c}{v_g} \beta_w \frac{\Delta \lambda_0}{\lambda_0} = -\frac{c}{v_g} \beta_w \frac{\Delta \nu_0}{\nu_0} \quad (1.21)$$

Thus the fractional change in λ_g for the accelerator is $\frac{c}{v_g}$ times as large as the fractional change in resonant wavelength.

A change in guide wavelength will, in general, have a serious effect on acceleration; electrons, riding initially on the wave crest will slip away from the region of maximum electric field. Since the

electrical length of an accelerator cavity is $\frac{2\pi d}{\lambda_g}$ radians, the phase shift due to errors in frequency or construction will be

$$\Delta \phi = \Delta \left(\frac{2\pi d}{\lambda_g} \right) = - \frac{2\pi d}{\lambda_g^2} \Delta \lambda_g \quad \text{if } d \text{ is constant} \quad (1.22)$$

If the accelerator operates in the " π " mode with $d = \frac{\lambda_g}{4}$, then

$$\Delta \phi = - \frac{\pi}{2} \frac{(\Delta \lambda_g)}{\lambda_g} \quad (1.23)$$

From 1.21

$$\Delta \phi = + \frac{\pi}{2} \frac{c}{v_g} \beta w \frac{(\Delta v_0)}{v_0} \quad (1.24)$$

If $2a$ is the dimension in error, the phase shift may be calculated from

$$\Delta \phi = \frac{\pi}{2} \frac{c}{v_g} \beta w \frac{\partial v_0}{\partial (2a)} \Delta (2a) \quad (1.25)$$

if the partial derivative is known. A similar method may be used to determine the phase shift due to changes in $2b$, or d . Although $\frac{\partial v_0}{\partial (2a)}$, etc. may be calculated theoretically, they may easily be determined experimentally by methods described in the next section.

The results of many such measurements on cavities having $2a$, $2b$, and d close to the design values already quoted are:

$$\begin{aligned} \frac{\partial v_0}{\partial (2a)} &= + .45 \text{ m.c.p.s./mil} \\ \frac{\partial v_0}{\partial (2b)} &= - 1.0 \text{ m.c.p.s./mil} \\ \frac{\partial v_0}{\partial d} &= - .45 \text{ m.c.p.s./mil} \end{aligned} \quad (1.26)$$

The resulting phase shifts for an error in each dimension of 1 mil are therefore

$$\begin{aligned}\Delta\phi_{2a} &= .44^\circ/\text{cavity} \\ \Delta\phi_{2b} &= .99^\circ/\text{cavity} \\ \Delta\phi_d &= .44^\circ/\text{cavity}\end{aligned}\tag{1.27}$$

For the complete 72 cavity accelerator the phase shift would be 32° for a 1 mil error in 2a or d, and 71° for the 2b dimension. If a design dimension were to vary in a random way along the accelerator, one would expect very little energy loss. Likewise, a constant "mistake" of 1 mil on one dimension in each cavity would not be serious because resonant operation could still be obtained by a slight shift in operating frequency. The type of error to guard against is a systematic shift of values during machining which would allow a taper in a dimension along the accelerator. If 2b tapers regularly by only 1 mil from the input to the output end of the structure, the integrated energy will be only ~75% of the design value.

It was decided to attempt to hold all dimensions - particularly 2b - to within .001" for the whole constant velocity section. With the exception of a few cavities, this was achieved.

II R.F. Testing of the Constant Velocity Structure

2.1 R.F. Tests for v_p , v_g and Q

General studies by Brillouin^{11,12)} on wave propagation in periodic structures and application of the theory by J. C. Slater¹³⁾ to accelerators show that a loaded wave guide behaves like a band pass filter. In such a structure, a plot of frequency against guide wave number has the shape of fig. 8: ν_0 is seen to be a periodic function of the reciprocal of guide wavelength within the pass band. The points shown indicate the infinite set of Fourier components propagated corresponding to the chosen frequency ν_0 .

The slope of the radius vector OA is seen to be $\frac{(1/\lambda_0)}{1/\lambda_g} = \frac{v_p}{c}$.

The slope of BC, tangent to the curve at A, is given by $d(1/\lambda_0)/d(1/\lambda_g) =$

$\frac{v_g}{c}$ (from equation 1.18). If $\frac{1}{\lambda_g} = \frac{1}{2d}$ the group velocity is seen

to be zero; the physical explanation for this is that the incident wave is scattered at each disc so that the reflected waves interfere constructively; the combination of incident and reflected waves thus produces a standing wave in the tube with no propagation of energy along it. At $\lambda_g = 4d$ the group velocity has its maximum value.

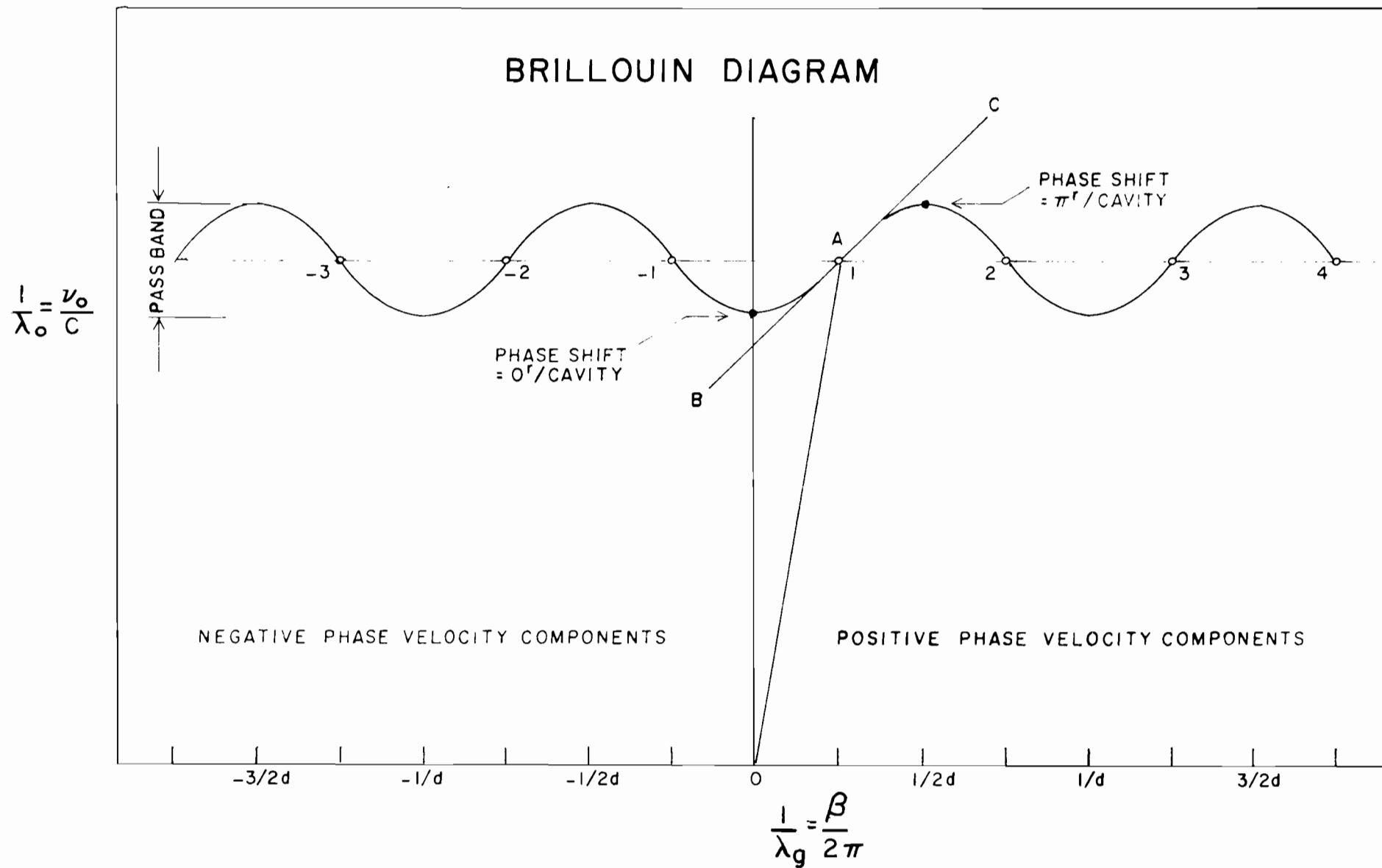


FIGURE 8

This is one reason for the popularity of the use of the $\pi/2$ mode in travelling wave accelerators - it is advantageous to fill the tube quickly with power so that the remaining time of the pulse is available for acceleration.

The apparatus for cavity measurements has been described in considerable detail by Chodorow et al⁶⁾ and is illustrated in fig. 9 . A test section of the type shown may be formed by capping n cavities with flat copper plates, clamped tightly to provide good electrical contact. Input and output loops or probes in one end plate are connected to a test oscillator and detector. There are $(n + 1)$ resonant modes in such a section corresponding to each standing wave pattern which can exist. For the 4-cavity sections used in preliminary tests, the resonances correspond with phase shifts of $0, \frac{\pi}{4}, \frac{\pi}{2}, \frac{3\pi}{4},$ and π radians. These resonant frequencies lie on the Brillouin diagram for the structure; therefore $v_p, v_g,$ and Q may be found with measurements of the five resonant frequencies. In particular, the central resonance should be the design frequency for the accelerator, since the $\pi/2$ mode is the one desired.

The test cavities with $2a = 1.185", 2b = 3.233", d = 1.055"$ and $\gamma d = .233"$ gave too high a value (by about 6% from the theory) for the $\pi/2$ mode resonance. It was necessary to machine each cavity,

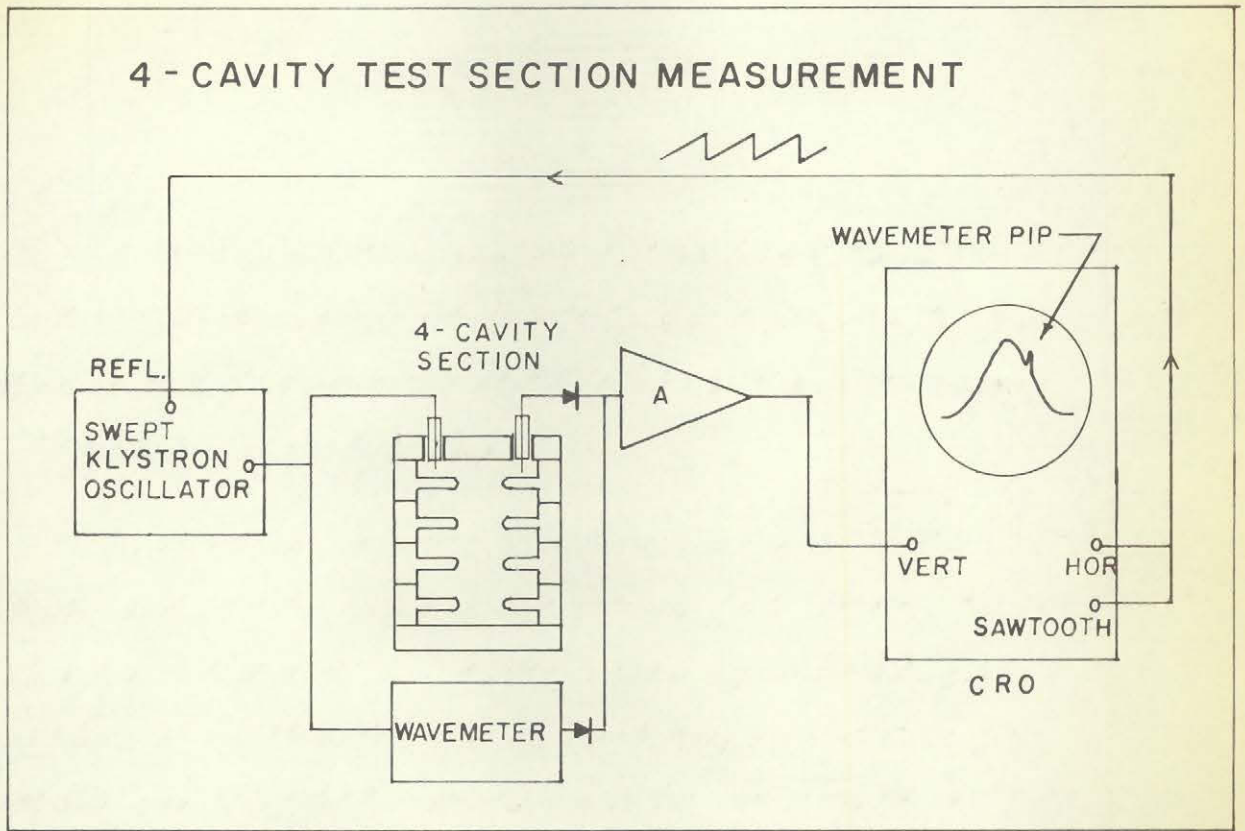
observing resonances after each change. The 2b dimension is the most "sensitive" of the accelerator parameters, and was accordingly chosen as the variable one; the amount of machining necessary changed the value of b/a , and hence the attenuation, only slightly. The results of the initial measurements and tests are shown in Table 3. The $f_1 - f_5$ values are the five resonant frequencies for the Brillouin diagram.

Table 3
Cavity Resonances

2a (in.) $\pm .0005$	2b (in.) $\pm .0005$	d (in.) $\pm .0005$	ηd (in.) $\pm .0005$	f_1 (Mcps) $\pm .3$	f_2	f_3 $(\frac{\pi}{2})$	f_4	f_5
1.185	3.233	1.055	.233	2896.9	2919.5	2969.4	3019.5	3037.5
1.185	3.233	1.055	.228	2893.2	2915.1	2964.2	3013.8	3033.7
1.185	3.247	1.055	.228	2879.4	2899.6	2948.6	2996.9	3016.4
1.185	3.300	1.055	.228	2830.4	2850.0	2897.4	2942.8	2961.1
1.185	3.365	1.055	.228	2778.3	2791.4	2836.3	2879.7	2896.5
1.185	3.405	1.055	.228	-	2758.7	2800.6	2842.8	2859.3

Q was measured in two ways. The first method involves moving the wavemeter pip on the swept frequency CRU trace to the half power points of the resonance, and measuring these frequencies. In the second method (illustrated in fig. 9), the klystron is pulsed briefly, and the energy

4 - CAVITY TEST SECTION MEASUREMENT



MEASUREMENT OF Q BY RINGING

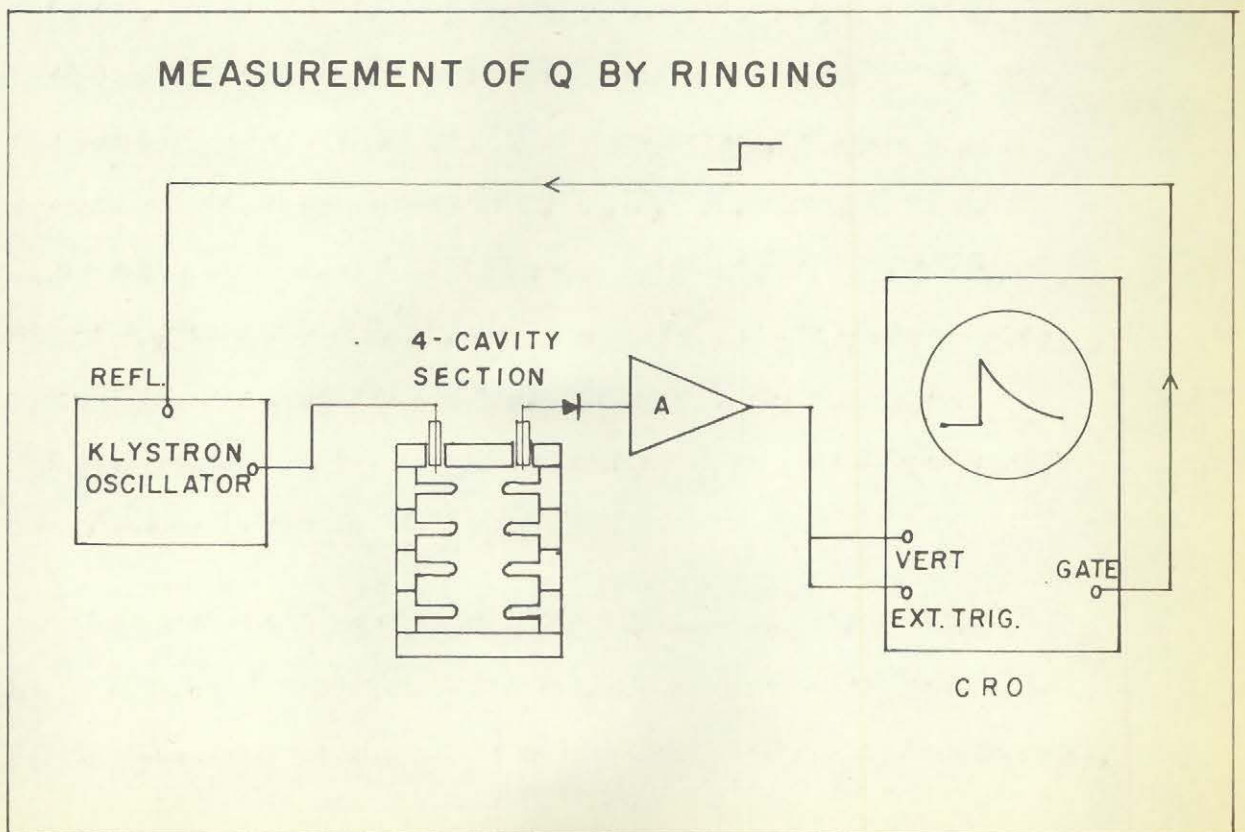


FIGURE 9

decay curve is observed on the CRO screen. In method 1, half power frequencies 270 KCPS apart give a value for Q of 10,400; in method 2, a ringing time of $\Delta t = 0.60 \mu\text{sec}$ gives a Q of $w\Delta t = 10,500$.

Unfortunately, when the first two foot section of 22 cavities was completed, the $\pi/2$ resonance was found to be at 2808.m.c.p.s. The reason for the change is obscure, but it seems likely that the loop input used in the first tests disturbed the resonant frequencies. The 24 cavity section was corrected by opening out the 2b dimension to 3.415" . A great many measurements were made on the corrected section; the mean value of central resonant frequency was 2800.6 m.c.p.s., with maximum deviations of +1.5, and -1.0 m.c.p.s. for various 4 cavity combinations used as test sections.

Fig. 10 shows the Brillouin diagram obtained when the resonant frequencies of the corrected 24 section stack are plotted. The curve gives a value of $\frac{v_g}{c} = .038$ for the $\frac{\pi}{2}$ mode corresponding to an accelerator attenuation (equation 1.7) of .078 nepers per metre.

2.2 Determination of Shunt Resistance r

The definition of cavity impedance R_c ^{14,15,16,17)} differs somewhat from the travelling wave shunt impedance defined in equation 1.9 . Hansen and Post¹⁴⁾ describe the measurement of cavity impedance;

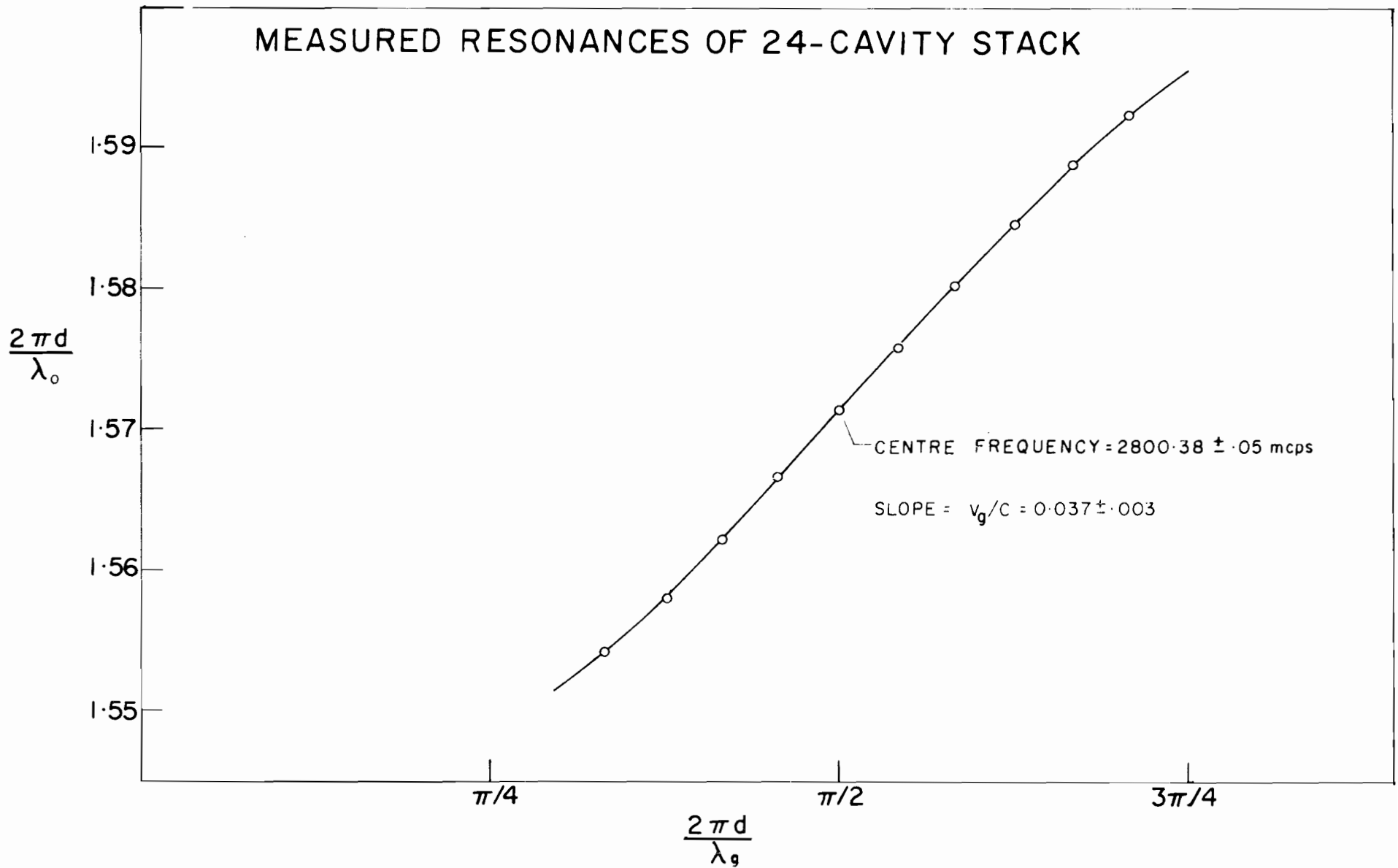


FIGURE 10

however there is a mistake in their final formula. The theory is repeated here in M.K.S. units.

The shunt resistance of a cavity is defined as

$$R_c = \frac{(\int E \cdot ds)^2}{P_1} \quad (2.1)$$

where

R_c = shunt resistance in ohms

ds - element of path along which the resistance is measured
(the axis, in this case.)

P_1 = power loss in watts

E = field along ds (volts/metre)

From equation 1.4

$$P_1 = \frac{\omega_0}{Q} W_c S \quad (2.2)$$

where W_c is the energy stored in unit length of the cavity.

Then

$$\frac{R_c}{Q} = \frac{\left[\int E \cdot ds \right]^2}{\omega_0 W_c S} \quad (2.3)$$

If a conducting "button" of arbitrary shape is introduced into the cavity to perturb the field, and hence the resonant wavelength, one can show ¹⁴⁾ that the fractional change is

$$\frac{\Delta \lambda}{\lambda} = \frac{1}{2} \frac{\int (\epsilon_0 E^2 - \mu_0 H^2) d\tau}{W_c \cdot S} \quad (2.4)$$

where E is here the unperturbed field at the button, and $\Delta\tau$ is its volume.

Using the known properties of a field of axial symmetry bounded by a plane surface, Hansen and Post¹⁴⁾ give the following approximation to the integral in 2.4 :

$$\int_{\Delta\tau} (\epsilon E^2 - \mu H^2) d\tau \doteq \pi r^2 d \left[1 - r^2 \left(\frac{3}{8} k^2 - \frac{1}{4} k_3^2 \right) \right] \epsilon_0 E^2 \quad (2.5)$$

where

$$k = \frac{2\pi}{\lambda} \quad k_3 = \frac{2\pi}{\lambda_g} = k \text{ in this case}$$

r = radius of metal plug

d = depth of plug .

Combining 2.3, 2.4, and 2.5 :

$$\frac{R_c}{Q} = \frac{s}{\pi c \epsilon_0} \frac{1}{1 - r^2 \left(\frac{3}{8} k^2 - \frac{1}{4} k_3^2 \right)} \frac{(\Delta\lambda)}{\Delta\tau} \left[\frac{\int E \cdot ds}{E \cdot s} \right]^2 \quad (2.6)$$

The factor $\left[\frac{\int E \cdot ds}{E \cdot s} \right]^2$ remains to be determined. This is most

conveniently done by moving a dielectric bead along the cavity, and observing the frequency shift. Formula 2.4 again applies, but ϵ and μ must be multiplied by "shape factors" depending on the material and shape of the bead.

Several bead and plug measurements were made. An example of the type of curve one obtains with a lucite bead is shown in fig. 11. It is

DETERMINATION OF r' BY FREQUENCY PERTURBATION

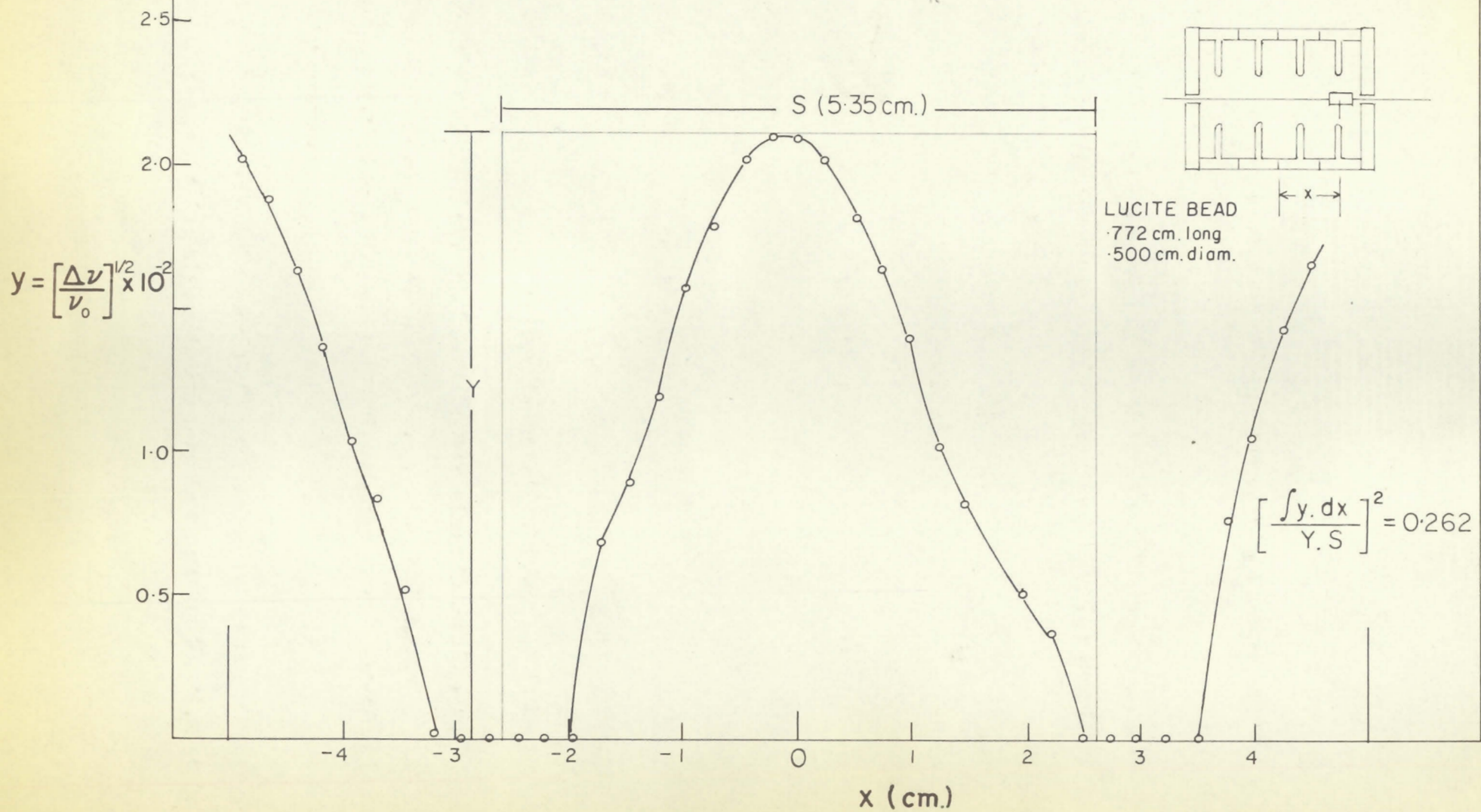


FIGURE II

doubtful that either frequency shift measurement will give a result to better than 5% accuracy. For a 2 cavity section

$$\frac{\Delta \lambda}{\Delta \tau} \doteq 600 \text{ m}^{-2} \text{ and } \left[\frac{\int E \cdot ds}{E \cdot s} \right]^2 = .277$$

giving a value of $\frac{R_c}{Q}$ of ~ 30.8 ohms/cavity.

The link between cavity impedance and travelling wave impedance may be derived from the definition

$$r = \frac{E_p^2}{\frac{dP}{ds}}, \quad (1.9)$$

Since r and E_p are constants for a particular cavity geometry, then

$$r = \frac{E_p^2 S}{P}, \text{ and } R_{TW} = \frac{[E_p \cdot S]^2}{P} \quad (2.7)$$

where P is the power lost in length S . For travelling waves

$$P = \frac{\omega_0 W_{TW}}{Q}$$

Here W_{TW} denotes energy stored per unit length of the travelling wave; this is the same as the W of equation 1.4.

Since

$$W_{TW} = 2W_c \quad P = 2P_1$$

Also

$$E_p = \sqrt{2} E_{RMS}$$

Therefore

$$R_{TW} = \frac{[E_{RMS} \cdot S]^2}{P_o}$$

So

$$R_{TW} = \left[\frac{E_f \text{ RMS} \cdot S}{\int E_f \text{ RMS} \cdot ds} \right] R_c \quad (2.8)$$

The symbol $E_f \text{ RMS}$ refers to the electric field of the Fourier component responsible for electron acceleration - i.e. the fundamental component. A Fourier analysis must therefore be carried out on the curves of fig. 11 in order to find the bracketed term of equation 2.8 .

The curve for the smaller bead gave a factor of 3.3, and for the larger, 3.5. Taking $R_c = 3.03 \times 10^5$ ohms $S = 2.68$ cm (for one cavity) we obtain

$$r = \frac{R_{TW}}{S} = 3.9 \times 10^7 \text{ ohms/metre,}$$

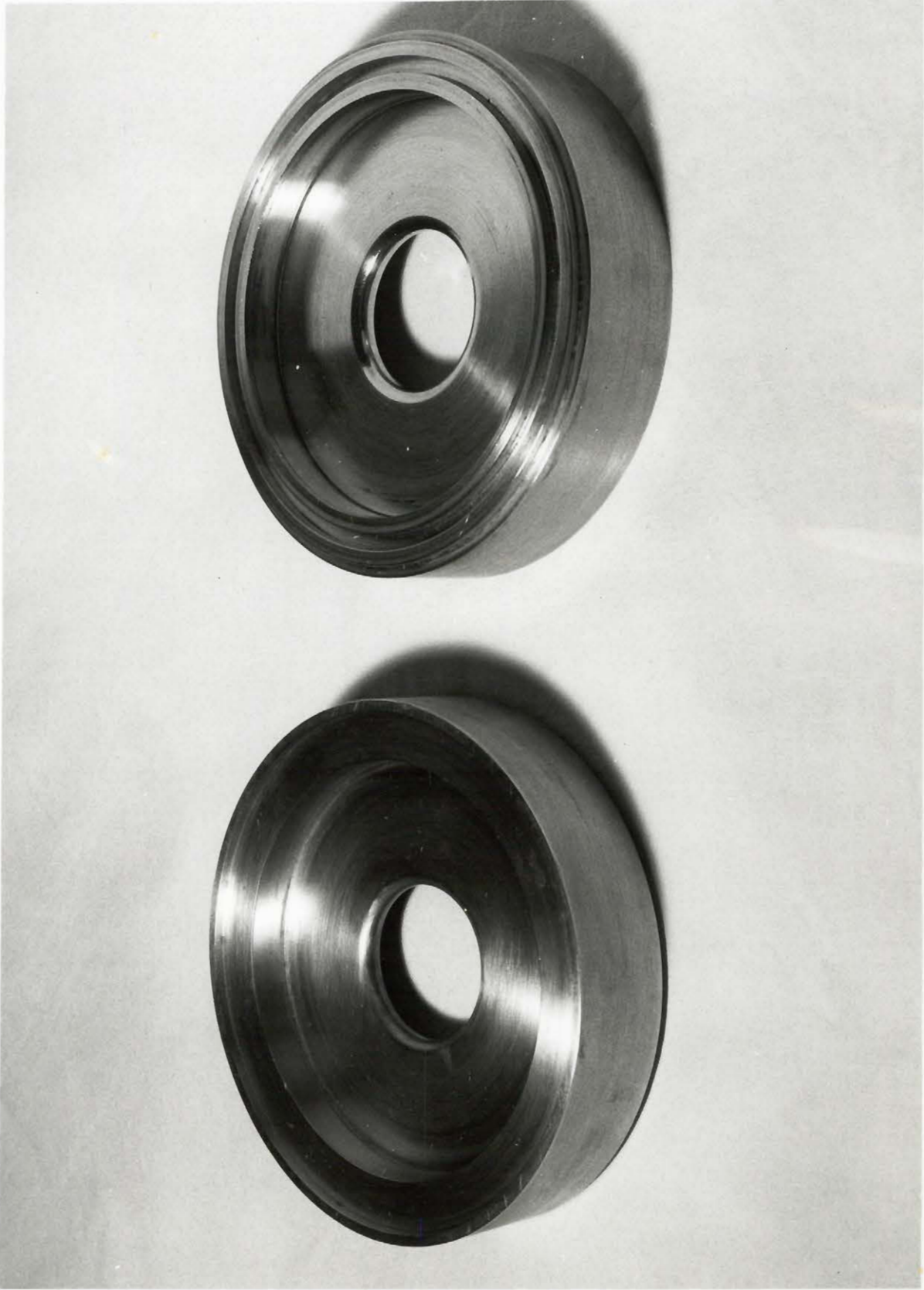
which checks well with the design value of 4×10^7 ohms per metre.

The test cavities were therefore considered suitable for the final design, and were machined to the shape of fig. 12. The .002" step on the face proved necessary to ensure proper contact, and the O-ring groove was included to provide the vacuum seal between cavities.

Figure 12

Accelerator cavities.

This upper and lower view shows finished accelerator cavities with the O-ring, and locating grooves. Since the electrical contact is made by pressure alone, a .002" step is provided on one cavity face. This is visible on the inner rim of the right hand cavity.



The first section of 24 cavities had central resonances close to the design frequency of 2800 m.c.p.s. The third and fourth sections, however resonated at ~2796 m.c.p.s. This difference has not been explained. It was first thought that small systematic errors in cavity dimensions were responsible, but careful measurement indicated that the slight differences present should have caused a higher resonant frequency (of about 2801 m.c.p.s.). The copper stock used for the odd sections was from a different batch than the previous one, but for conductivities giving $Q \sim 10,000$ there should be measurable dimensional differences in the two sets. Exactly the same difficulty was experienced with the Mark III Stanford accelerator⁶⁾; the reason proposed was variation in hardness among the batches. Since the Mark III accelerator was constructed by shrinking discs into a cylinder, this could conceivably cause dimensional changes sufficient to account for the deviations. With our structure it is difficult to see how this could be the case; the resonance at 2796 m.c.p.s. remained unchanged with different tensions in the tie rods for the section.

It was decided that the safest way to correct the error was to electroplate copper to change the 2b dimension from 3.415" to 3.411". It is difficult to do this in an ordinary plating bath, since most of the surface must be masked.

A brush plating technique was eventually used, and all cavities in the section were corrected.

2.3 Impedance Measurements

The accelerator waveguide should be perfectly matched at the output end to a resistive load so that no reflected wave will reach the magnetron. A constant flow water load with vacuum seals was made for the R.V.H. accelerator; a thermocouple with junctions in the water input and output lines provides a direct reading of microwave power output. The dummy load coupler must, then, match the TM_{01} mode of the corrugated cylinder to the dominant (TE_{10}) mode of the rectangular guide enclosing the load.

The impedance measurements necessary for the trial-and-error procedure of matching involve the use of a shorting plunger, and a resistive plunger (fig. 13). Measurements must be made for VSWR in the rectangular guide as the shorting and resistive plungers are moved along the accelerator cavities. The short circuit measurements give a direct indication of phase shift throughout the accelerator and may be used to locate errors in individual cavities; the resistive plunger measurements indicate the VSWR of the trial match between the two guides.

IMPEDANCE & PHASE SHIFT MEASUREMENTS

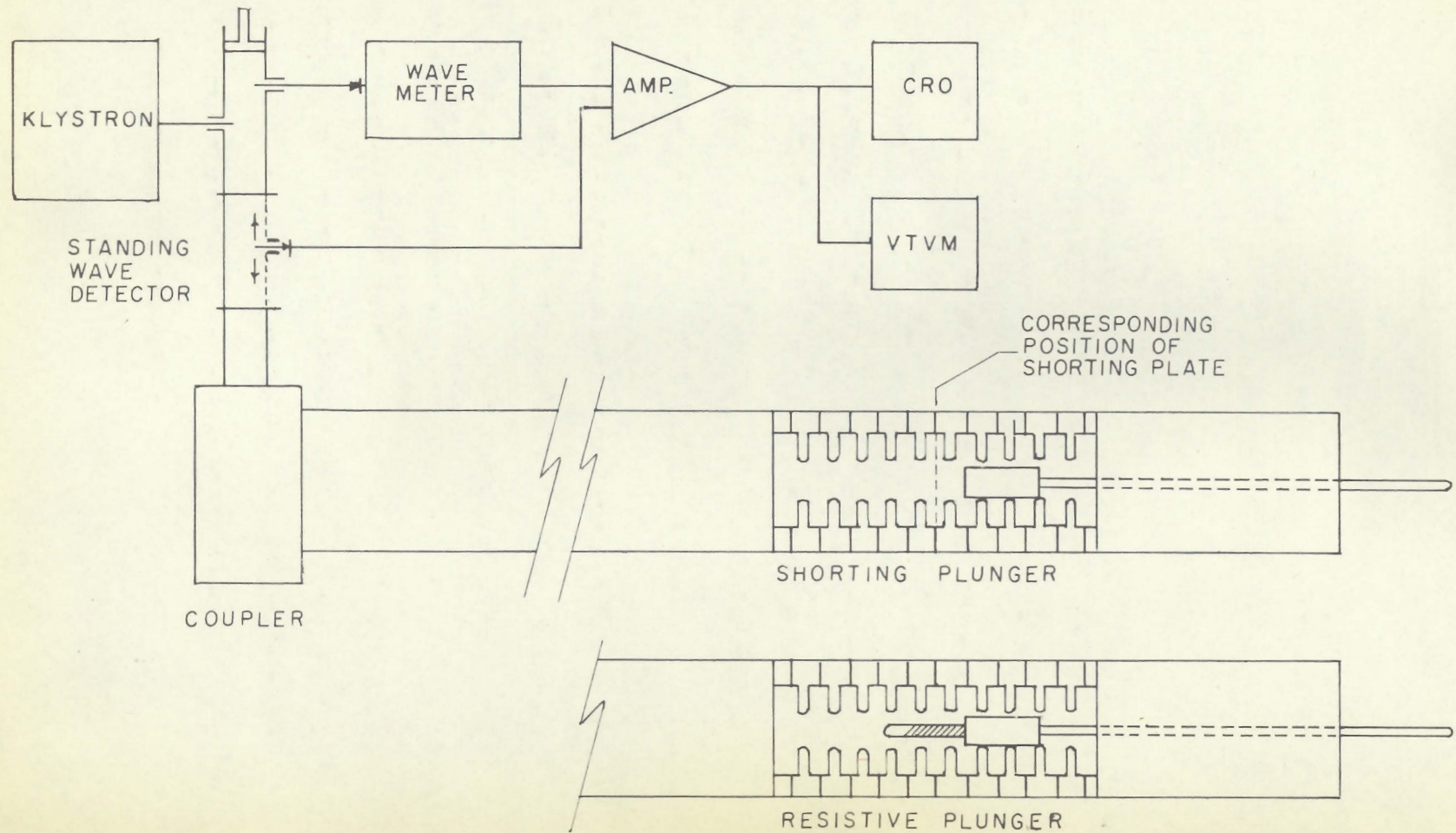


FIGURE 13

For the $\frac{\pi}{2}$ mode the insertion of the shorting plunger into a cavity will cause a minimum of axial field to exist at that point. If a copper cap is placed across the mid-plane of a cavity, a maximum axial field will occur at the plate (as in the 4 cavity test sections) The shorting plunger, then, N cavities from the accelerator input will reflect power in the same way as a plane conductor at the mid-plane of cavity N-1 . A high standing wave ratio will be observed at the input as the plunger is moved along the accelerator axis, and the locus of impedance will be a spiral on a Smith chart. In cavities with loose coupling (as in the constant velocity section of the accelerator) the shorting plunger has no detuning effect on the preceding cavity. The input impedance measurement exhibits so-called "dwell points" - for about 2 cm. of plunger movement in a cavity the input impedance remains constant, shifting quickly around to the opposite side of the Smith chart as the end of the plunger passes a disc. A check on the accuracy of the short circuit measurements is, of course, possible since this design permits the actual capping of cavities.

The shorting plunger may be changed to a resistive one by inserting a length of resistance card or strip in the reflecting end so that it projects into cavities on the input side. In the ideal case the strip may be tailored in such a way that the dwell

points (corresponding with those of the short circuit measurement) coincide, and indicate the input impedance directly. This is difficult to do, but if the impedance locus on the chart is a reasonably localized ellipse the centroid will be close to the actual match point. All loads made in the course of this work consisted of $3" \times \frac{1}{8}"$ strips cut from a 300 ohm/square resistance card. It was found that a reasonable impedance locus could be obtained if some of the conducting material was scraped away from about 1" of the end of the strip.

Figs. 14 and 15 show the final design of the buncher (input) and dummy load (output) couplers. The shape of the buncher coupler cavity differs from the output one, and bears some resemblance to the "doorknob" transformers of early British accelerators¹⁸⁾. Originally both couplers had ordinary cylindrical cavities - the revised shape for the buncher coupler was chosen when later measurements showed considerable beam spreading close to the accelerator input. It was thought that fringing fields at the input hole caused the spreading; with the doorknob the injected electrons are well into the magnetic field of the focusing coils before they experience any R.F. forces.

The coupler cavities must be resonant at the chosen design frequency; in addition, an inductive impedance must be provided

at the transition to match the rectangular to the cylindrical guide. The "windows" shown in the rectangular guides of fig. 14 and 15 provide this inductance.

The matching procedure is as follows: the first trial coupler is capped and connected to the circuit of fig. 13. The position of a minimum on the standing wave detector then gives a reference phase for the impedance measurements. A length of accelerator is then connected to the coupler, and the measurements of VSWR and minimum position are made while the resistive load is moved through two cavities at the output. The impedance "ellipse" is plotted on the Smith chart, its centroid giving an approximate matched impedance. The position of the ellipse indicates whether the cavity has too low or too high a resonant frequency, and if the window's dimension gives sufficient inductance. The window may be filed to reduce the inductance, and a small removable shaped plug at the axis of the coupler may be machined to adjust the resonant frequency. Another test is made to determine the impedance, and the parameters are adjusted until the impedance ellipse surrounds the centre of the Smith chart. The first completely soldered dummy load coupler had a VSWR (measured with the resistive load) of 1.10; the first buncher coupler had an unusually good VSWR of 1.02. The ratio proved to be extremely sensitive to changes of even .001" in either window width or cavity size. An exhaustive discussion of accelerator faults

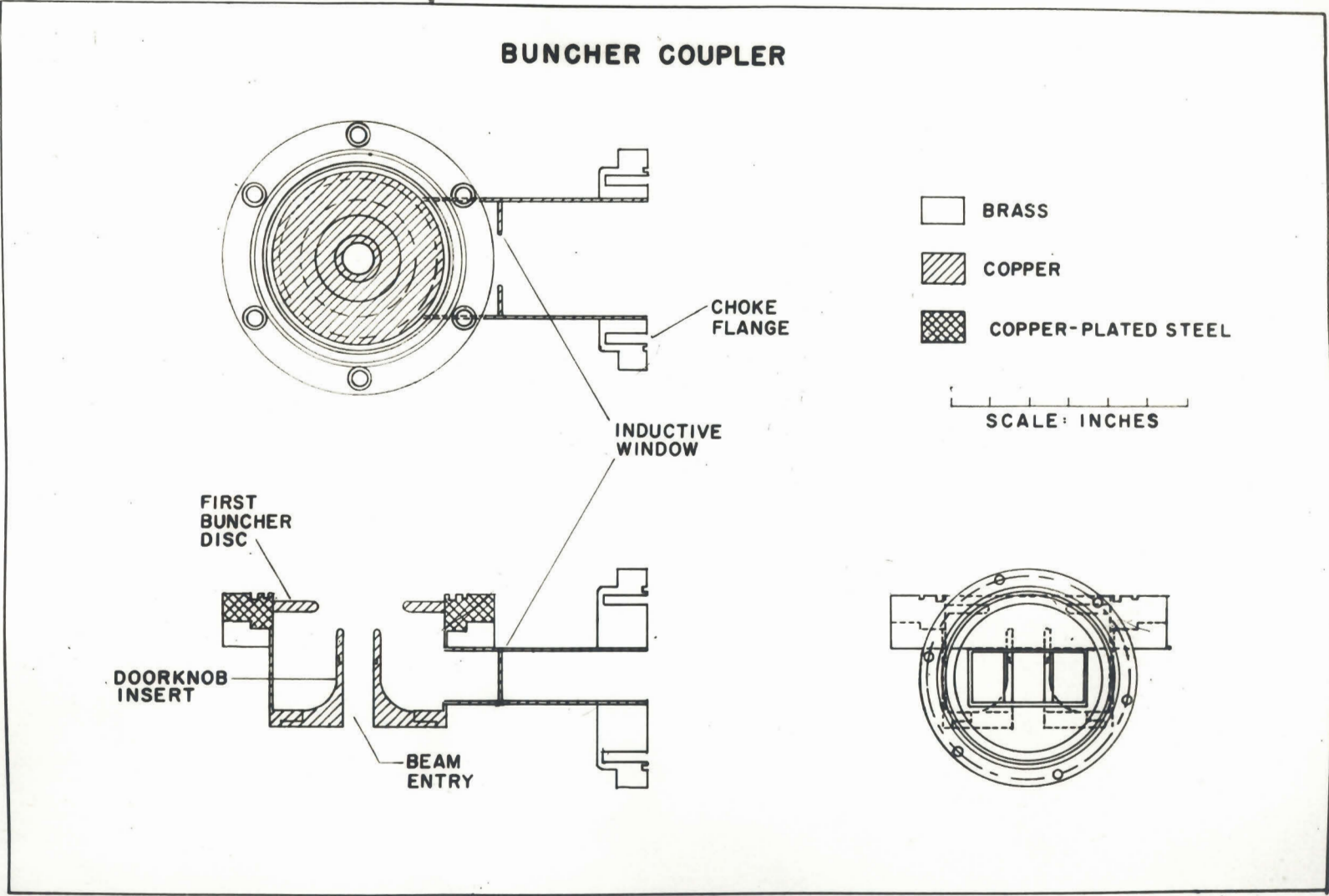


FIGURE 14

DUMMY LOAD COUPLER

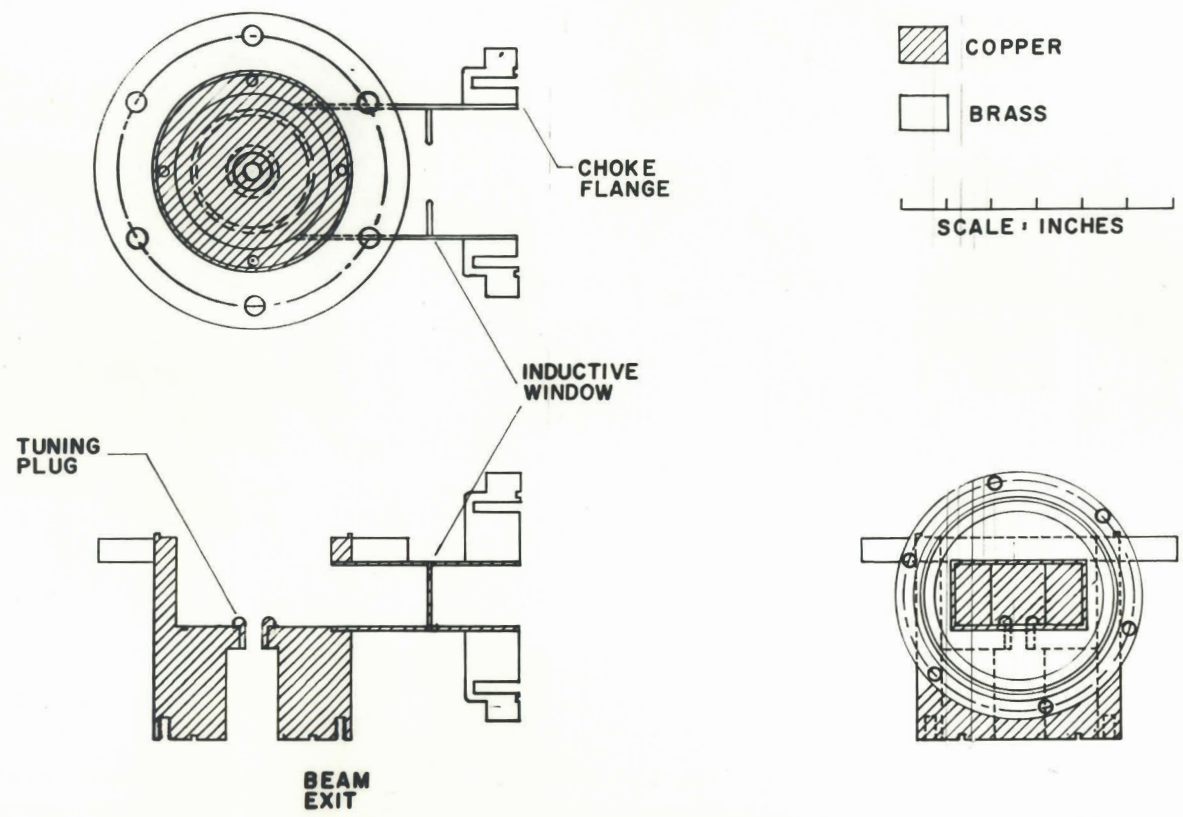


FIGURE 15

which may be revealed by this method has been given by Mallory¹⁹⁾.

With the completed couplers, it was possible to measure the attenuation of the first two-foot section. This was done in two ways. In the first, a crystal probe in the input rectangular guide was calibrated against the standing wave detector probe and placed in the output guide; the amplitudes of input and output signals then gave the power loss. In the second, the shorting plunger VSWR's were plotted on a Smith chart giving a reasonably circular figure about the centre. The mean radius then gives the reflection coefficient Γ for the system and the attenuation is found from

$$I = \frac{1}{2L} \log_e \frac{1}{|\Gamma|} \quad (2-9)$$

The value obtained from the first method was .086 nepers/metre; the second gave a value of .092 nepers/metre . These agree closely with the design value of Table 2 .

The QK 338 and QK 327 magnetrons should not operate with a load of VSWR > 1.5 . A plot of SWR against frequency for this first coupler showed that the ratio was less than 1.5 over a range of 9 m.c.p.s., centred at 2799 m.c.p.s.

III Design and Construction of Buncher Cavities

3.1 Choice of α and β for Longitudinal Orbits

If the accelerator injection energy is 80 KeV, a section must be designed which will pick up as many electrons as possible, gather them into a small phase spread, accelerate these from $v_p = .5 c$ to $v_p = c$, and place the resulting bunches close to the crest of the R.F. wave so that they may receive maximum energy in the succeeding constant velocity section²⁰. The small phase spread is necessary if it is desired to have a sharp energy spectrum at the output. One can, of course, design very long bunchers in order to obtain highly monochromatic beams. The problem with most accelerators is to optimize the bunching process so that the buncher energy output is reasonably high, and the phase spread sufficiently narrow.

If one assumes that the amplitudes of all Fourier components of the accelerating field are very much smaller than the fundamental, the equation of longitudinal motion of an electron on the axis may be written

$$\frac{d(m\dot{z})}{dt} = eE \sin \left(\omega t - \frac{2\pi z}{\lambda_g} \right) = eE \sin \omega \left(t - \frac{z}{v_p} \right) \quad (3.1)$$

where

m = mass of the moving electron

e = electronic charge
 E = axial electric field
 z = distance along accelerator axis
 Phase convention: at t = 0, the axial field is zero
 at the z = 0 position.

The momentum $m\dot{z}$ may be written

$$m\dot{z} = m_0 \dot{z} \sqrt{1 - \frac{\dot{z}^2}{c^2}} = \gamma m_0 \dot{z} \quad (3.2)$$

where m_0 is the rest mass of the electron.

It is convenient to introduce other dimensionless coordinates to simplify the equation of motion. These are

$$\xi = \frac{z}{\lambda_0} = \text{distance along accelerator in free space wavelengths}$$

$$\alpha = \frac{eE\lambda_0}{m_0 c^2} = \text{maximum energy gained by the electron on a wave of amplitude } E \text{ in units of the electronic rest mass.}$$

$$\beta_w = \frac{v_p}{c}$$

$$\beta_e = \frac{v_e}{c}, \text{ where } v_e \text{ is the electron velocity in the laboratory system.}$$

$$\tau = vt = \text{time, in number of R.F. cycles}$$

If Δ represents the phase angle of the electron with respect to a position of zero axial field (i.e. $\Delta = -90^\circ$ representing the position of maximum forward accelerating field), the equation of motion in dimensionless form is

$$\frac{d(\gamma \dot{\xi})}{d\tau} = -\alpha \sin \Delta, \text{ where } \dot{\xi} = \frac{d\xi}{d\tau}$$

Using the definitions of $\dot{\xi}$ and τ , the equations of motion become

$$\frac{d\gamma}{d\xi} = -\alpha \sin \Delta \quad (3.3), \text{ and} \quad \frac{d\Delta}{d\xi} = \frac{1}{\beta_w} - \frac{1}{\beta_e} \quad (3.4)$$

From the definition of shunt impedance r (equation 1.9), the estimated axial field of the R.V.H. constant velocity section is $\sim 5.3 \times 10^6$ volts/meter, so that at the input of this section $\alpha \doteq 1$.

Chu²¹⁾ has shown that bunching action exists if β_e , or α , or both, are made to increase monotonically in the initial portion of the accelerator. A numerical example given shows that the α constant, β variable case gives very inefficient bunching action. The β constant, α varying case gives much more efficient bunching. Although this case is treated mathematically by Chu, it is readily apparent that the problem is similar to that of a pendulum having a steadily increasing restoring force over a period of several cycles. The motion of the electron referred to axes moving with the phase velocity of the wave is oscillatory about the equilibrium position $\Delta = 0$. If the restoring force is steadily increased, the amplitude of oscillation will decrease. In addition, the relativistic increase in mass will assist the bunching process.

The most satisfactory method of bunching involves simultaneously increasing values of α and β . A low initial β implies a high final to initial electron mass which will assist bunching, and, incidentally permit more cycles of oscillation per free space wavelength. β should be increased slowly at first so that the equilibrium position

remains close to $\Delta = 0$; after the amplitude of oscillation has decreased considerably, and the field strength has increased, a higher $d\beta/d\xi$ is permissible. In the R.V.H. design the 80 kv. magnetron pulse is used for the electron gun making the choice of $\beta_w = .5$ an attractive one. The initial value of α should be low to assist bunching. It may be shown⁶⁾ that if β is initially 0.5, a value of $\alpha \geq 0.84$ is sufficient to cause some injected electrons to reverse direction, and thus be lost from the beam.

For these reasons the values of α and β for the R.V.H. accelerator were chosen to be .1 and .5 respectively at the buncher input. There is considerable freedom in choosing $\alpha = f(\xi)$ along the buncher - usually, an analytic trial function reduces numerical work. Once such a function has been chosen, the equations of motion are used to study phase orbits throughout the buncher, or for that matter, the complete accelerator. Analog computers have recently been devised^{22,23)} to handle this integration, but in the present work it was necessary to carry out the first calculations by hand. Later, when the IBM 650 computer was available the process was much simplified. In the integration suitably small steps of $\delta\xi$ are decided on along with desired input phase angle Δ ; one then uses equation 3.3 to find the value of γ at a distance $\delta\xi$ from the accelerator input, and 3.4 to find a new value for Δ at the position $\delta\xi$. The procedure is repeated until the values of Δ and γ are found as functions of ξ for the whole buncher.

The functions $\alpha(\xi)$ and $\beta(\xi)$ chosen for this accelerator are shown in Fig. 16. The "stepped" nature of α and β after cavity 10 saved a great deal of extra testing and machining which would have been necessary for smooth curves; the original trial buncher design had only 14 cavities and a succeeding phase shifting section of 5 cavities, but the increase in α and β proved too fast for proper bunching. Figures 17, 18, and 19 show buncher orbits computed at frequencies of 2800, 2798 and 2802 m.c.p.s. The effect of the phase shifting section included from cavities 14 to 20 of the second accelerator section is clearly seen in the three figures. In fig. 17, for example, electrons which have slipped to a phase angle of $\Delta \doteq -100^\circ$ are allowed to move back to $\Delta \doteq -70^\circ$. The phase slip in the next two sections is not serious with most electrons completing the orbit just at the wave crest.

Table 4 shows calculated orbit values of final (output) phase angle Δ_{out} , and total energy for electrons of various input phase angles Δ_{in} . An additional calculation for $\beta_{e(in)} = .478$ was carried out; it was thought that since the magnetron pulse provides the gun accelerating voltage, a variation in pulse voltage from 80 to 70 kv might lower the output energy.

An energy loss of 15% is noted for frequency errors of ± 1 m.c.p.s. With a 2 m.c.p.s. error the energy is only half the design

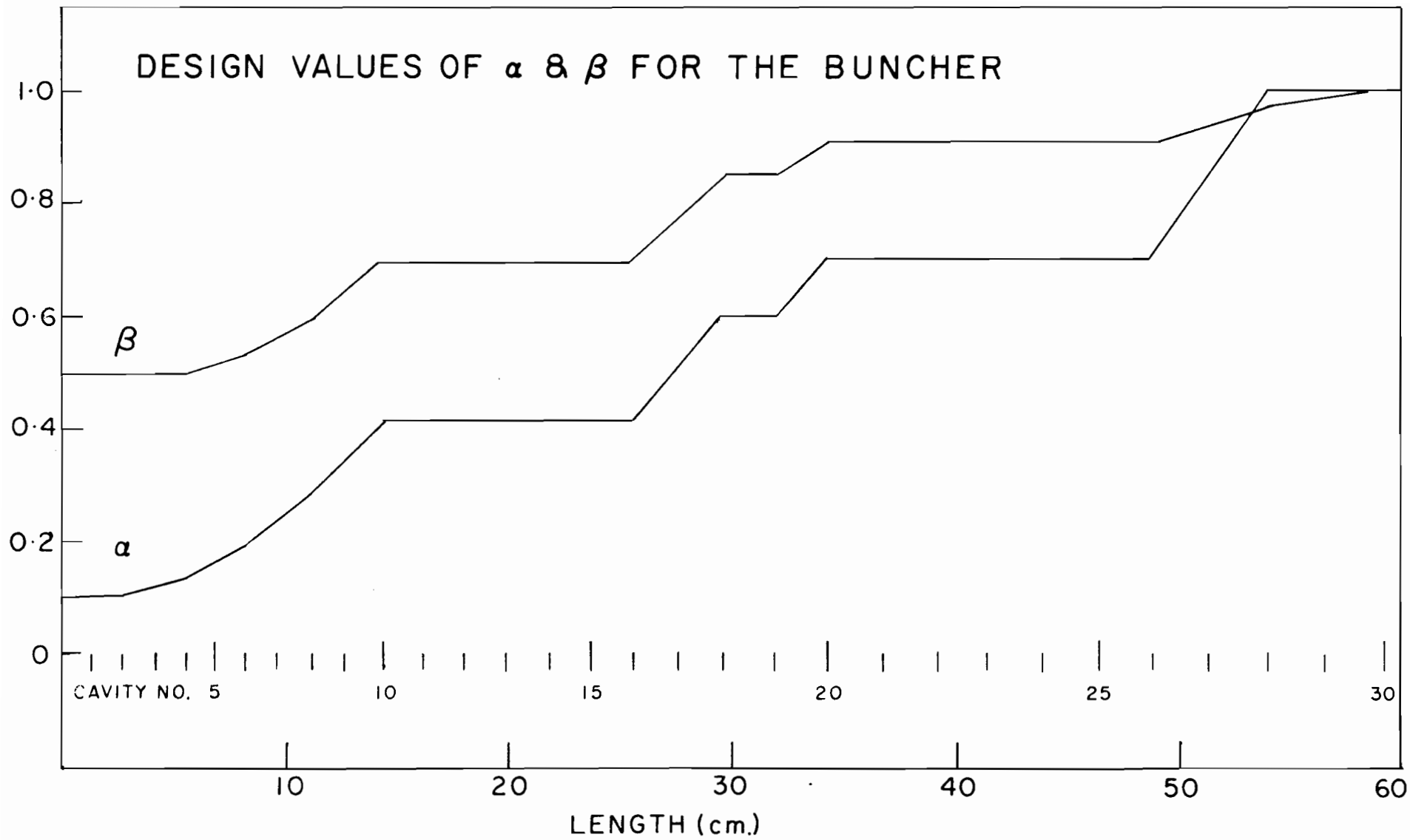


FIGURE 16

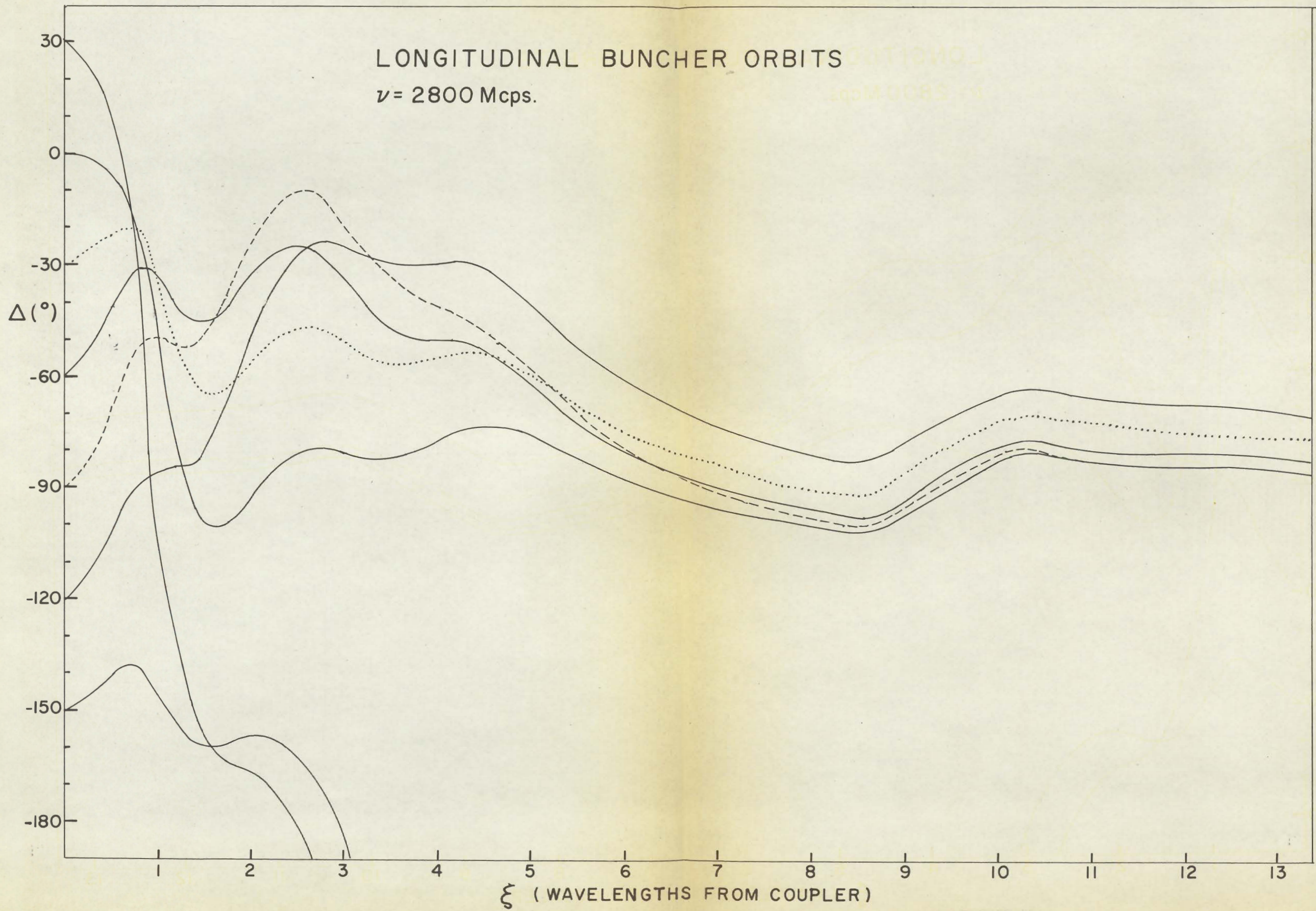


FIGURE 17

LONGITUDINAL BUNCHER ORBITS
 $\nu = 2798$ Mcps.

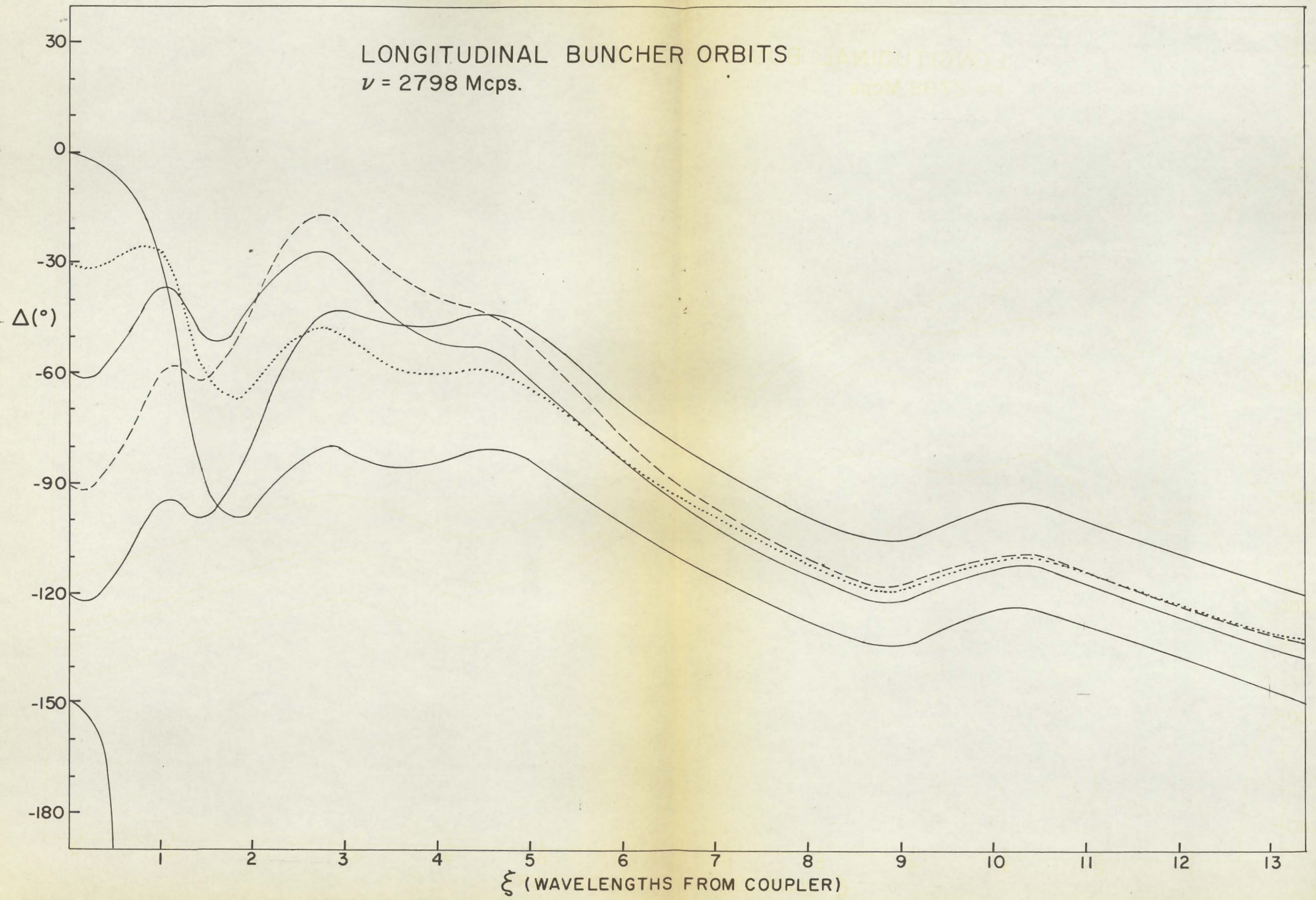


FIGURE 18

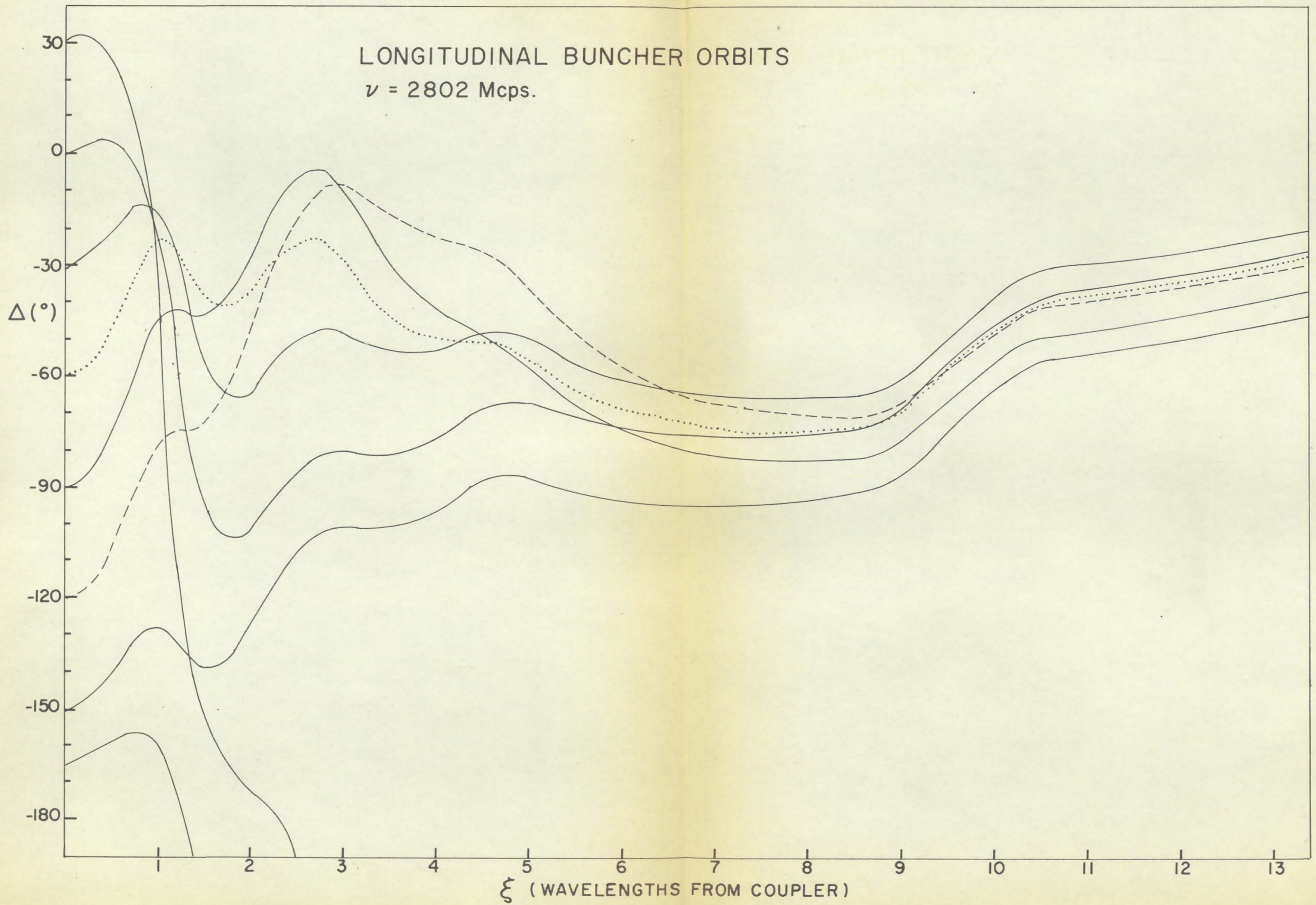


FIGURE 19

Table 4

Orbit Calculations

$\beta_{e(in)}$	0.5											
	.478 (70kv.)											
f m.c.p.s. $\Delta_{in}^{(o)}$	$\Delta_{out}^{(o)}$ 2798 E _{MeV}	$\Delta_{out}^{(o)}$ 2799 E _{MeV}	$\Delta_{out}^{(o)}$ 2800 E _{MeV}	$\Delta_{out}^{(o)}$ 2801 E _{MeV}	$\Delta_{out}^{(o)}$ 2802 E _{MeV}	$\Delta_{out}^{(o)}$ 2800 E _{MeV}						
+15		-450	0.4	-158	6.3	-89	9.4	-29	8.8	-98	10.4	
0	-227	4.1	-156	8.6	-93	10.5	-32	8.6	+23	4.7	-80	10.0
-15	-210	5.6	-145	9.3	-84	10.3	-25	7.7	+25	3.8	-79	9.8
-30	-208	5.7	-144	9.2	-84	10.1	-26	7.7	+25	3.9	-82	9.9
-45	-210	5.4	-147	9.0	-87	10.1	-30	8.0	+22	4.2	-86	9.9
-60	-213	5.1	-151	8.7	-92	10.1	-34	8.4	+19	4.1	-88	9.9
-75	-214	5.0	-153	8.5	-95	10.1	-38	8.6	+16	5.2	-88	9.8
-90	-209	5.4	-151	8.6	-95	10.0	-39	8.7	+13	5.5	-84	9.7
-105	-200	6.2	-144	8.9	-90	9.9	-37	8.4	+13	5.3	-76	9.4
-120	-192	7.0	-133	9.5	-79	9.6	-29	7.5	+17	4.5	-80	10.1
-135	-241	3.0	-144	9.5	-75	9.8	-19	6.6	+20	3.2		
-150									+11	6.5		

value. These losses are indeed serious; however the calculation for the low value of β_e predicts an output energy loss of only 200 keV. Electrons within initial phase angles from 0 to -135° - over 1/3 of the total injected current - should be picked up and accelerated to within 10% of the maximum energy. Electrons more than 20° outside these limits suffer a serious slip in phase angle and are eventually thrown into the cavity walls. Some of these will extract energy from the R.F. wave, and contribute to beam loading.

The problem of accelerator orbits has been over-simplified for purposes of rapid calculation. For example $\alpha(\xi)$ was assumed to be exactly 1.0 for the whole constant velocity section, whereas there must, of course, be exponential attenuation. The effect of beam loading^{7,24)} is almost impossible to include in the calculations even if a definite beam current is assumed. However, the buncher orbits should be reasonably accurate, and if most electrons are riding on the wave crest after the phase shift sections, the accelerator should function properly.

3.2 Dimensions of Buncher Cavities

The design problem remaining is the calculation of a, b, and d to give the correct buncher values of $\alpha(\xi)$ and $\beta(\xi)$. The

values of d can be calculated immediately if the buncher is constructed to operate in the $\pi/2$ mode. As in constant velocity sections

$$d = \frac{\lambda_g}{4} = \frac{\beta_w(\xi)}{4} \lambda_0 = 1.055 \beta(\xi) \text{ (in inches).}$$

$\alpha(\xi)$ is determined mainly by the hole diameter $2a$ of the buncher irises, and $2b$, the remaining dimension may then be changed to adjust the cavity resonant frequency. Four cavity tests of the type described in chapter 2 had to be done for each buncher cavity - i.e. $2a$, and d were machined to exactly the theoretical value, and $2b$ was changed until the central resonance was at 2800 m.c.p.s.

Chu and Hansen¹⁰⁾ have investigated the problem of power flow in disc-loaded guides. Their calculations show that the Poynting vector magnitude is given by the following expression:

$$P = \text{const.} \frac{a^4 \alpha^2}{\beta_w} \frac{J_1^2(k'a) - J_0(k'a)J_2(k'a)}{(k'a)^2} \quad (3.5)$$

$$= \text{const.} \frac{a^4 \alpha^2}{\beta_w} F(k'a)$$

$$\text{where } k = \frac{2\pi}{\lambda_0} \quad \text{and} \quad k' = k \frac{\sqrt{\beta_w^2 - 1}}{\beta_w}$$

Assuming a constant power flow throughout the buncher

$$\frac{a^4 \alpha^2 F(k'a)}{\beta_w} = K \quad (3.6)$$

K, the constant in this equation may be found by inserting in 3.6 the values $a = 1.503$ cm, $\alpha = 1.0$, $\beta = 1.0$ and $(k' a) = 0$ (i.e. $F(k' a) = 1$) to match the first cavity of the constant velocity section following the buncher. Equation 3.6 is then solved for the "a" of each buncher cavity. Since a appears in the argument of the Bessel functions this must be done by successive approximations.

A necessary condition for the continuity of the solutions of Maxwell's equations in the regions $r < a$, and $a < r < b$ within the guide has been found to be¹⁰⁾

$$\frac{1}{k' a} \frac{J_1(k' a)}{J_0(k' a)} = \frac{1}{(1-\eta)ka} \frac{J_1(ka)N_0(kb) - N_1(ka)J_0(kb)}{J_0(ka)N_0(kb) - N_0(ka)J_0(kb)} \quad (3.7)$$

where $\eta d =$ iris thickness, as before.

The values of a (ξ) computed from 3.6 may now be used in 3.7, and a similar procedure of successive approximations is used to determine the value of b for each cavity.

The results of the calculations for a , b , and d are shown in Table 5. The 2b (measured) column is the actual outer diameter after the adjustments made during the 4 cavity resonance tests. These values are all $\sim .020$ " larger than the calculated ones; fortunately, material could be turned off to make the necessary correction. It will be noticed that both 2a and 2b decrease

Table 5

Buncher Parameters and Dimension

	Cavity No.	α	β	d (in)	2a (in)	2b Calc. (in)	2b (measured)	
Buncher	1		.500	.527	2.250	4.346	4.359 (5)	
	2		.501	.528	2.228	4.327	4.342 (5)	
	3		.504	.531	2.163	4.270	4.288	
	4		.509	.536	2.072	4.191	4.208	
	5		.517	.545	1.972	4.102	4.117	
	6		.533	.561	1.875	4.013	4.032	
	7		.556	.586	1.809	3.932	3.955	
	8		.590	.622	1.710	3.843	3.871	
	9		.639	.672	1.644	3.762	3.791	
	10-14		.701	.739	1.583	3.689	3.711	
	15		.701	.739	1.583	3.689	3.711	
	16		.774	.816	1.523	3.610	3.645	
	17		.774	.816	1.523	3.610	3.645	
	18		.856	.902	1.461	3.546	3.570	
	19		.856	.902	1.461	3.546	3.570	
	20-24		.909	.957	1.384	3.494	3.513	
	25		.909	.957	1.384	3.494	3.513	
	26		.950	1.001	1.317	3.458	3.479	
	27		.950	1.001	1.317	3.458	3.479	
	28		.986	1.039	1.265	3.431	3.451	
	29		1.000	1.054	1.185	3.406	3.415	
	2nd Section	1-12		1.000	1.054	1.185	3.406	3.415
		13		1.000	1.054	1.185	3.406	3.415
		14		.986	1.039	1.265	3.431	3.451
		15-18		.950	1.001	1.317	3.458	3.479
		19		.950	1.001	1.317	3.458	3.479
		20		.986	1.039	1.265	3.431	3.451
		21		1.000	1.054	1.185	3.406	3.415

towards the output end of the buncher, while d increases. It was therefore possible to construct a 4-cavity test section for cavity 29, make the Brillouin diagram measurements, and turn off all dimensions on the lathe to produce cavity 28, etc. This procedure was carried out to check all buncher dimensions.

3.3 Phase Shift Measurements and Bandwidth

The shorting plunger measurement described in section 2.1 would be an attractive way of testing the buncher for any cumulative phase shift. This is not possible, however; a plunger small enough to insert through the irises of the buncher output cannot effectively detune the wider cavities near the input. It is possible, though, to cap each cavity in turn with a flat copper plate, and to measure the phase change with an SWR detector in the rectangular input guide. The results of these tests for the buncher and one $\beta_w = 1$ section are plotted in fig. 20. The shift appears to be rather large, notably close to cavity 23, where it amounts to $.13 \lambda_g$, however it was hoped that since most of the bunching action takes place in the first 45 cm of the section the phase error would, at worst, place the electron packet at the wrong phase of the wave. The cumulative error is very small and, if necessary, a correction could be made by changing the phase shift cavities of the first $\beta = 1$

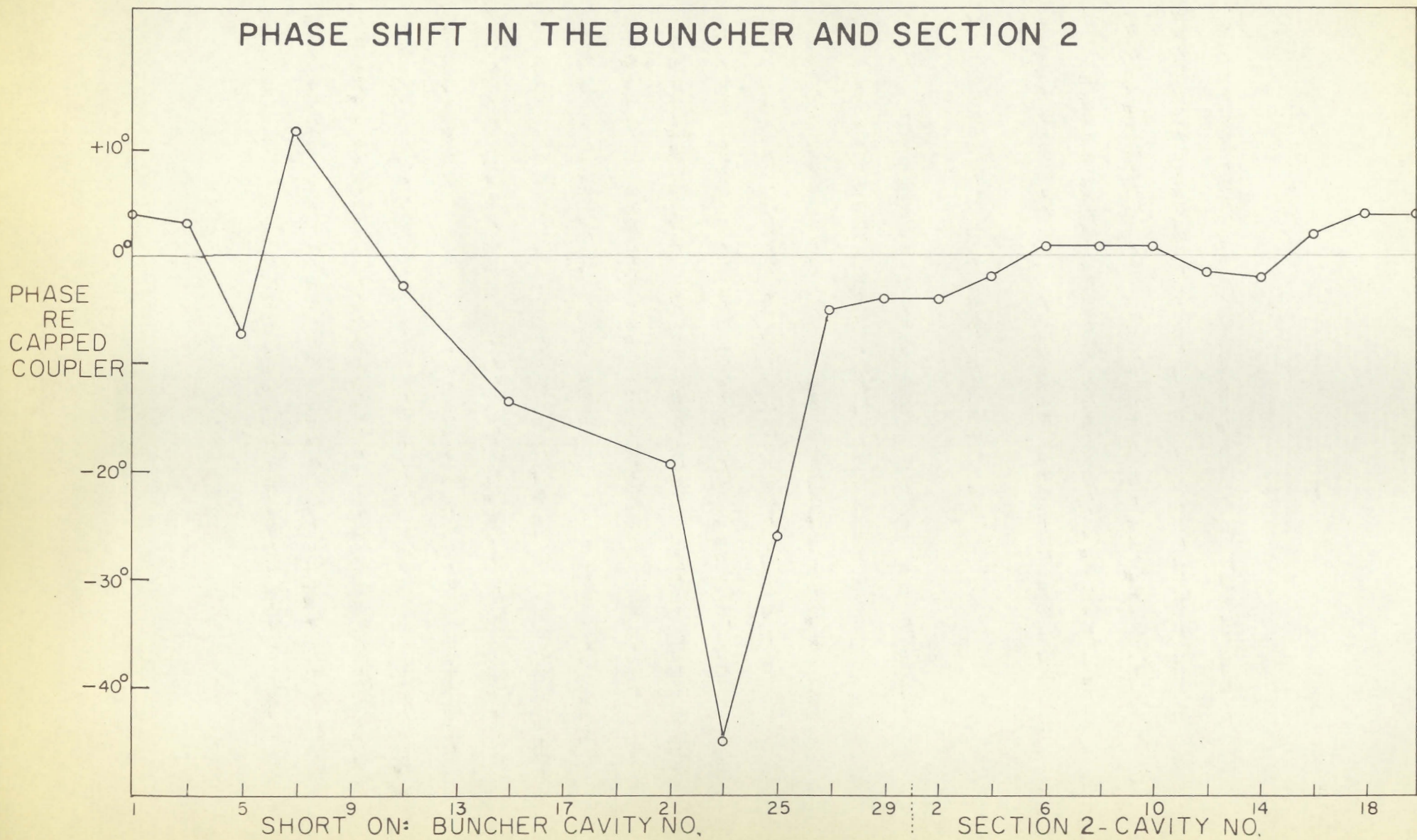


FIGURE 20

section. This fortunately did not prove necessary, but the performance of the completed accelerator would no doubt be improved if cavities 11-27 could be corrected.

The specifications of the QK 338, or QK 327 magnetrons list a VSWR = 1.5 as the maximum permissible mismatch. For this reason it was necessary to measure the bandwidth of the system at low power to guard against any reflections unnoticed in the phase shift measurement. Such reflections can cause sparking at the ceramic output window of the magnetron, and if this is sustained, will cause window failure. It was intended at the outset to use fixed frequency tubes chosen to operate close to 2800 m.c.p.s., and to make any fine tuning adjustments by inserting a slight mismatch in the rectangular guide close to the magnetron window. This is difficult to do, and can be harmful to the magnetron if the operating band of the system is too narrow. Bandwidth measurements were made many times for couplers, and for separate accelerator sections. Fig. 21 shows the result for the complete structure operating into a water dummy load. For a standing wave ratio of 1.5 the bandwidth is seen to be 4.4 m.c.p.s. This is certainly narrow, but at the time was not thought to be a serious enough problem to require the use of a tunable magnetron.

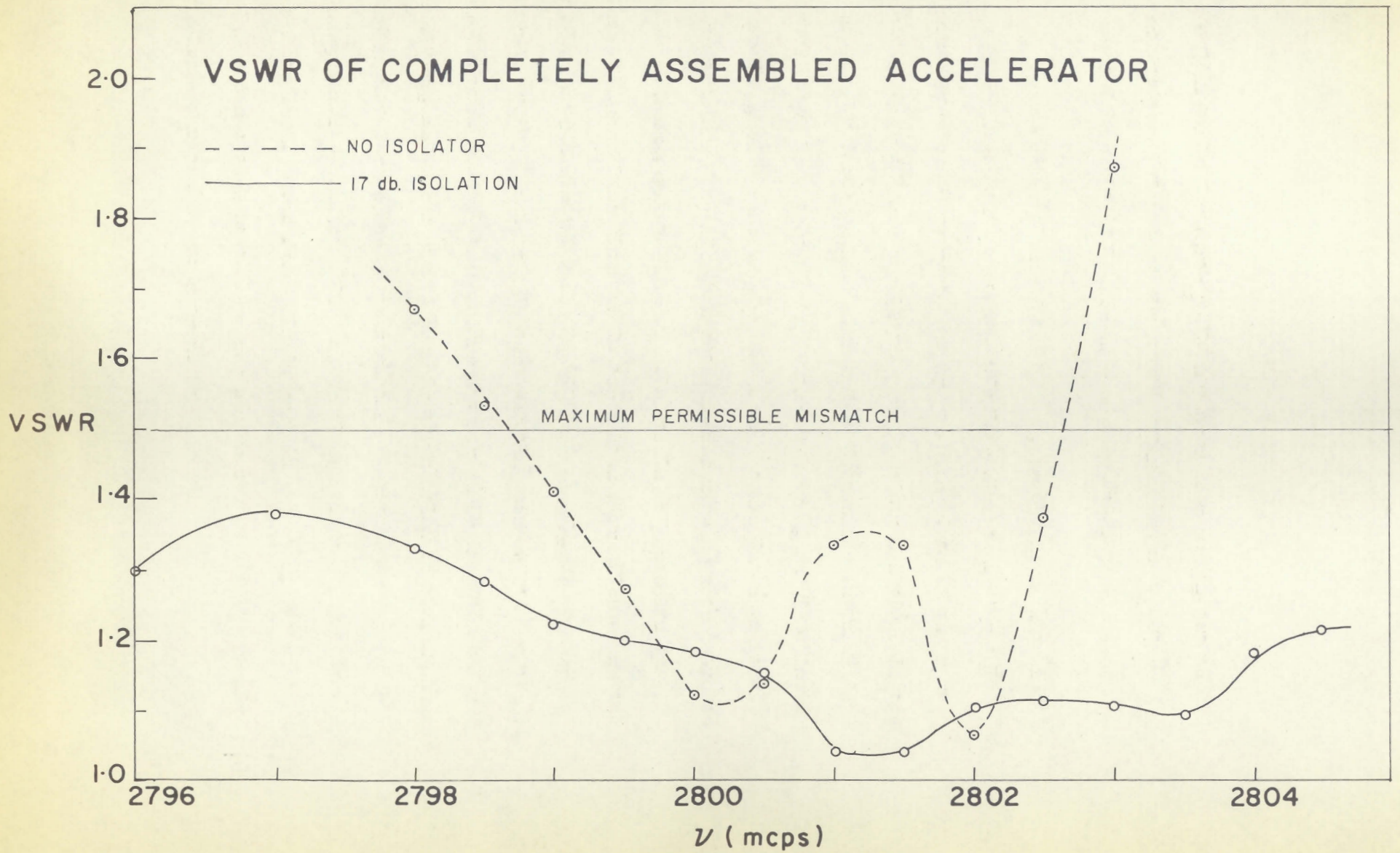


FIGURE 21

IV The Electron Gun, and Focusing System

4.1 Gun Designs

Even with ideal transverse focusing along the entire accelerator, beam losses in the buncher are inevitable. It is probable that more beam loss will occur if the beam is to be steered magnetically through 90° at the output end. It was stated that a current of 20 microamp. should be available at the accelerator target; therefore a minimum of 60 μ amp. (much more, if possible) should be the average current injected by the gun. It is also important to confine the beam to a diameter of a few millimetres - this simplifies the buncher focusing requirements, as well as the design of the steering magnet, and X-ray head.

Earlier accelerators often operated quite successfully using only a simple tungsten filament directly behind the buncher coupler. Such a device, injecting electrons continuously, is unlikely to produce a good output energy spectrum. In the first place, the electrons entering will have very low energies so that the acceptance angle of the buncher will be small. For any respectable average output current the injected current must be large; therefore the magnetron must, at every pulse, operate into a loaded system constituting a large mismatch. Ideally, then, electrons entering the guide should have energies of 80 kv to match the initial $\beta_w = .5$

cavities of the buncher. It is also desirable to pulse the gun separately after the complete accelerator is filled with R.F. power.

All of the gun designs of the present work are, in geometry, similar to the Pierce type, using a focusing electrode surrounding the cathode. Usually the Pierce gun is designed to operate in the space charge limited region, whereas an 80 kv accelerator gun can have a much smaller perveance. It was decided to construct the gun in the style of a slightly convergent Pierce type, but with conical approximations to the usual curved cathode. Some preliminary work was done with an electrolytic tank to explore the feasibility of several electrode shapes. The shape selected for the first actual beam test had a cathode cone of half angle 48° surrounding a $\frac{1}{2}$ " diameter flat tungsten spiral, and a convex anode of half angle 75° with a central $\frac{1}{2}$ " diameter hole. The two electrodes were mounted in a glass tube along with a collecting electrode 25 cm behind the anode. After the tube was evacuated, the relative electrode positions could be changed externally with a small permanent magnet. The anode voltage used was 2 kv for this model. With a total emitted current of 1 ma, the partition (i.e. $\frac{\text{Collector current}}{\text{total current}}$) was as high as 80% with careful adjustment of the spacings. It was also noted that a negative bias of 100 - 200 volts applied to the focusing electrode was sufficient to cut off the beam completely.

The structure was then modified for testing on the assembled buncher section with a 23 cm space between the gun anode and the back of the buncher coupler. This space accommodated a 3" diameter vacuum gate valve, and a pump-out connection. No high voltage DC supply was available at the time, so the main modulator pulse was used up to 60 kv for testing. Although 70% of the beam passed through the anode, none was observed at the first buncher cavity. Subsequent tests indicated that the beam was divergent in the field free space following the anode, so that most of the accelerated electrons struck the back of the buncher coupler. Many attempts were made to focus the beam with cylindrical permanent magnets with only slight success - 15% transmission was eventually obtained, but it was apparent that this was in a diffuse beam spread over the whole half inch diameter of the entrance hole. It was however, noted that the gun was capable of transmitting a peak current over 200 ma through the anode, and it was decided to remount the gun assembly, using the back of the coupler as the anode.

Tests with the preceding gun showed that the cathode cone angle was critical between 40° and 45° , giving the best partition at 42° , while a change in anode angle made very little difference to the gun's operation. The flat back face of the coupler was therefore not altered. Tests made with pulse voltages of 20 - 75 kv, and with

a filament power of 85 watts showed that 50% of the beam was transmitted into the coupler. With this filament power, it was necessary to provide cooling for the gun cathode with the focusing cone. Transformer oil pumped through a small heat exchanger was used as the coolant for these high voltage electrodes.

4.2 D. C. Pulsing System

To avoid the necessity of pulsing with a completely separate 80 kv pulse generator, it was proposed to operate the final gun model as a triode, with the focusing cone acting as a grid. The cathode may then be kept at a D.C. voltage of -80 kv with the grid bias sufficiently large to cut off the current; if μ is high enough for this triode, a relatively small pulsing unit can then be used to inject current into the accelerator after it has been filled with R.F. power.

Measurements of the static characteristics of the gun were made at cathode voltages up to 35 kv. These gave a value of μ from 15 to 35 depending on the position of the focusing cone with respect to the cathode. With a μ of 30, the gun current will be cut off with a bias of about 2.5 kv, if the accelerating voltage is 75 kv.

At the time the pulser was constructed, no 80 kv D.C. supply

was available, and the system could only be tested at accelerating voltages up to 35 kv. The collecting electrode was mounted on a sliding probe inserted at the output end of the accelerator, and in this test the buncher focusing coils were adjusted for maximum current. With the cathode at -30 kv, and a 1 μ sec, 1500 v pulse (300 p.p.s. repetition rate), as much as 110 ma peak current was observed. The filament power required for this was 116 watts, which was disappointingly high. The filament in use at this time was a spiral of .020" diameter tungsten 8 cm long and the lifetime predicted at this power is less than 10 hours²⁵⁾ .

Unfortunately, all attempts to use the pulsing system described above ultimately failed. The vacuum system used for the accelerator has never reduced the pressure below .01 microns, and at this pressure the gun invariably broke down at D.C. cathode voltages above 55 kv. With a 75 kv pulse applied directly to the cathode this happens only during the outgassing period required following long periods when the system is opened to air. The D.C. system was therefore abandoned, even though it was realized that most of the other feasible methods would probably result in a poorer beam energy spectrum.

The simplest alternative is to use the magnetron pulse as the accelerating voltage. This voltage varies somewhat with different

magnetrons (70 - 80 kv), but the buncher orbit calculations indicated that relatively small changes in injection voltage have a negligible effect on output energy. There is no appreciable extra load on the modulator, since the average magnetron current is 65 ma. The filling time of the R.V.H. accelerator is only 0.2 μ sec. so that there should be little beam deterioration at least on the rise of the pulse.

4.3 The Present Electron gun

With the second gun, the pressure of the accelerator system invariably rose after several minutes of operation from 2×10^{-5} mm. to 3×10^{-5} mm. This, in part could be blamed on the inefficiency of the gun, which made it necessary to use filament powers of 100 watts or more, causing severe heating of the whole cathode structure. Breakdown between the cathode and buncher coupler occurred frequently, even with the magnetron pulse as the accelerating voltage, and it was soon apparent that a new gun design was necessary. Any breakdown in the system causes an immediate pressure burst, which almost always results in a spark at the ceramic magnetron window.

The focusing cone design for the third gun was suggested by High Voltage Engineering Corporation. The cathode, shown in fig. 22,

ELECTRON GUN

- BRASS
- ▨ CERAMIC
- ▧ OFHC COPPER

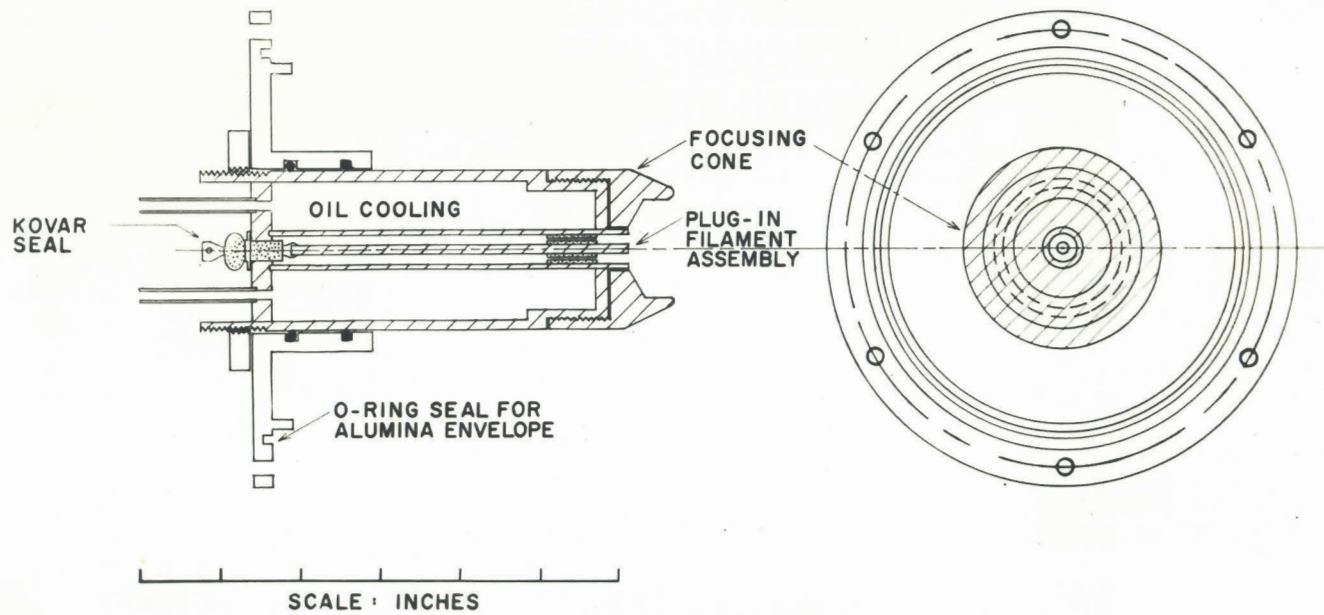


FIGURE 22

was made of OFHC copper parts, preassembled, and brazed with solder rings in a hydrogen furnace. This eliminated the need for flux, which was a serious problem in the previous gun. Since it had been noted in earlier measurements that the gun performance depended rather critically on the position of the filament inside the cone, the latter was left movable, and was threaded on the main gun cylinder; in addition, the cylinder itself can be moved along the gun axis in the sliding O-ring seal. The first guns had been mounted in lucite envelopes having exhaust connections to the diffusion pump; the final gun is enclosed in a cylinder of Coors AL-100 alumina.

Several types and shapes of cathode have been tried. The flat tungsten spiral provides a high beam current but results in a poor spot size. Tantalum filaments were used for a time, but proved unsatisfactory, burning out frequently after very short lives either at the tantalum-nicked spot weld, or at sharp bends in the wire. One indirectly heated barium-nicked oxide cathode, similar to types used in magnetrons was inserted. This required an elaborate forming and baking procedure. Although the spot shape at the output was somewhat better than with the directly heated cathodes, the current was much lower. It was also realized that the time lag of the indirectly heated cathode would very

probably be a serious drawback if the filament control is the only one to be used to vary X-ray dose rates.

The filament finally decided on was perhaps the simplest design of all, consisting of a 3 mm diameter longitudinal spiral of .010" diameter tungsten wire, $6 \frac{1}{2}$ cm long, mounted with its axis normal to the accelerator axis. This has proved to be a good compromise for output current, spot size, and filament life.

4.4 Magnetic Focusing

In the appendix a description of the transverse forces exerted on the electron is given. It can be seen from equation (a. 1.4) that if both the electron and the wave are travelling at the velocity of light, then $k^2 = k_e^2 = k^2 z_0$, and that $F_r = 0$. The analysis shows that when $v_p = v_e = c$, the radial magnetic force becomes exactly equal and opposite to the radial electric force. No transverse focusing should then be necessary in the $\beta = 1$ portions of the accelerator unless corrections are required for preceding radial drift. This is exactly the reason for the feasibility of long electron accelerators. Even assuming an initial radial electron velocity, the resultant defocusing need not be serious; the radial momentum of the electron remains constant, so the velocity must decrease during acceleration as mass increases. The radial displacement then varies only logarithmically with accelerator length.

Neal states⁶⁾ that the magnitude of the minimum axial field required to prevent radial drift for electrons riding ahead of the wave crest is

$$\begin{aligned}
 B &= 2 \frac{\sqrt{\pi} m_0 c^2}{e \lambda_0} \left[\frac{\alpha (1 - \beta^2)^{1/2} \cos \Delta}{\beta} \right]^{1/2} \\
 &= 565 \left[\frac{\alpha \sqrt{1 - \beta^2}}{\beta} \right]^{1/2} \text{ gauss} \qquad 4.1
 \end{aligned}$$

(with the design wavelength of 10.706 cm)

Inserting values for α and β along the buncher results in a field which is at no point higher than 375 gauss; this is certainly easily obtained with air cored solenoids of modest size.

Before the corrections described in section 3.1 had been carried out, the buncher consisted of only 19 cavities with a total length of 16". Hence the solenoid was much shorter than the system used at present. The original coil had five windings, of approximately equal spacing, covering the first 14 buncher cavities. These windings had 1600, 3300, 2300, 2100, and 1500 turns with a current requirement of one ampere for each coil; and an 80 v, 5 amp power supply of the three phase quadrature type was constructed.

With the completion of the longer buncher section, it became apparent that the focusing provided by this coil system was inadequate. A more detailed investigation of the equations of transverse motion of an electron in the buncher was carried out, and it was found that the required field, as given by equation 4.1, is

only adequate if the electron happens to have the correct initial angular velocity. It seems more reasonable to design for the case in which the initial angular velocity of an off-axis electron is zero. It is shown in the appendix that in the worst case, with the electron riding at $\Delta = -0^\circ$, the field should be $\sqrt{2}$ times the value given by equation 4.1; with this field, the electron starting at a radius R_0 off axis will stay within a radius of $\sqrt{2} R_0$. It is certainly inevitable that an electron entering the focusing field will acquire some angular velocity even in the buncher coupler due to the radial component of magnetic flux; in this case it is shown that the focusing of the axial field lines is even more effective. This "required field" as well as actual field obtained with optimum focusing are plotted in fig. 23 .

AXIAL MAGNETIC FIELD

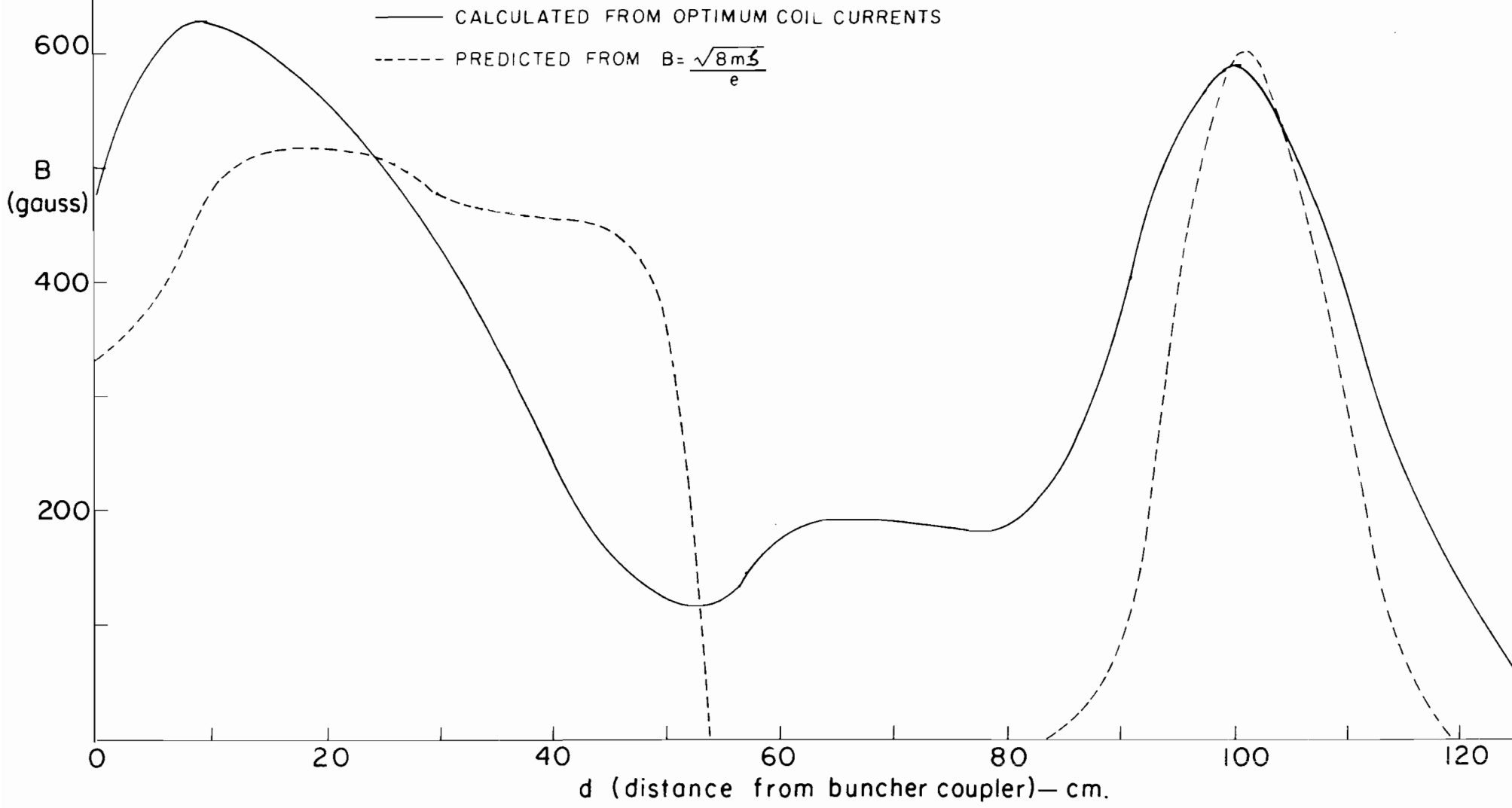


FIGURE 23

V Accelerator tests at High Power

5.1 Experience with Magnetrons

The QK 327 tunable magnetron was still in the development stage during early accelerator work. The first tests were carried out with a 4 MeV accelerator consisting of the buncher, and one two-foot constant velocity section having a bandwidth of 10 m.c.p.s. centred at 2797 m.c.p.s. It was therefore thought that the QK 338 tube, selected on frequency (at 2800 m.c.p.s.) would perform satisfactorily, even if the QK 327 proved to be necessary for the complete four section accelerator. This was only partly true, and many difficulties were encountered.

The first tubes were tested on water loads, operating into both pressure and vacuum systems, and in general performed fairly well. However, these tubes invariably developed cracks across the output ceramic windows when attempts were made to operate them with the short accelerator as load and with the tube operating into a vacuum. The cracks were always in the direction of the electric vector, and it was assumed that sparking was the cause of the failure at 4 megawatts input power. Later observations showed that the windows cracked only after the magnetron power was turned off; this led to the discovery that the entire window

was operating at temperatures higher than the design maximum of 160° C . This was caused by poor heat conduction away from the ceramic to the magnetron output flange. With the tube operating into a pressurized system (as in radar applications) the window is cooled by convection.

To correct this, an 8" section of pressure waveguide was inserted. This has a circular ceramic window mounted diagonally across the output end, and water cooling on the guide walls. Such sections are capable of transmitting up to 10 kilowatts of average power without damage; in our application, both windows are cooled by the enclosed air at 40 p.s.i. pressure. As a safety measure, a small compressor provides the system with clean dry air, which is continuously bled off. Since this section was installed several magnetrons have been used. None has failed because of window damage, although on occasion severe sparking has occurred within the guide. The VSWR of the section itself has been measured to be 1.08 .

The first tests on the two section accelerator revealed a problem which has continued to be a serious drawback to the intended use of fixed frequency tubes. The frequency of the first QK 338 had been measured as 2802 m.c.p.s. with the tube operating into a wide band match. With the accelerator as load

the frequency was pulled to 2806 m.c.p.s., well out of the permissible operating bandwidth. A mismatch of VSWR = 1.3 was made with a rectangular bar, mounted in teflon insulating supports, and inserted close to the magnetron window. This had little effect on the operating frequency, pulling it at most 1.5 m.c.p.s.

It was found necessary to construct line stretchers at the accelerator input to pull the operating point of the magnetron far enough around the Riecke diagram to result in a frequency of 2800 m.c.p.s. This was successful and the magnetron was eventually operated into the accelerator at pulse power outputs as high as 2.2 megawatts. Above this level (55 ma average current) the frequency jumped to 2803.5 m.c.p.s. With a combination of line stretcher, and inserted mismatch the magnetron ran very stably at its full rated power output (3.9 Mw. , 80 kv pulse voltage, 75 ma average current, and 330 p.p.s. repetition rate).

The first electron beam measurements were made with this two section accelerator system. With the gun operating as a pulsed triode, only weak X-rays of energy less than 100 keV were observed. The gun was then pulsed directly with the main modulator. Average beam currents of .02 microamperes were measured with a Faraday cup collector, and a galvanometer. The

energy was then measured by magnetic deflection; whereas 4 MeV was the design value, only 1 MeV was observed.

After a study of the change in accelerator operation at different frequencies it was realized that the buncher design was at fault. The replacement of four $\beta > 1$ cavities of the buncher with $\beta = 1$ cavities immediately improved the output yielding an energy of 2.4 MeV, and higher beam current. The buncher was then redesigned (as described in section 3.1) and another completed two foot section was added to the two previously tested. After a good match had again been obtained, beam tests were performed, indicating an energy of 4.5 MeV at 2800.2 m.c.p.s., and an average current of 1 μ amp. Contrary to expectation, the energy improved somewhat at higher frequencies, reaching a maximum of 5.6 MeV at 2802.2 m.c.p.s.

The adjustment of frequency proved to be even more difficult with the tunable QK 327 magnetron. This tube, operated at low power levels, refused to oscillate in the tuning range between 2776 m.c.p.s. and 2810 m.c.p.s., skipping over the whole region. A bandwidth check at low power indicated a VSWR < 1.5 from 2798.7 to 2803.3 m.c.p.s., with the acceptable value of 1.15 at 2800 m.c.p.s. The probable reason for this skipping is discussed in the following section.

5.2 Frequency Skipping and Long-line Effect

The type of tuning problem described is characteristic of magnetrons coupled through long guides into a mismatch^{26,27}.

If the magnetron is considered as a simple parallel resonant circuit, the input susceptance of the line is seen by the magnetron as a reflected susceptance B . For a mismatch of $VSWR = 1.5$ the input susceptance will vary with phase angle; the maximum deviations of B may be easily found (on a Smith chart, for example) as $\pm .417$. If P , (the magnetron pulling figure) is defined as the total frequency spread as this mismatch is varied through all possible phase angles, the relation between natural resonant frequency ν_0 , and pulled frequency ν can be shown to be

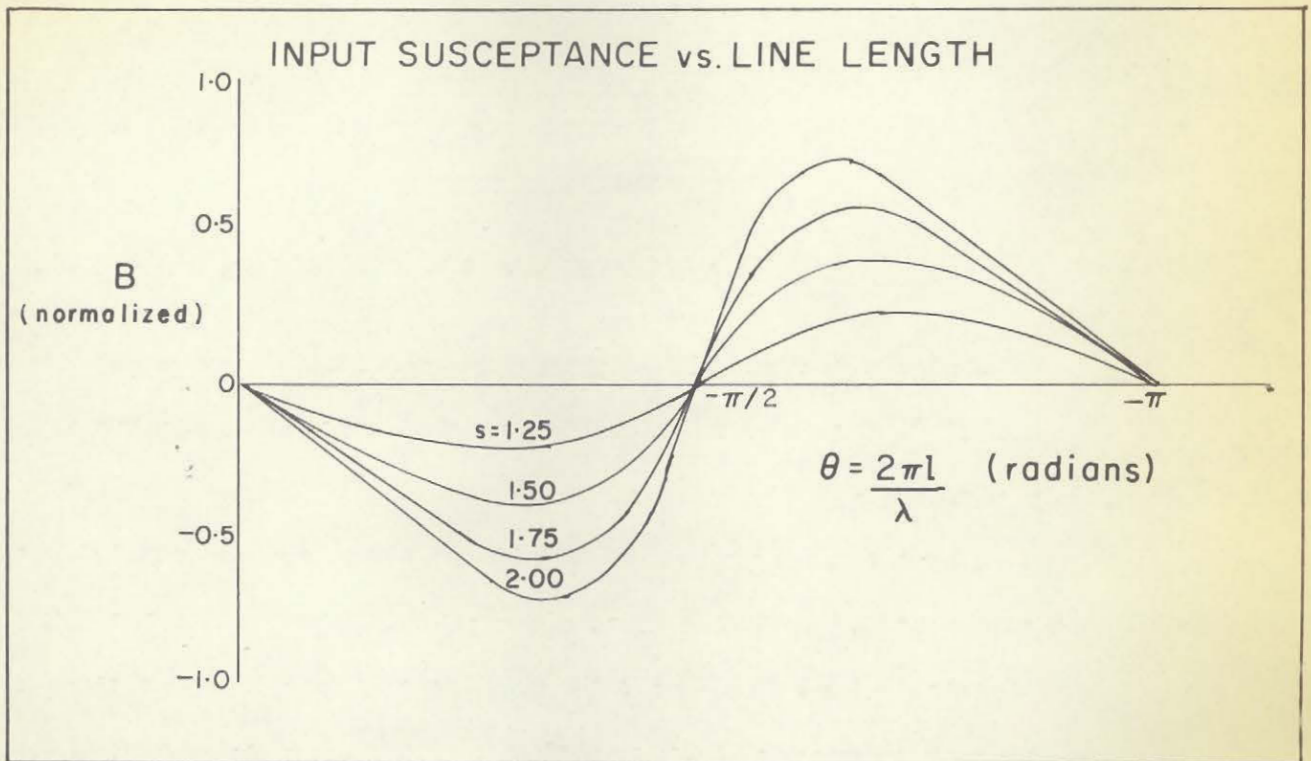
$$\nu_0 = \nu + \frac{BP}{2(.417)} = \nu + \frac{BP}{.83} \quad (5.1)$$

If the mismatch is considered to be purely resistive, of $VSWR = s$, and at the end of a line of electrical length θ , it may be shown that the input susceptance is

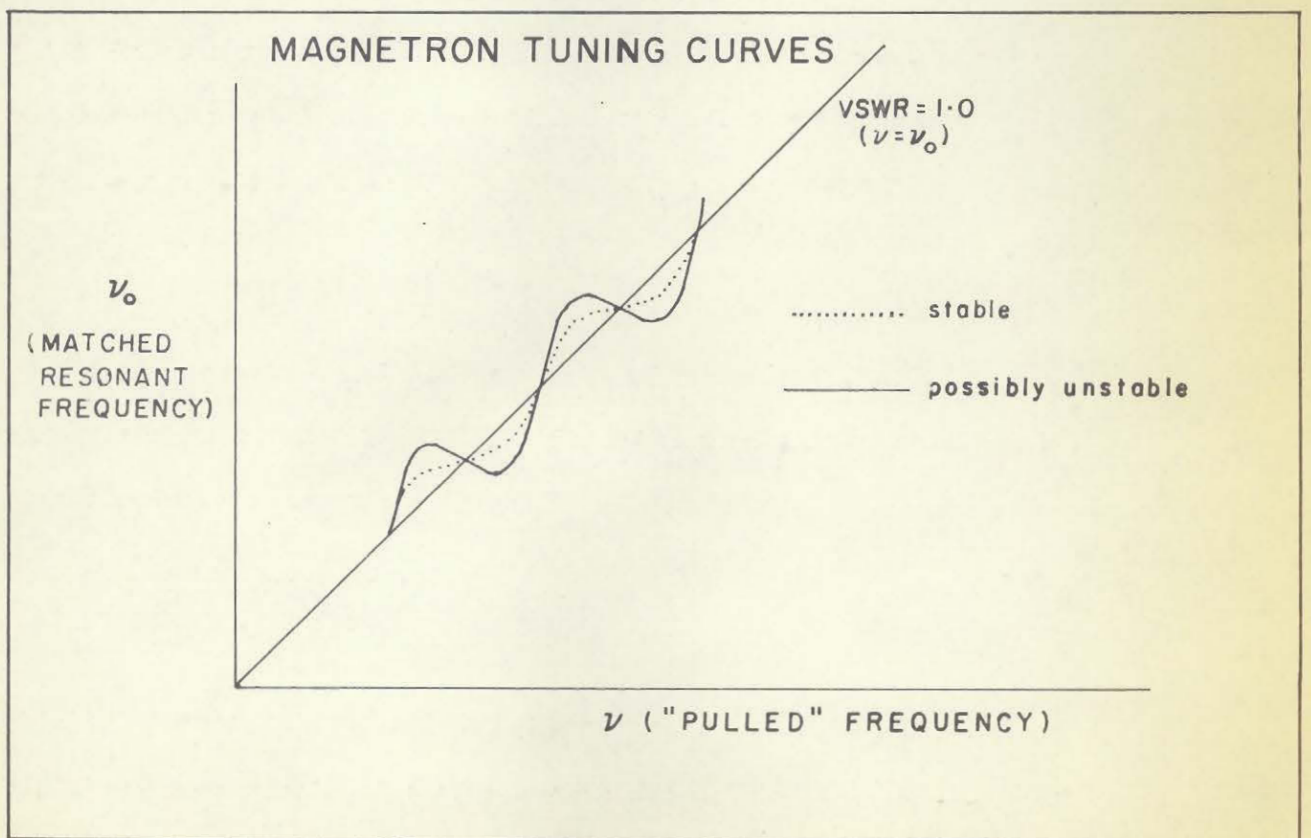
$$B = \frac{\text{Sin } 2 \theta}{\frac{s^2 + 1}{s^2 - 1} + \cos 2 \theta} \quad (5.2)$$

This is plotted in fig. 24(a). Equations 5.1 and 5.2 give the tuning characteristic of the magnetron shown in fig. 23(b), namely

$$\nu_0 = \nu + \frac{P}{.83} \frac{\text{Sin } 2 \theta}{\cos 2 \theta + \frac{s^2 + 1}{s^2 - 1}} \quad (5.3)$$



(a)



(b)

FIGURE 24

With large susceptance the curve of v_0 vs v may not be single valued - i.e. the magnetron may "skip" frequency. If single-valuedness is taken as the criterion of stability of magnetron operation, the condition is therefore that

$$\frac{dv_0}{dv} = 0 \text{ at } \theta = \frac{n\pi}{2} \quad (\text{with } n \text{ odd})$$

And

$$\frac{dv_0}{dv} = 1 + \frac{P}{.83} \left[\frac{1 + \left(\frac{s^2 + 1}{s^2 - 1}\right) \cos 2\theta}{\left(\cos 2\theta + \frac{s^2 + 1}{s^2 - 1}\right)^2} \right] 2 \frac{d\theta}{dv} \quad (5.3)$$

Now, for the accelerator

$$\frac{d\theta}{dv} = \frac{d\left(\frac{2\pi L}{\lambda_g}\right)}{dv} = \frac{2\pi L}{c} \frac{d\left(\frac{1}{\lambda_g}\right)}{d\left(\frac{1}{\lambda_0}\right)} = \frac{2\pi L}{v_g}$$

Therefore

$$\frac{dv_0}{dv} = 1 + \frac{15.12 L P}{v_g} \frac{1 + \left(\frac{s^2 + 1}{s^2 - 1}\right) \cos 2\theta}{\left(\cos 2\theta + \frac{s^2 + 1}{s^2 - 1}\right)^2} \quad (5.4)$$

and $\frac{dv_0}{dv}$ will be zero for the critical line length L_{MAX} - (i.e. the maximum line length for stable magnetron operation at $\theta = -\frac{\pi}{2}, -\frac{3\pi}{2}, \dots = \frac{2n+1}{2} \frac{\pi}{2} \dots$) This gives a value of

$$L_{MAX} = \frac{v_g}{7.56 P(s^2 - 1)} \quad (5.5)$$

The same analysis carried out for an unloaded line yields a value of $L_{MAX} c/v_g$ times the above value. Actually stable operation may be

achieved with lines longer than L_{MAX} if, for example, the magnetron operating frequency happens to lie at a single valued ν_0 of the tuning curve. With longer lines, and larger standing wave ratios the problem may, however, be serious.

Values of L_{MAX} for three pulling figures are plotted in fig. 25. For the QK 327 magnetron the pulling figure is 15 m.c.p.s., and with the pressure section in the system, the operating VSWR cannot be less than 1.1. This indicates a maximum permissible line length of less than 50 cm, so that unless the magnetron happens, by chance, to operate in a quasi-stable condition just at the operating frequency, there is little hope of avoiding frequency skip. One solution to the problem is to decrease the pulling figure by introducing attenuation in the waveguide between the magnetron and the accelerator. This, however, is wasteful of power, and will necessarily reduce the available electron energy. Recently, ferrite isolators have become available at megawatt power levels, and provide a more satisfactory solution. The isolator chosen for this application has a backward attenuation of 17 db, and a forward attenuation of only 0.25 db.

The accelerator bandwidth was again measured with the isolator inserted, and the results are shown with the previous measurement in fig. 24. The minimum VSWR occurs at about 2801.3 m.c.p.s. with

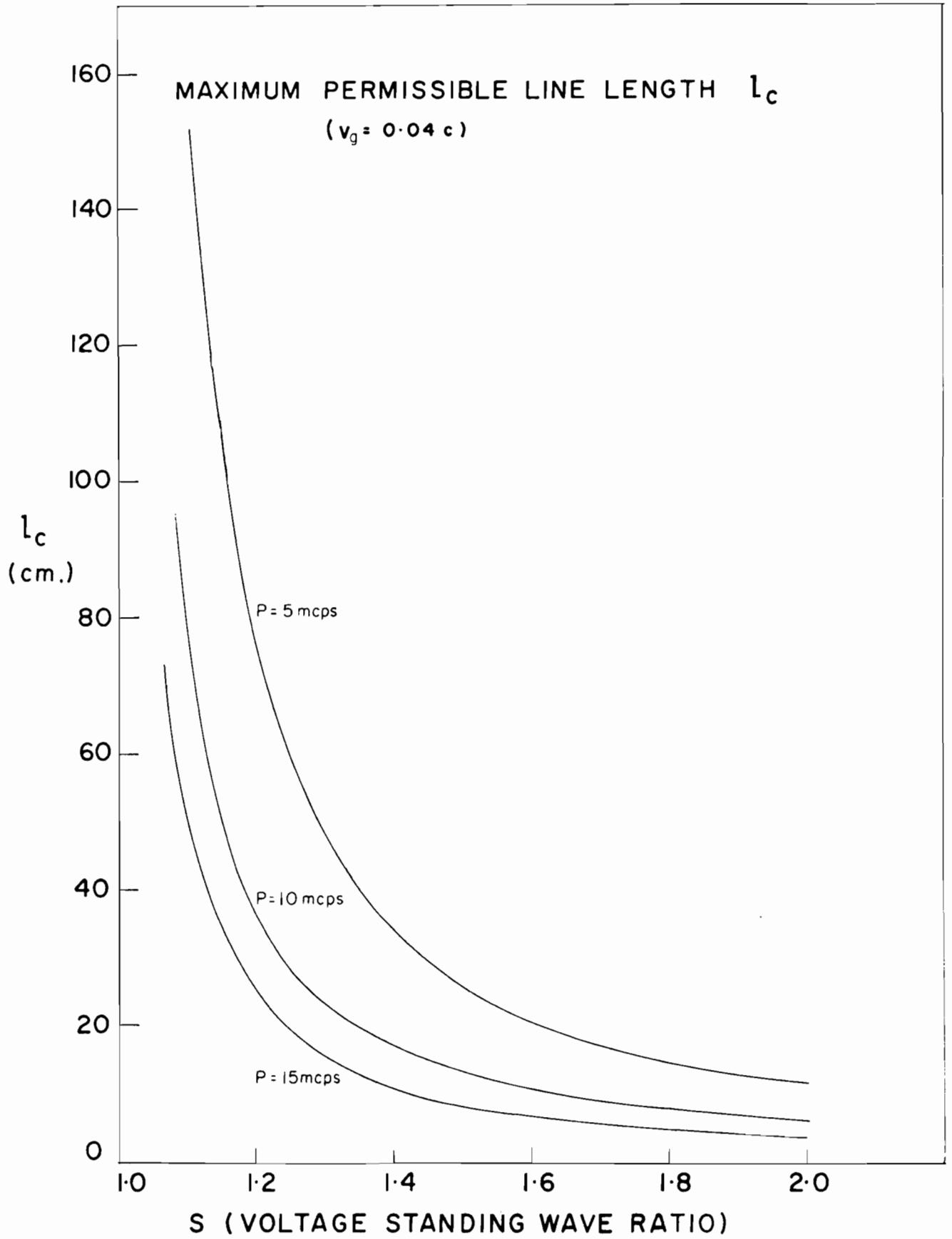


FIGURE 25

the isolator inserted, and not at the previous value of 2800 m.c.p.s.; this is perhaps a result of the increased line length. At 2801 m.c.p.s. the VSWR value of 1.04 is a considerable improvement on the ratio without isolation.

At high power, magnetron operation is improved, but frequency skipping still occurs. In the region of interest, the magnetron operates quite stably at 2801.1 m.c.p.s., but on tuning jumps to 2803.5 m.c.p.s. or 2798.1 m.c.p.s. At the latter value some breakdown occurs in the isolator. At present, a magnetron with frequency adjustable over a small range (resembling in other specifications the QK 338) is under development. It is hoped that the pulling figure of this tube will be low enough to cure the skipping completely, and to permit operation of the accelerator with no external tuning control whatever.

5.3 Measurements of Accelerator Performance

Since the first crude beam measurements indicated a very low output energy (< 3 MeV) and beam currents of the order of only .1 μ amp. many improvements had to be made in the operating parameters of the accelerator. In order to make reasonable evaluations of the effect of a design change it was necessary to know not only the peak energy, and average current output, but also the shape of the energy spectrum, the loading due to the

beam, and the transverse distribution of electrons. The following sections describe the equipment and techniques used.

(a) Measurement of Beam Current

The simplest, and most direct method of measuring current is to catch the beam at an anode, and to measure the collected charge. Considerable care must be taken to avoid errors, especially at low electron currents, and high energies; secondary emission from the anode material, for example, will reduce the collected charge, as will the collection of any positive ions from the surrounding atmosphere²⁸⁾. If a metal of high Z is used for the catcher, pair production near the surface may give a falsely low indication because of the higher absorption cross-section for positrons. Accordingly, the anode constructed was in the form of a Faraday cup, consisting of 3" of carbon backed by 2" of lead. In the first measurements, a manually operated slideback electrometer was used to measure the charge stored on a collecting condenser, in order to keep the cup potential at ground during the measurement. There was, however, found to be no loss in accuracy when the electrometer was connected as an ordinary current meter between the cup and ground. At average currents greater than 5 μ amp, the electrometer is unnecessary; an ordinary microammeter

may be used, or the current pulse may be observed on an oscilloscope.

If the electron energy is known the beam current may be checked by two simple methods. In the first, the beam is absorbed in a water calorimeter²⁹⁾ and the beam power is calculated from the observed heating. Alternatively, the beam may be intercepted by a target of high Z material, and the forward X-ray intensity measured at 1 metre from the target. Curves due to Miller³⁰⁾, and others³¹⁾ may then be used to find the corresponding beam current. The X-ray output is, however, a rapidly varying function of both electron energy and current, and estimates obtained by this method are unlikely to be accurate within 10% .

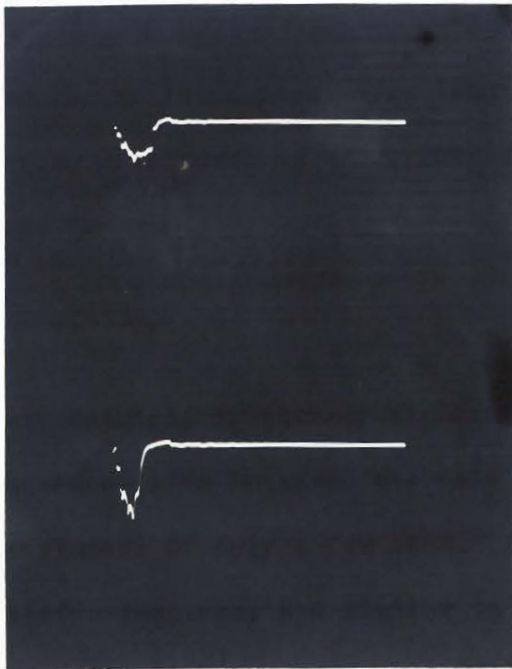
More recently, a transmission current monitor has been used. The beam passes through a ferrite ring 1 1/4" O.D. with a square 1/4" cross section. A winding of 30 turns of no. 30 cotton covered wire on this toroid forms the secondary, while the beam itself may be thought of as the primary "winding". If this secondary, of inductance L , is connected to an amplifier, of input resistance R , the pulse will be differentiated with time constant L/R ; the design must therefore ensure that L/R is large

compared to the 2 μ sec pulse length. If L is increased by putting more turns on the secondary(N), the output current, which is

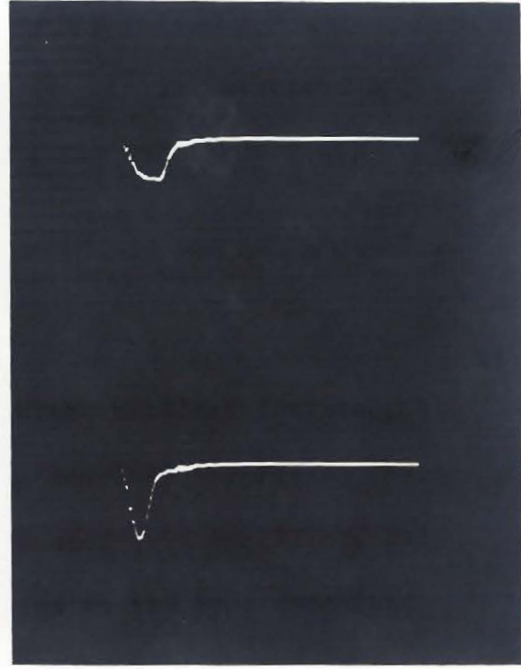
$$\frac{L_{\text{beam}}}{N},$$

(very nearly), is thereby reduced. With the first ferrites, the inductance with 30 turns was only 50 μ henries, permitting input resistances of only a few ohms. A grounded grid amplifier, using positive feedback, and similar in design to the type described by Bess et al³²⁾ was made: this functioned well on a bench test, with no observable differentiation of a generator pulse.

Unfortunately the noise level at the amplifier input caused by the 80 kv magnetron pulse was so high that the circuit could not be used under actual conditions. The toroid used now is completely shielded at the output end of the accelerator, and has a much higher inductance (0.5 millihenries). This, with an input resistance of 30 ohms has a time constant of 17 μ sec, which is adequate. The pulse obtained is shown in fig. 26, along with the extremely simple circuit. This consists of a grounded base input amplifier with an emitter follower output. The whole circuit is mounted within the shield on the accelerator head with an enclosed battery power supply. The output pulses may be viewed on an oscilloscope, rectified by a peak voltmeter to read peak current, or integrated to give average current.

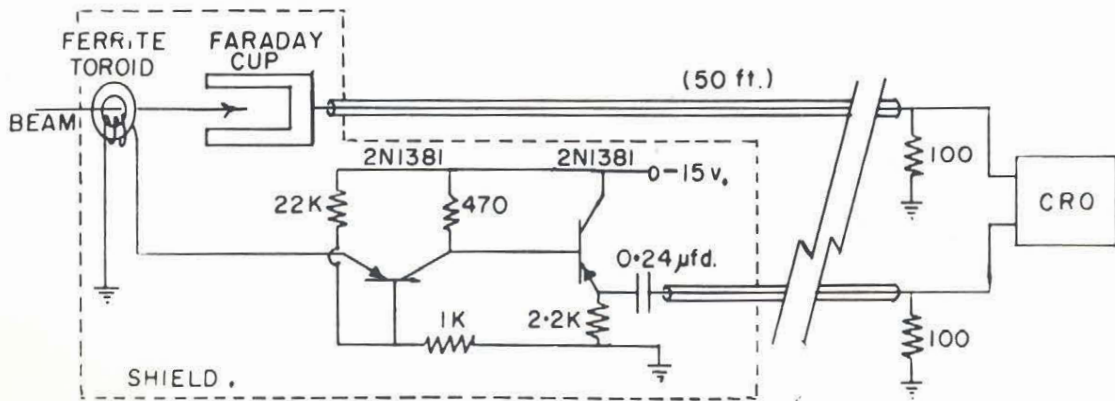


FARADAY CUP



TOROIDAL MONITOR

UPPER PULSE - 60 ma. PEAK CURRENT
 LOWER PULSE - 90 ma. PEAK CURRENT (SHORTENED)



MONITOR CIRCUIT

OBSERVATION OF BEAM CURRENT

(b) Energy Measurement

All the energy spectrum measurements to be described were made by mounting the Faraday cup on the end of a magnetic deflection system. The beam first passed through a 1/32" hole in an aluminum collimator, and entered a curved vacuum chamber mounted between the poles of an electromagnet. The output collimator - an aluminum plate with a slot 1/32" wide - was mounted to collect electrons deflected by the field through a fixed angle of 15°. The fringing field, and irregular shape of the pole tips gives rise to considerable error if an attempt is made to calculate energy directly from the deflection geometry. The calibration of the deflecting system was therefore done by the "floating wire" method described by Mallory¹⁹⁾. The current I and tension T in a wire suspended in a magnetic field may be adjusted so that the position of the wire represents the path of an electron travelling in the opposite sense to electrons in the wire, and having a momentum

$$p = \frac{Te}{I} .$$

It is, of course, difficult to eliminate error in the measurement of tension as well as to ensure that the alignment of the wire with marks representing the collimator slits is accurate, and this is the chief limitation of the method.

Range measurements in aluminum will give a value for the maximum energy in the beam. If the energy spectrum has been improved to the point that the magnetic deflection measurement shows a sharp peak, the range measurement provides a useful check on the magnetic one. There is considerable freedom in the choice of "end-point" in the range measurement, and the deflection method is preferable. Eventually, the beam current was improved to such an extent that it was possible to make range measurements on "monochromatic" electrons emerging from the output slit of the deflecting system. Agreement between the two methods, and estimates of error in the floating wire calibration indicate accuracy to within 5% of all energies quoted.

When the beam current and energy are known, the average output microwave power (determined from the dummy load thermocouple reading) gives an approximate value for the beam current within the accelerator; this, in turn, assists evaluations of the effectiveness of transverse focusing. Short of disassembling the whole accelerator, and putting the dummy load coupler at the end of a shorter section, this is the only practical way of estimating the internal current. Although probes can be used inside the waveguide to study the gun current, nothing can be inserted while the power source is operating.

The equations of section 1.1 may be used to predict the power entering the water load, but a sufficiently accurate approximation is given by the following considerations. The attenuation of the complete accelerator structure has been calculated - and measured - to be 2 db, and the isolator insertion loss is .25 db . Therefore 59% of the input power should be observed at the thermocouple, with no internal beam. Additional losses due to beam loading should be given by the product of average beam current, and electron energy at the output. If the observed loading indicates a much higher current than that collected in the Faraday cup, it is probable that the beam diverges to the accelerator walls near the output end. If, on the other hand, there is poor beam transmission, and little indication of loading, one must suspect phasing errors in the buncher; a poor energy spectrum may confirm this possibility.

(c) Transverse Distribution

The most accurate quantitative method of determining the distribution of current within the beam spot is to use a system of collimating discs which intercept successive radial portions, and to measure the power absorbed, or beam current collected at each disc²⁹). Such a method may give a false idea of distribution if the main "spot" is off-axis. What was desired for this work was a qualitative device which would give

some idea of the position of the beam spot, and an indication of relative current density within the intense portion. In the earliest tests long exposures (3 min) on X-ray film gave sufficient indication of the distribution and intensity of the beam, but the method was time consuming. When average currents of $1 \mu\text{amp}$ or more were obtained the darkening of glass slides placed at the output window gave, in a few seconds, a good indication of spot size and position. The degree of darkening of glass is not a reliable indicator of current density - ordinary photographic printing paper is more satisfactory in this respect. The emulsion darkens during a short exposure, and fixing is only required if a permanent record is desired. In addition, the backing will char during an exposure of several seconds, showing the most intense part of the beam.

A fluorescent screen was only used to indicate the presence or absence of a beam. No remote viewing device was available, and with the screen only 30 cm from the output window scattering always made the spot appear diffuse, and about 5 cm in diameter.

5.4 Improvement of Accelerator Operation

The first beam tests on the complete accelerator were made before the buncher had been redesigned (see section 5.1), using the gun described in section 4.1. Although the peak energy was 7.3 MeV,

the energy spread was 55%, and a current of 1 μ amp could only be obtained by operating the gun filament above 100 watts. In an attempt to determine the injected current, an insulated axial probe was constructed which could be pushed axially down the accelerator guide from the output end. For the same filament power, a current of 23 μ amp could be picked up with a 1/2" diameter collector as far as 30 cm from the input coupler. From all measurements it appeared that an increase in field near the accelerator input was necessary.

At the same time it was decided to redesign the buncher, and to change the shape of the input coupler by inserting the "doorknob" transformer. It was thought that if serious R.F. defocusing fields existed close to the exit hole of the gun the doorknob would provide shielding up to the first accelerator cavity. A new flange of cold-rolled steel was made for the coupler, and a disc (of copper-plated steel) was shrunk into the coupler to place the first cavity close to the end of the doorknob. This flange acts as a magnetic shield, preventing the buncher field from penetrating to the gun cathode where its effect may be serious. Tests performed after this system had again been matched showed that the energy and energy spread had improved slightly, but that in other respects the performance was

EFFECT OF MAGNETRON FREQUENCY SPECTRUM ON OUTPUT ENERGY

----- FIXED FREQUENCY MAGNETRON AT 2801.2 Mcps (POOR FREQUENCY SPECTRUM)
—— TUNABLE MAGNETRON AT 2801.1 Mcps (IMPROVED FREQUENCY SPECTRUM)

CURRENT
(arbitrary units)

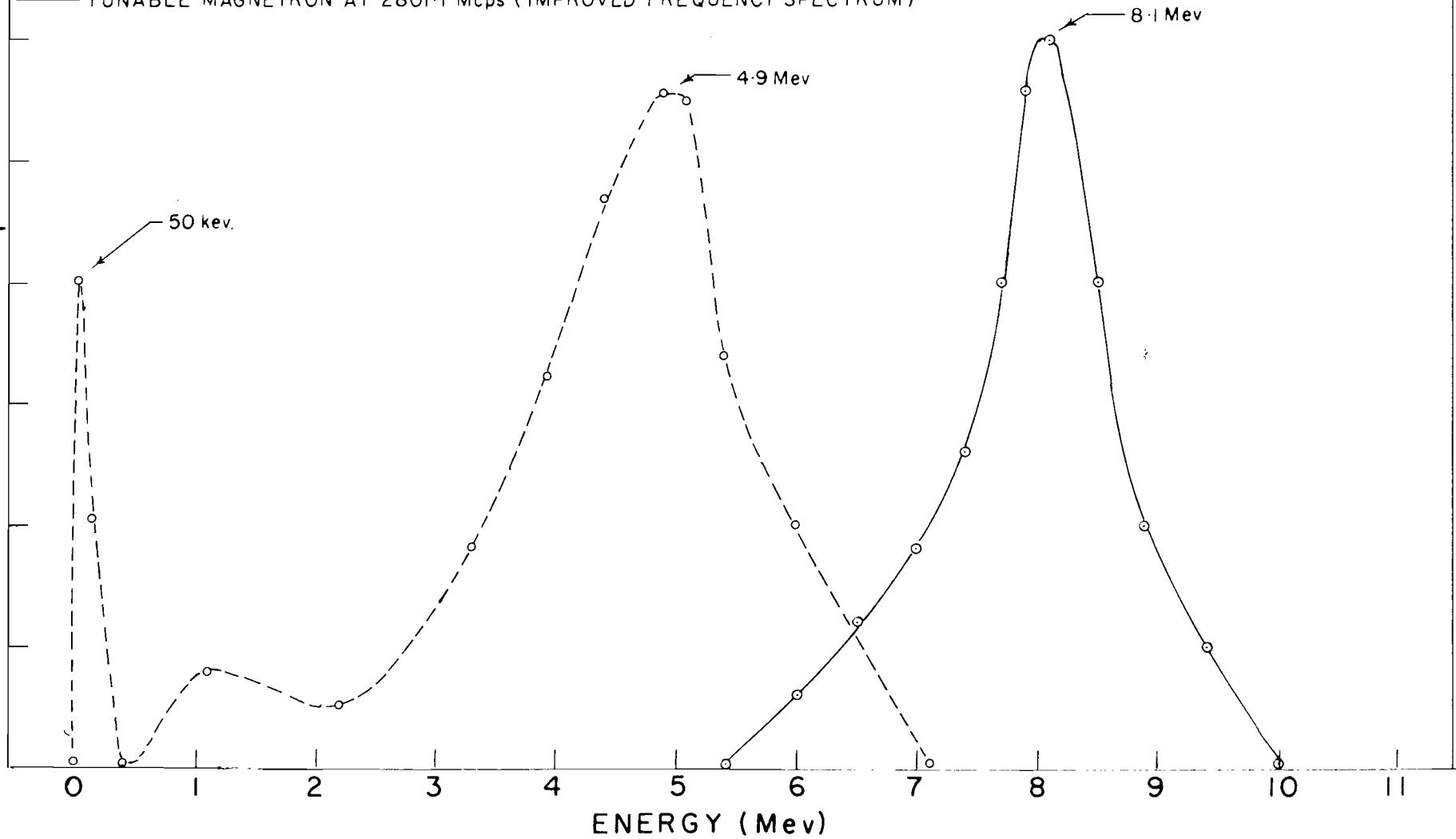


FIGURE 27

worse. The beam current was particularly poor; only $.1 \mu\text{amp}$ could be obtained with 100 watts filament power. The magnetrons in use at the time compounded the difficulty. At the infrequent times when the tubes operated at the design frequency, or slightly below it, their poor frequency spectrum resulted in the sort of energy output shown in fig. 27. A new QK 327 tunable tube cured this difficulty. The spectrum is plotted on the same graph, and it is apparent that the low energy electrons are completely eliminated. The current showed only a slight improvement, being $3.5 \mu\text{amp}$ with the same filament power.

It was realized that more magnetic focusing was required to prevent the beam from spreading in the accelerator. An elementary study of beam loading proved this. An electromagnet was placed at several positions beside the accelerator to steer the beam into the wall, and the reading on the thermocouple was recorded. Only a very slight decrease in loading was noted with the magnet beyond the buncher; therefore most of the beam diverged on leaving the focusing coils, and was intercepted by the discs of the second section. This was confirmed by operating only the first two accelerator sections. As much as $80 \mu\text{amp}$ current could be collected in the rather diffuse beam at the end of the second section. To check the operation of the buncher an energy measurement was made. The result (fig. 28) indicates a 3.15 MeV beam with only 6% energy

spread. This is 1 MeV lower than the energy predicted from orbit calculations, but with correct phasing, a total energy of 9 MeV could still be expected at the end of four sections. A recent spectrum measurement for the complete accelerator is included in this figure.

To improve the beam current and spot size two changes were made. The gun was replaced with the one described in section 4.3 (fig. 21) and the plane spiral filament was changed to the helical winding. With the axis of the helix placed 90° to that of the gun, the winding appears as a source about 4 mm square. The focusing coils were rewound, and two auxiliary coils were made to be placed on the second accelerator section. In addition, a small auxiliary coil, wound on a mild steel core was made, to be inserted between the gun and the buncher coupler. These coils now have the following windings and dimensions:

<u>System</u>	<u>Coil</u>	<u>Length</u>	<u>Turns</u>	<u>Wire</u>	<u>Position</u>
Main	1	2 3/8"	1500	No.18 QF	Starts at buncher
Main	2	5 1/4"	3300	16	Coupler flange
Main	3	5 1/4"	3300	16	
Main	4	2 3/8"	1500	18	

<u>System</u>	<u>Coil</u>	<u>Length</u>	<u>Turns</u>	<u>Wire</u>	<u>Position</u>
Auxiliary	5	5 3/8"	3000	No. 16	Starts at section 2
Auxiliary	6	5 3/8"	3000	16	Starts 15" along section 2
Gun Coil		1 1/8"	2500	28	Between gun anode and buncher coupler

5.5 Present Accelerator Performance

The changes described in the preceding section produced the desired result. The average and peak current output are shown in fig. 29. The reason for the drop in average current is apparent from the photographs of the current pulse in fig. 26. Above average currents of 50 μ amp, the tail of the pulse is shortened, and the duty cycle is reduced^{33,34)}. This current is however, more than adequate for therapy.

With optimum adjustments of the currents in the focusing coils, the beam spot can be confined to an elliptical cross section with axes 9 x 4 mm. About 80% of this beam falls within the nearly circular 4 mm diameter spot shown by the burned area of the insert of photographic printing paper.



The energy spectrum of the present beam is shown in fig. 28 . Spectra for four different beam currents yield the following information

Table 6
Accelerator Operation

<u>Current (μamp)</u>	<u>3</u> <u>("No load")</u>	<u>15</u>	<u>28</u>	<u>52</u>
Filament power (watts)	28	35	40	46
Input R.F. average power (watts)	2310	2310	2310	2310
Power to walls (40% of input) (watts)	925	925	925	925
Power absorbed by beam (i_{AV}) (watts)	24	119	211	362
Estimated power remaining (watts)	1361	1266	1174	1023
Power observed at thermocouple	1370	1300	1135	972
Peak energy (MeV)	8.00	7.90	7.52	7.00
Percent drop from "No load" energy	-	1.0	6.0	12.5
Predicted percent drop (equation 1.14)	-	1.8	3.6	6.7
Energy spread (half value) %	11.3	6.9	9.3	10.3

The design peak power for the accelerator is 4 megawatts while the QK 327 will deliver only 3.5 Mw . Presumably, then, the accelerator energy could be increased to 8.6 MeV if a QK 338 tube could be used. However, it was noted in section 5.4 that the energy from the first two

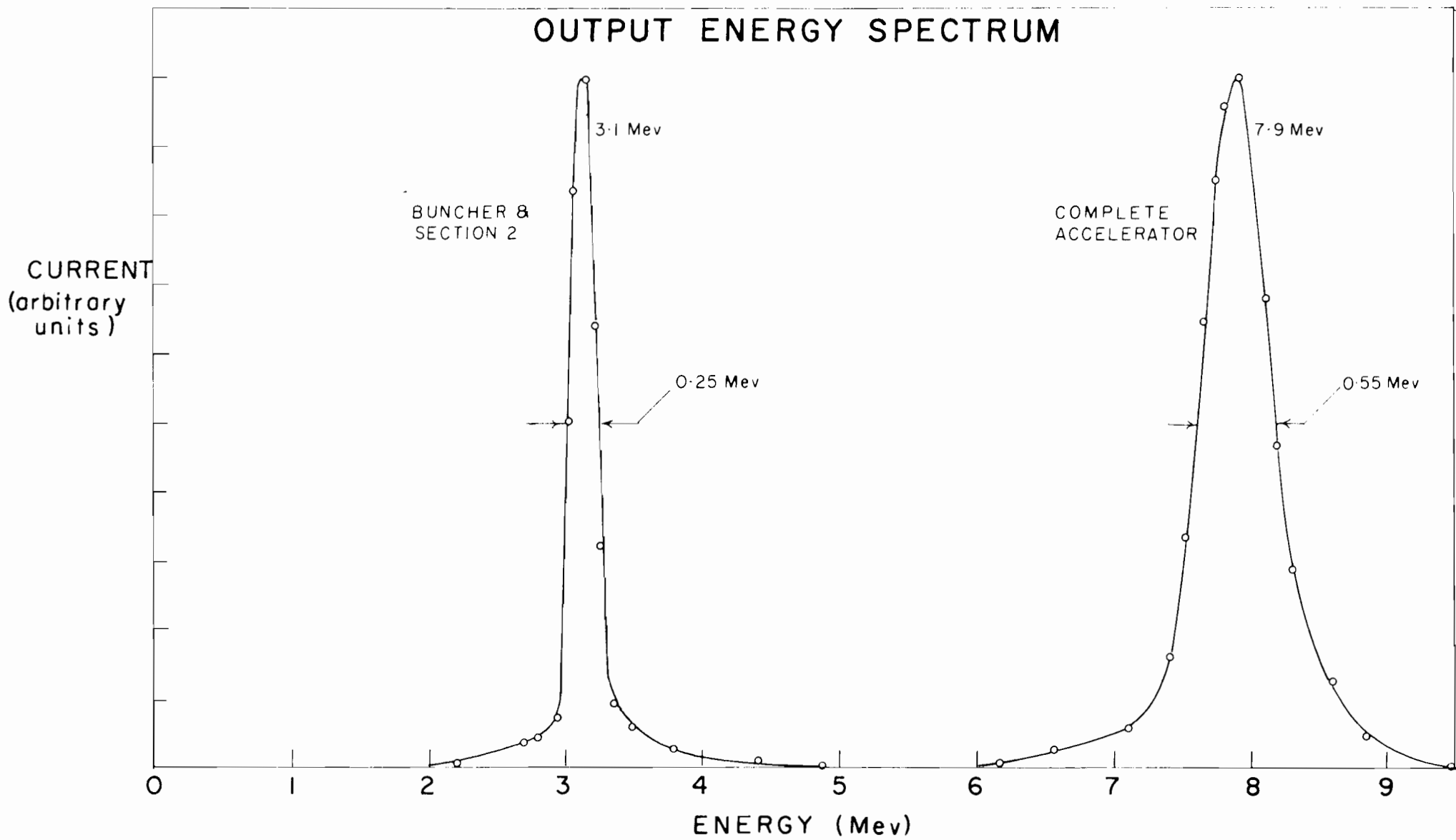


FIGURE 28

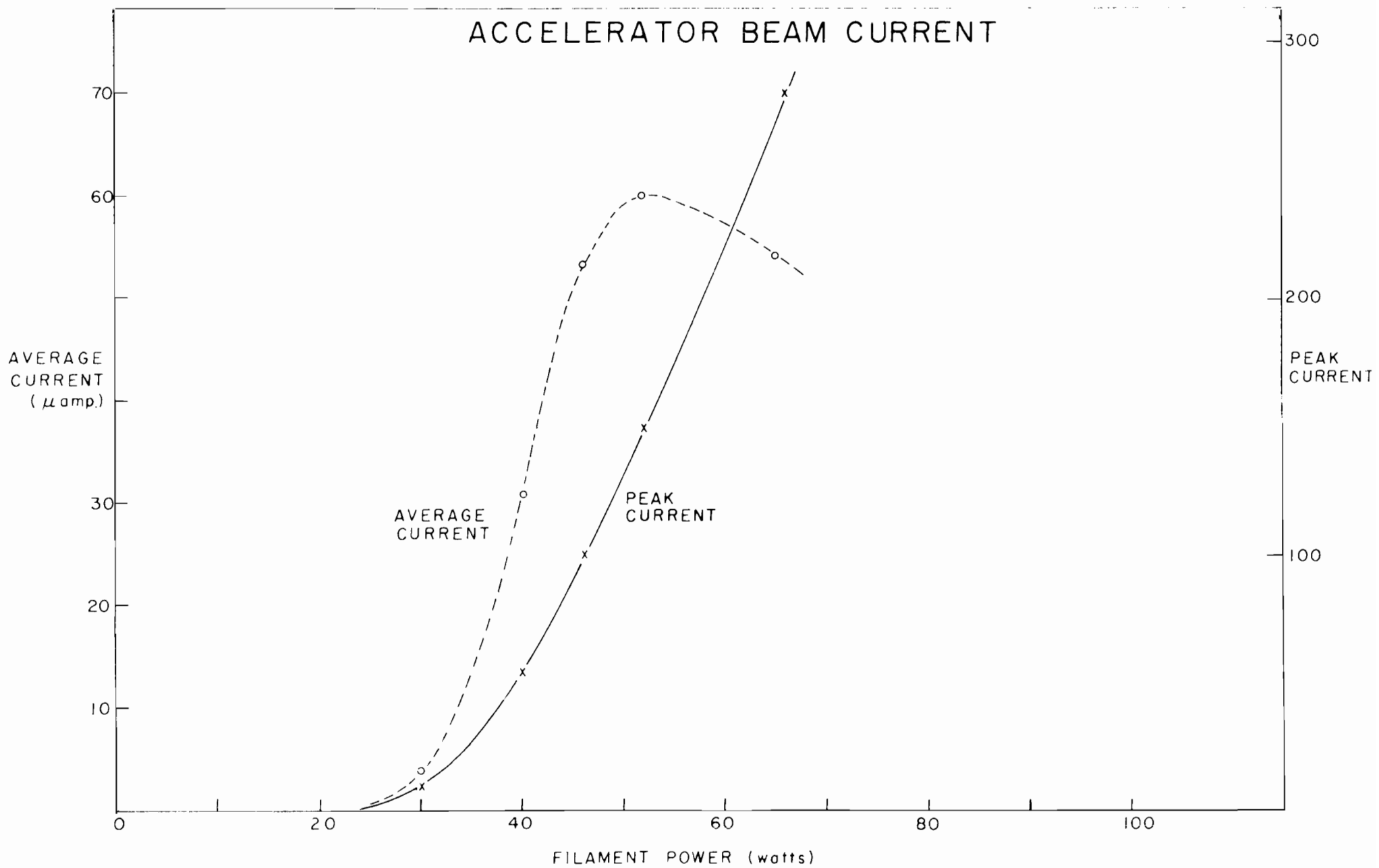


FIGURE 29

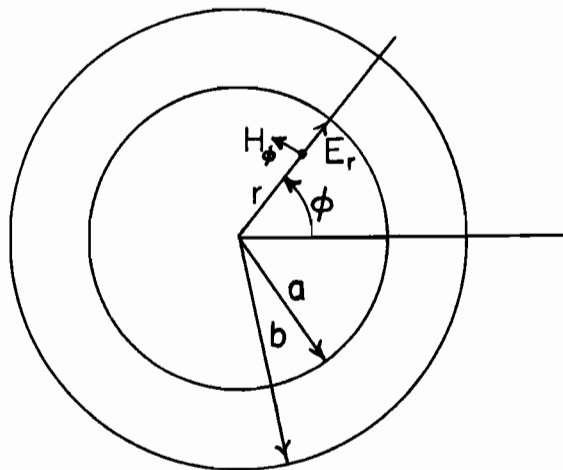
sections was 3.15 MeV; therefore the gain in the last two sections is only 5 MeV, and not the expected 6. This indicates a phasing error in the buncher which places the electrons some 30° away from the wave crest. This could most easily be corrected with a phase shift section of several cavities between sections 2 and 3. This step might entail further matching at the accelerator input, so no changes are planned at present. In any case, the medical advantages of a 10 MeV over an 8 MeV accelerator are practically insignificant.

Appendix

The Transverse Electron Motion

The problem of magnetic focusing has been discussed by R.-Shersby-Harvie³⁵⁾ and in more detail by E. L. Chu²¹. If one were confident of the accuracy of all phase shifts and design parameters, the equations of motion derived by Chu could be integrated in a stepwise fashion on a computer, using the same procedure as for the longitudinal orbits. Since the coils for the R.V.H. buncher were wound on six forms (fig. 30), the field strengths could be adjusted by separate adjustment of the coil current. It was necessary, however, to have some idea of the field necessary to confine the beam to a cross-section of 7 mm or less. In this appendix certain approximations are made to simplify the focusing problem, so that an idea of the interaction of the electron and the fields may be obtained; an estimate of the minimum field required is obtained.

A. 1 Accelerator R.F. fields.



It may be shown³⁶⁾ that if Fourier components higher than the fundamental are neglected, the solutions of Maxwell's equations in a disc-loaded guide are:

$$E_z = E_0 J_0(k_{r0}r) \sin \Delta \quad (\text{a.1.1}) \text{ longitudinal electric}$$

$$E_r = E_0 \frac{(k_{z0})}{k_{r0}} J_1(k_{r0}r) \cos \Delta \quad (\text{a.1.2}) \text{ radial electric}$$

$$H_\phi = \frac{E_0}{Z_0} \left(\frac{k}{k_{r0}} \right) J_1(k_{r0}r) \cos \Delta \quad (\text{a.1.3}) \text{ transverse magnetic}$$

where $\Delta = -90^\circ$ represents the crest of the longitudinal electric wave, as before, and

$$k = \frac{2\pi}{\lambda_0}, \quad k_{r0} = k \sqrt{1 - \frac{c^2}{v_p^2}}, \quad k_{z0} = \frac{2\pi}{\lambda_g} = \frac{2\pi c}{\lambda_0 v_p}$$

The radial force on an electron moving through the r.f. field lines is then the sum of the electric and magnetic forces; for an electron in advance of the crest, the radial electric force tends to spread the beam, while the magnetic force has a focusing effect.

The resultant radial force is then:

$$\vec{F}_r = e\vec{E}_r - e(\vec{v}_e \times \vec{B}_\phi) = e\vec{E}_r - e\mu_0(\vec{v}_e \times \vec{H}_\phi)$$

Expressing H_ϕ in terms of E_r (from a.1.2) we have

$$\begin{aligned} \vec{F}_r &= e\vec{E}_r \left[1 - \frac{\mu_0 v_e \cdot v_p}{z_0 c} \right] = e\vec{E}_r \left[1 - \frac{\mu_0 v_e v_p}{\sqrt{\frac{\mu_0 c}{\epsilon_0}}} \right] = e\vec{E}_r \left(1 - \frac{v_e v_p}{c^2} \right) \\ &= e\vec{E}_r (1 - \beta_e \beta_w) \end{aligned} \quad (\text{a.1.4})$$

Thus, an electron travelling close to the velocity of light will not be defocused by the r.f. fields, regardless of its phase.

Inserting the expression for E_r (from a.1.2)

$$\vec{F}_r = \frac{e\vec{E}_0 J_1(k_{r0}r) (1 - \beta_e \beta_w) \cos \Delta}{\sqrt{\beta_w^2 - 1}}$$

$$\begin{aligned} \text{If } r \text{ is small, } J_1(k_{r0}r) &\doteq \frac{k_{r0}r}{2} = \frac{k}{2} \sqrt{1 - \frac{1}{\beta_w^2}} r \\ &= \frac{k}{2\beta_w} \sqrt{\beta_w^2 - 1} \cdot r \end{aligned}$$

and the expression becomes

$$\vec{F}_r = \frac{e\vec{E}_0 k (1 - \beta_e \beta_w) r \cos \Delta}{2\beta_w} \quad (\text{a.1.5})$$

It is more convenient to write this in terms of the dimensionless field strength parameter

$$\begin{aligned} \alpha &= \frac{eE_0 \lambda_0}{m_0 c^2} : \\ F_r &= \frac{m_0 c^2 \pi}{\lambda_0^2} \frac{\alpha (1 - \beta^2)}{\beta} r \cos \Delta \end{aligned} \quad (\text{a.1.6})$$

(if $\beta_e \doteq \beta_w$)

i.e. for a given position and time in the buncher the radial force on the electron may be written

$$F_r = \zeta r \quad \text{where} \quad \zeta = \frac{m_0 c^2 \pi}{\lambda_0^2} \frac{\alpha (1 - \beta^2) \cos \Delta}{\beta}$$

(a constant of position)

$$= 2.24 \times 10^{-11} \frac{\alpha(1 - \beta^2)}{\beta} \cos\Delta \text{ newtons/meter for this}$$

accelerator. Therefore, when β is small, there must always be a defocusing force on off-axis electrons, with the exception of those riding at, or behind, the wave crest.

A.2 Equations of Radial Motion

In order to confine the radial electron motion to within a given limit an axial magnetic field B may be provided by means of a solenoid enclosing the buncher. If one assumes that transverse electron velocities in the buncher are small compared with c , the radial equations of motion are, in polar coordinates:

$$m\ddot{r} = \mathcal{L}r + m\dot{\theta}^2 r - Be\dot{\theta} \quad (\text{a.2.1})$$

$$\frac{m}{r} \frac{d}{dt} (r^2 \dot{\theta}) = Be\dot{r} \quad (\text{a.2.2})$$

These resemble the equations of motion of an electron in a magnetron, except for the term $\mathcal{L}r$ in (a.2.1). In the magnetron equations the radial electric potential is considered to be obtained from a D.C. voltage applied between concentric cylinders, and is therefore logarithmic, giving a force proportional to $1/r$.

To avoid the necessity of a numerical integration (which would have to be carried out if a complete orbit were desired) we will suppose that \mathcal{L} is constant during the electron's radial motion.

This will not necessarily be true, in the initial part of the buncher where Δ changes rapidly, and it may not be true in the last part unless

$$\frac{\omega (1 - \beta^2)}{\beta}$$

happens to be approximately constant. If the electron is assumed to have

$$\dot{r} = 0 \quad \dot{\theta} = 0,$$

and

$$r = R_0$$

initially, equation (a.2.2) may be integrated to give

$$\dot{\theta} = \frac{B_e}{2m} \left[1 - \frac{R_0^2}{r^2} \right] \quad (\text{a.2.3})$$

Substituting in (a.2.1):

$$m\ddot{r} = \zeta r - \frac{B_e^2 r^2}{4m} + \frac{B_e^2}{4m} \frac{R_0^4}{r^3} \quad (\text{a.2.4})$$

whose integral is the radial electron velocity

$$\dot{r}^2 = Ar^2 + \frac{C}{r^2} + K \quad (\text{a.2.5})$$

where

$$A = \left(\zeta - \frac{B_e^2}{4m} \right) \quad K = \left(\frac{B_e^2}{2m} - \zeta \right) R_0^2$$

$$C = - \frac{B_e^2 R_0^4}{4m^2}$$

If \dot{r} is set equal to zero in (a.2.5) the two solutions of the quartic equation are

$$r^2 = R_0^2, \text{ and } r^2 = \frac{R_0^2}{1 - \frac{4m\zeta}{B^2 e^2}}$$

The second solution indicates that the electron follows some curved path outwards, reaching a maximum "final" radius R_f given by

$$R_f = \frac{R_0}{\sqrt{1 - \frac{4m\zeta}{B^2 e^2}}} \tag{a.2.6}$$

This is real only if $B \geq 2 \sqrt{\frac{m\zeta}{e}}$.

Chodorow et al³⁷⁾ take the equality as being the condition for confinement of the beam, but (a.2.6) shows that $R_f = \infty$ if this is true. In our work we have chosen a value of $B = 2 \sqrt{2} \frac{\sqrt{m\zeta}}{e}$ as a sufficient field for confinement, in which case $R_f = \sqrt{2} R_0$. This value of the field is plotted in fig. 22.

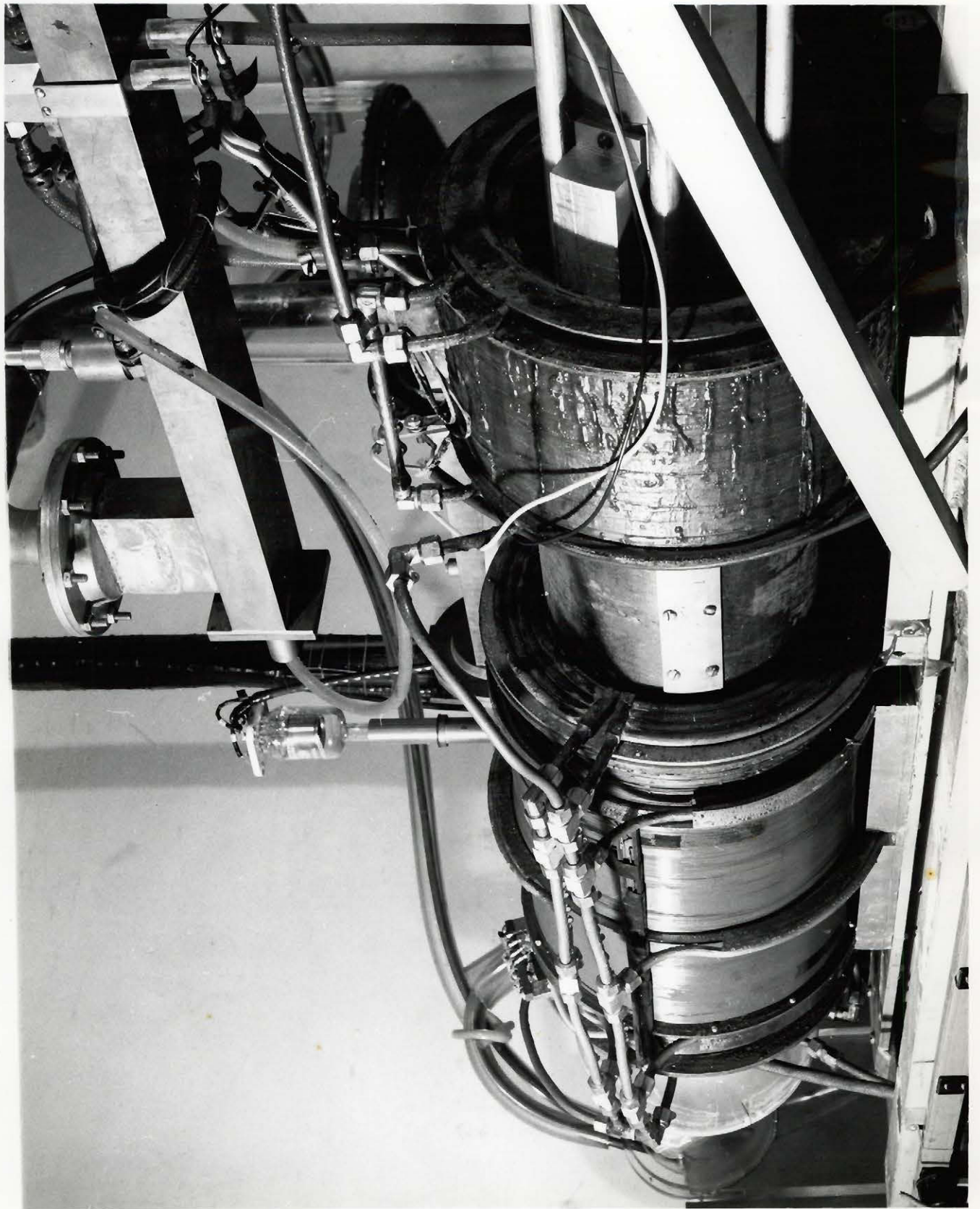
The equation of the path of the electron starting at rest in the cross sectional plane is obtained by solving (a.2.3) and (a.2.5):

$$r^2 = \frac{R_0^2 \left[1 - \frac{2m\zeta}{B^2 e^2} \left(1 + \cos \frac{Be}{m} \sqrt{1 - \frac{4m\zeta}{B^2 e^2}} t \right) \right]}{1 - \frac{4m\zeta}{B^2 e^2}} \tag{a.2.7}$$

Figure 30

Buncher focusing coils.

Five of the coils surrounding the buncher and second section are shown. At the extreme left, part of the electron gun envelope is visible. The rectangular guide above is the water load for the output power.



TRANSVERSE ORBITS WITH $\dot{\theta}_0 = 0$

1. $B = \frac{\sqrt{8m\zeta}}{e}$

2. $B = \frac{\sqrt{6m\zeta}}{e}$

3. $B = \frac{\sqrt{4.84m\zeta}}{e}$

4. $B = \frac{\sqrt{4.5m\zeta}}{e}$

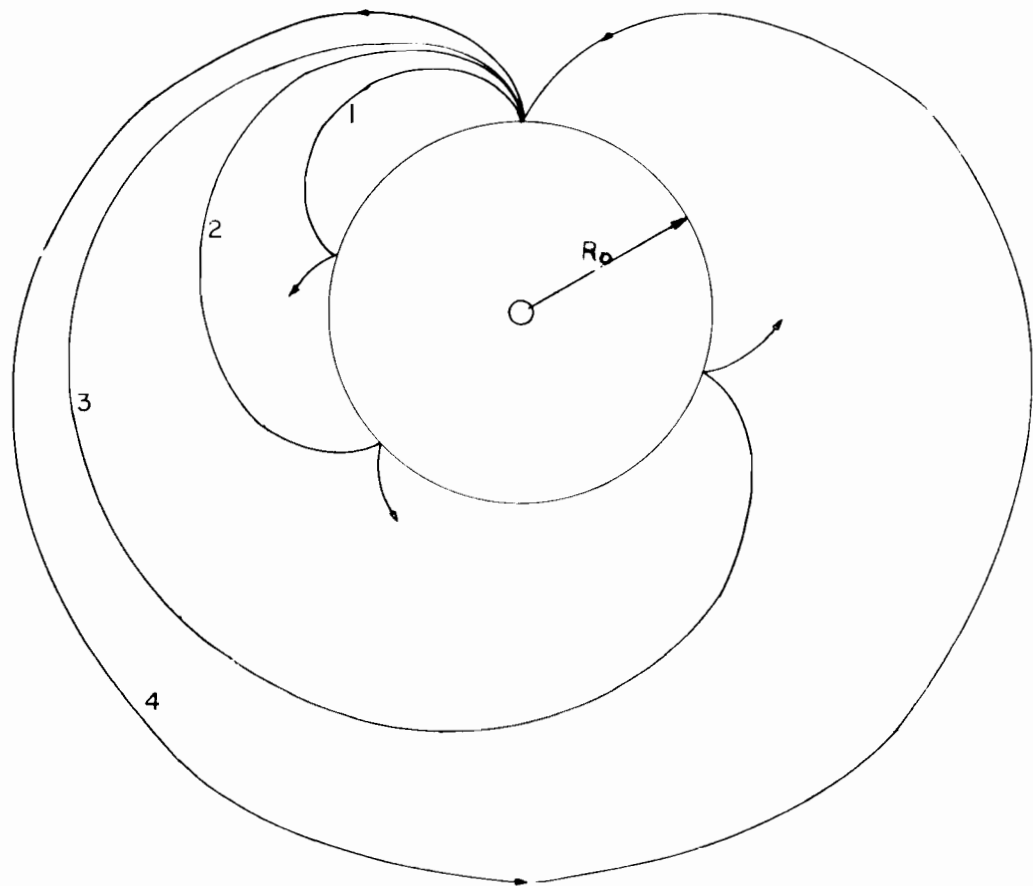


FIGURE 31

and

$$\theta = \frac{Be t}{2m} - \tan^{-1} \left[\frac{\tan \frac{Be}{2m} \sqrt{1 - \frac{4m\zeta}{B^2 e^2}} t}{\sqrt{1 - \frac{4m\zeta}{B^2 e^2}}} \right] \quad (\text{a.2.8})$$

The paths of the electron for several axial field strengths and $\Delta = 0$ are shown in fig. 31. These orbits are epicycloids, generated by a point on the circumference of a circle rolling around a fixed circle of radius R_0 . The radius of the moving circle for any field may be found from (a.2.6); it is simply

$$\frac{R_f - R_0}{2}$$

It may be noted that the limiting case of field

$$B = 2 \frac{\sqrt{m\zeta}}{e}$$

corresponds with a rolling circle of infinite radius - i.e., a straight line.

A.3 Electrons with Initial Angular Velocity

It is probable that electrons, before entering the buncher r.f. fields will acquire some angular velocity from the stray radial field lines of the buncher coils. The case of radial focusing with initial angular velocity is therefore of practical interest. The equations of motions are again (a.2.1) and (a.2.2) but the initial

conditions are now

$$r = R_0, \dot{r} = 0 \quad \dot{\theta} = \dot{\theta}_0 .$$

From (a.2.2):

$$\dot{\theta} = \frac{Be}{2m} \left[1 - \left(\frac{R_0}{r} \right)^2 \right] + \left(\frac{R_0}{r} \right)^2 \dot{\theta}_0 \quad (\text{a.3.1})$$

After substitution in (a.2.1)

$$m\ddot{r} = \left(\frac{\mathcal{L}}{m} - \frac{B^2 e^2}{4m^2} \right) \frac{1}{r} + \left[\frac{B^2 e^2 R_0^4}{4m^2} + R_0^4 \dot{\theta}_0^2 - \frac{Be}{m} R_0^4 \dot{\theta}_0 \right] \frac{1}{r^3} \quad (\text{a.3.2})$$

This may be integrated to give the same equation as before:

$$\dot{r}^2 = Ar^2 + C/r^2 + K \quad (\text{a.2.5})$$

but the constants are now:

$$A = \frac{\mathcal{L}}{m} - \frac{B^2 e^2}{4m^2} \quad C = \left[-\frac{B^2 e^2}{4m^2} + \frac{Be}{m} \dot{\theta}_0 - \dot{\theta}_0^2 \right] R_0^4$$

$$K = \left[\frac{B^2 e^2}{2m^2} - \frac{\mathcal{L}}{m} + \dot{\theta}_0^2 - \frac{Be}{m} \dot{\theta}_0 \right] R_0^2$$

As before, one may set

$$\dot{r} = 0$$

in equation (a.2.5) to find the "final"radius .

The equations of the path of the electron are obtained by

integrating (a.3.1) and (a.3.2) . They are:

$$r^2 = R_0^2 \left[1 + \frac{\frac{2m^2}{B^2 e^2} (\dot{\theta}_0^2 - \frac{Be}{m} \dot{\theta}_0 + \frac{\mathcal{L}}{m}) (1 - \cos \frac{Be}{m} \sqrt{1 - \frac{4m\mathcal{L}}{B^2 e^2}} \cdot t)}{1 - \frac{4m\mathcal{L}}{B^2 e^2}} \right] \quad (\text{a.3.3})$$

and

$$\theta = \frac{Be}{2m} t - \tan^{-1} \left[\frac{(1 - \frac{2m\dot{\theta}_0}{Be}) \tan \frac{Be}{2m} \sqrt{1 - \frac{4m\zeta}{B^2 e^2}} t}{\sqrt{1 - \frac{4m\zeta}{B^2 e^2}}} \right] \quad (a.3.4)$$

Figure 32 shows orbits for the field

$$B = 2 \frac{\sqrt{2} \sqrt{m\zeta}}{e}, \text{ and with } \Delta = 0$$

taking $\dot{\theta}_0$ as parameter. The general form of the path may be deduced from the behaviour of the orbits in fig. 32. It may be noted that if the orbit is to be circular, the term

$$\left(\dot{\theta}_0^2 - \frac{Be}{m} \dot{\theta}_0 + \frac{\zeta}{m} \right)$$

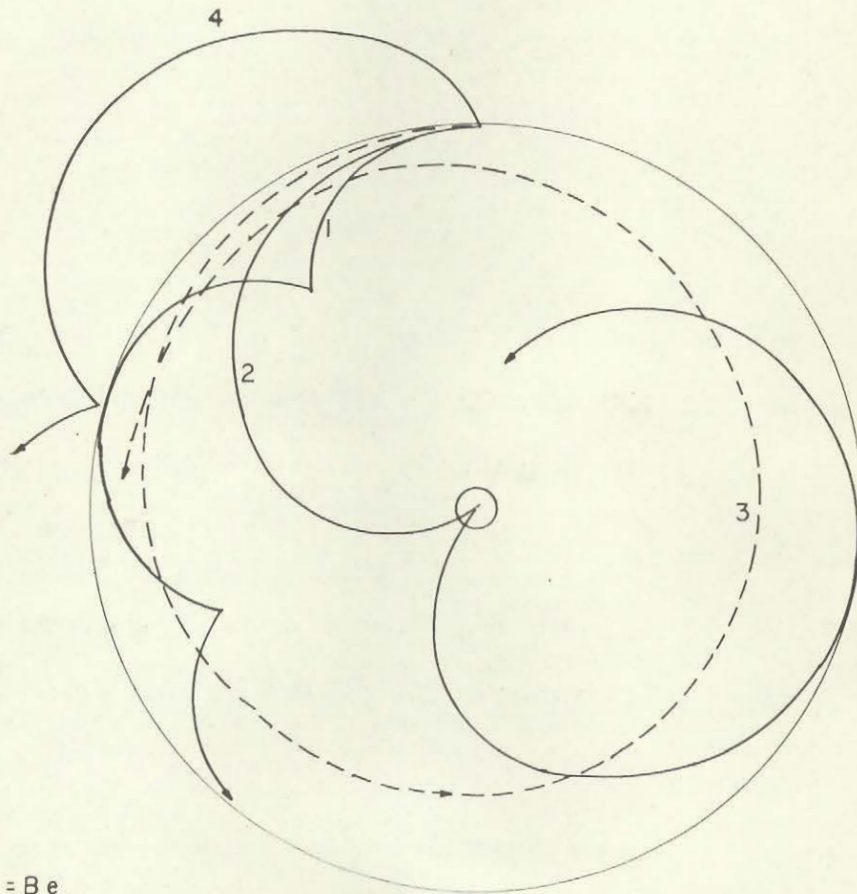
in equation (a.3.3) must be zero. These are then in general two possible angular velocities for the circular orbit

$$\begin{aligned} & (\dot{\theta}_c \mp): \\ & \dot{\theta}_c \pm = \frac{Be}{2m} \left[1 \pm \sqrt{1 - \frac{4m\zeta}{B^2 e^2}} \right] \end{aligned} \quad (a.3.5)$$

If $0 < \dot{\theta} < \dot{\theta}_{c-}$, the orbits lie between R_0 and R_f (defined in a.2.6). For $\dot{\theta}_{c-} < \dot{\theta} < \frac{Be}{2m}$ the orbit always lies within R_0 , and if the angular velocity = $\frac{Be}{2m}$, the electron will just reach the accelerator axis.

If $\frac{Be}{2m} < \dot{\theta} < \dot{\theta}_{c+}$, the orbits still lie within R_0 but have a different

TRANSVERSE ORBITS WITH $B = \frac{\sqrt{8m\zeta}}{e}$
 PARAMETER $\dot{\theta}_0$



1. $\dot{\theta}_0 = \frac{Be}{4m}$

2. $\dot{\theta}_0 = \frac{Be}{2m}$

3. $\dot{\theta}_0 = \frac{3}{4} \frac{Be}{m}$

4. $\dot{\theta}_0 = \frac{Be}{m}$

FIGURE 32

form (orbit 3 of fig. 32), until $\dot{\theta} = \dot{\theta}_{c+}$, giving the second circular orbit. If $\dot{\theta} > \dot{\theta}_{c+}$ (orbit 4 of fig. 32) the path is again entirely outside R_0 .

It should be noted that this simplified picture of transverse motion is only a crude approximation to what actually happens. For the accelerated electrons B , m , ζ and Δ change during the orbit, and the initial angular velocity is uncertain. In defence of the estimated value for the field it may be pointed out that the beam is confined to

$R_f \doteq \sqrt{2} R_0$ (the effective radius of the filament) in our case when the current in the buncher coils gives a field of ~600 gauss, compared with the 518 gauss calculated from

$$B = 2 \frac{\sqrt{2} \sqrt{m\zeta}}{e} .$$

It is necessary, too, to have a strong field (~500 gauss) along the second accelerator section. Fig. 23 shows the large (calculated and observed) field required to correct for the defocusing of the phase shifting cavities at this point.

Bibliography

1. G. Ising, Arkiv. Mat. Astron. Fysik 18, no. 30, 1, (1924-5)
2. R. Wideröe, Arch. Elektrotech 21, 387, (1928)
3. D. H. Sloan and E. O. Lawrence, Phys. Rev. 38, 2021 (1931)
4. J. W. Beams and L. B. Snoddy, Phys. Rev., 45, 287 (1934)
5. J. W. Beams and H. Trotter, Jr., Phys. Rev. 45, 849 (1934)
6. M. Chodorow, E. L. Ginzton, W. W. Hansen, R. L. Khyll,
R. B. Neal, W. K. H. Panofsky and the staff, W. W. Hansen
Laboratories of Physics, Stanford University, Stanford,
California, Rev. Sci. Inst. 26 no. 2, 134 (1955)
7. R. B. Neal, Report no. 185, Microwave Laboratory, Stanford
University (1953)
8. E. L. Ginzton, K. B. Mallory, and H. S. Kaplan, Stanford
Medical Bulletin, 15, no. 3
9. E. L. Ginzton, W. W. Hansen, and W. R. Kennedy, RSI 19 no2,
89 (1948)
10. E. L. Chu, and W. W. Hansen, J. Appl. Phys. 18, 996 (1947)
11. Leon Brillouin, Wave propagation in periodic structures
(McGraw-Hill, 1946)
12. L. Brillouin, J. Appl. Phys. 19, 1023, (1948)
13. J. C. Slater, Rev. Mod. Phys., 20, 473, (1948)
14. W. W. Hansen, and R. F. Post, J. Appl. Phys. 19, 1059 (1948)
15. G. L. Hall, and Philip Parzen, Proc. I.R.E. 41, 1769 (1953)
16. E. L. Nalos, Proc. I.R.E. 42, 1508 (1954)
17. S. W. Kitchen, and A. D. Schelberg, J. Appl. Phys. 26, 618, (1955)

18. L. B. Mullett, and B. G. Loach, Proc. Phys. Soc. (London), 61, 271, (1948)
19. K. B. Mallory, Tech. Report no. 46, H.E.P.L. Stanford (1955)
20. W. Walkinshaw, Proc. Phys. Soc. (London) 61, 246, (1948)
21. E. L. Chu, Report no. 140, Microwave Laboratory, Stanford University, Stanford, California
22. M. C. Crowley-Milling, Metropolitan Vickers Research Series no. 26, (1957)
23. P. T. Demos, Rev. Sci. Inst. 30, 543, (1959)
24. G. Saxon, Proc. Phys. Soc. (London) 47, 705, (1954)
25. K. R. Spangenberg, Vacuum Tubes (McGraw-Hill, 1948), p. 38.
26. H. J. Reich, P. F. Ordnung, H. L. Krauss, J. G. Skalnik, Microwave Theory and Techniques (D. Van Nostrand, 1953), p. 541
27. W. L. Pritchard, Paper; I.R.E. Symposium on Electron Reviews (1951)
28. K. L. Brown and G. W. Tautfest, Rev. Sci. Inst. 27, 696, (1956)
29. C. F. Bareford, and M. G. Kelliher, Philips Tech. Review, 15, 1, (1953)
30. C. W. Miller, Metropolitan Vickers, Research Series, no. 11, (1955)
31. Ginzton, Mallory and Kaplan, op. cit.; Graph on p. 129
32. L. Bess, J. Ovadia, and J. Valassis, Rev. Sci. Inst. 30, 985 (1959)
33. M. G. Kelliher and R. Beadle, Nature 187, 1099 (1960)
34. M. C. Crowley-Milling, T. R. Jarvis, C. W. Miller, G. Saxon, Nature 191, 4787 (1961)

35. R. B. R-Shersby-Harvie, Proc. Phys. Soc. (London) 61,
255, (1948)
36. J. A. Stratton, Electromagnetic Theory (McGraw-Hill, 1941) p. 360
37. Chodorow et al, op. cit. p. 188; equation no. 5.23